Contract No. N 62558 - 3960

Series of model tests on ducted propellers.

Final Report.

NEDERLANDSCH SCHEEPSBOUWKUNDIG PROEFSTATION

NETHERLANDS SHIP MODEL BASIN

Bureau of Ships Fundamental Hydromechanics Research Program SR009010l Administered by the David Taylor Model Basin, Washington, D.C. 20007

WAGENINGEN
NEDERLAND

Contract No. N 62558 - 3960

Series of model tests on ducted propellers.

Final Report.

SERIES OF MODEL TESTS ON DUCTED PROPELLERS.

Contract No. N62558-3960

Principal Investigator: Prof. Dr. Ir. J.D. van Manen.

Report by : Ir. M.W.C. Oosterveld.

Table of contents.

List of Figures.

List of symbols.

a	nozzle length in front of propeller disk.
A	propeller disk area
c	nozzle chord.
C_L	sectional lift coefficient of the nozzle
C_p	pressure coefficient, $\frac{p-p_\infty}{\frac{1}{2}\rho U^2}$
C_T	thrust coefficient, $\frac{T}{\frac{1}{2}\rho U^2 A}$
d	hub diameter
D	propeller diameter
E	loss of kinetic energy in the propeller slip stream.
J	advance coefficient
K_T	thrust coefficient, $\frac{T}{\rho n^2 D^4}$
K_Q	torque coefficient, $\frac{Q}{\rho n^2 D^5}$
p	local static pressure
p_∞	static pressure in the undisturbed stream
p_v	vapour pressure
$p_{1,1}$	static pressure upstream of the propeller plane
$p_{1,2}$	static pressure downstream of the propeller plane.
p_{mean}	mean static pressure at the propeller plane, $\frac{p_{1,1}+p_{1,2}}{2}$
$p_{min.}$	minimum static pressure at the exterior surface of the nozzle
Q	torque
R	propeller radius
T	thrust
T_p	thrust on propeller
T_n	thrust on nozzle
U	undisturbed stream velocity

u_1 average induced axial velocity at propeller plane

u_2 average induced axial velocity in the propeller slipstream at infinite

u_n average induced axial velocity by the nozzle at the propeller plane

u_r induced radial velocity at the propeller plane by the propeller flow field

α angle of attack of nozzle profile

γ vortex strength per unit area

θ angle between nozzle section and axial axis

ρ specific mass of fluid

σ_0 cavitation number of the undisturbed fluid

η efficiency

τ propeller thrust total thrust ratio, $\frac{T_p}{T}$

ω rotational velocity of the propeller

subscripts:

f friction

i ideal

p propeller

n nozzle

Abstract.

Results of an investigation into nozzle shapes, reducing the flow rate through the propeller, are presented. The purpose of this reduction is to prevent the occurrence of cavitation.
The investigation was carried out under Contract No. N62558 -3900 of the U.S. Department of the Navy, David Taylor Model Basin, through its U.S. Navy European Research Contract Program.

A theory is described for the numerical calculation of systematic series of nozzles shapes.

Three nozzles were selected, each designed for operating at the same thrust coefficient C_T, ($C_T = 0.92$) but for a different ratio τ between propeller thrust and total thrust (τ = 1.04; 1.18; 1.36). The shape of the nozzles was chosen to produce ram pressures at the propeller plane in order to delay the onset of cavitation. Tunnel experiments were carried out with the above nozzles.

The method of calculation for the performance characteristics of nozzle propeller systems gives results which compare favourably with the experimental results.

1. Introduction.

The ducted propeller, invented by Kort over 30 years ago, is now extensively used in cases where the ship screw is heavily loaded (e.g. tugs, towboats etc.). Since the duct increases the flow rate through the propeller, the latter operates at a more favourable loading.
The duct itself will generally produce a positive thrust.
The application of this kind of ducted propellers has extensively been dealt with in the literature. The theoretical investigations of Horn [1] , Dickmann and Weissinger[2] , [3] and the systematic experimental investigations of van Manen [4], [5] , may be mentioned in particular.

The range of applicability of the ducted propeller may be extended since the duct can also be used to reduce the flow rate through the propeller.

This second type of flow is used if retardation of propeller cavitation phenomena is desired. In this case the duct reduces the flow rate through the propeller, resulting in an increase of the static pressure at the propeller location. Ram pressures at the propeller plane are obtained if the mean static pressure at the propeller plane exceeds the static pressure in the undisturbed stream. In this way delay of the onset of propeller cavitation may be obtained. The duct itself will generally produce a negative thrust.

Interest has recently been shown in the application of the second duct type. The present report presents the results of investigations of ducts, suitable for building up "ram pressures" at the propeller location.

The investigation covered the following details:

1. Based on one-dimensional momentum considerations, expressions for the ideal efficiency of the propulsion system and the mean static pressure at the propeller plane were derived.
   In addition, a relation between total thrust, the ratio between propeller thrust and total thrust and the angle between nozzle profile and shaft line is given.

2. Representing the propeller by a uniformly loaded actuator disk rotating with finite angular velocity and the nozzle by distributions of ring vortices, sources and sinks, a theory was developed to calculate the flow field. Starting from the flow field, expressions for the propeller torque and thrust, the thrust on the nozzle, the static pressure along the nozzle and the shape of the camber of the nozzle were derived.
3. Systematic calculations were carried out with the above theory. The relation between the total thrust coefficient (K_T) and the advance coefficient was calculated for a number of nozzle shapes. In addition the ratio between propeller thrust and total thrust, the efficiency, the mean static pressure at the propeller and the minimum static pressure at the exterior surface of the nozzle were calculated.
4. Three nozzles were selected, each designed for operating at the same thrust coefficient C_T, but for a different ratio between propeller thrust and total thrust. The shape of the nozzles was chosen in such a way, that "ram pressures" were expected at the propeller plane.
   Cavitation tunnel experiments were carried out with the above nozzles and with a practical nozzle shape. Five screw models have been tested in combination with each of the nozzles . The propeller torque, the propeller thrust and the thrust on the nozzle were measured.
   Flow observations were performed. Separation phenomena and cavitation inception at the surface of the nozzle were recorded.
5. The validity of the approximate method for the calculation of the nozzle-propeller performance was tested, by a comparison with the experimental results.

2. Theoretical analysis of ducted propellers.

2.1. Momentum considerations.

Insight into the most important properties of ducted propellers can be obtained from momentum considerations. Figure 1 shows diagrammatically the simplified system by which the ducted propeller can be replaced.

The x, y, z body axis system is a right handed orthogonal triad with its origin in the centre of the propeller plane. x is positive in the direction of the uniform stream velocity u.

The propeller was replaced by a uniformly loaded actuator disk. The tangentially induced velocities were neglected.

The nozzle extends from $x = -c/2$ to $x = +c/2$, with a radius R at $x = 0$. The propeller was situated in the middle of the nozzle.

The total thrust T acting on the fluid owing to the working propeller and to the nozzle is:

$$T = \rho u_2 A (u + u_1) \qquad (2.1 - 1)$$

applying the momentum theorem over the control volume given in Figure 1.
u_1 and u_2 are the mean additional velocities in the slip stream at $x=0$ and $x=\infty$.
A denotes the actuator disk area at $x=0$.

The trust T_p developed by the propeller can be obtained by calculating the pressure difference across the actuator disk with Bernoulli's equation,

$$\left.\begin{aligned} p_{1,1} + \tfrac{1}{2}\rho(u+u_1)^2 &= p_\infty + \tfrac{1}{2}\rho u^2 \\ p_{1,2} + \tfrac{1}{2}\rho(u+u_1)^2 &= p_\infty + \tfrac{1}{2}\rho(u+u_2)^2 \end{aligned}\right\} \qquad (2.1-2)$$

and thus,

$$T_p = A(p_{1,2} - p_{1,1}) = \rho u u_2 A \left(1 + \frac{u_2}{2u}\right) \qquad (2.1-3)$$

where $P_{1,1}$ and $P_{1,2}$ denote the static pressures upstream and downstream of the actuator disk, respectively, and P_∞ denotes the static pressure for upstream and for downstream of the propeller.

The kinetic energy E lost in the propeller slip stream is given by,

$$E = \frac{1}{2}\rho(u+u_1)A u_2^2 \qquad (2.1\text{-}4)$$

Hence the ideal efficiency η_i of the propulsion device is defined by,

$$\eta_i = \frac{uT}{uT + E} = \frac{1}{1+\sqrt{1+\tau C_T}} \qquad (2.1\text{-}5)$$

where

$$\left.\begin{aligned} C_T &= \frac{T}{\frac{1}{2}\rho u^2 A} \\ \tau &= \frac{T_P}{T} \end{aligned}\right\} \qquad (2.1\text{-}6)$$

The mean value of the static pressure at the actuator disk P_{mean} can be calculated from:

$$P_{mean} = \frac{P_{1,1} + P_{1,2}}{2}$$

thus

$$C_{p_{mean}} = \frac{P_{mean} - P_\infty}{\frac{1}{2}\rho u^2} = 1 + \frac{\tau C_T}{2} - \left[\frac{C_T/2}{-1+\sqrt{1+\tau C_T}}\right]^2 \qquad (2.1\text{-}7)$$

The efficiency η_i and the mean static pressure coefficient at the actuator disk $C_{p_{mean}}$ are plotted as a function of the ratio τ between propeller thrust and total thrust, with the total thrust coefficient C_T as parameter, in the Figures 2 and 3 respectively.

It follows from these Figures that the efficiency η_i of the propulsion device decreases and the mean value of the static pressure at the propeller plane increases with increasing value of the ratio τ. Ram pressures at the propeller plane are only built up when τ exceeds 1.0. Consequently a negative thrust is acting on the duct in that case. The total thrust coefficient c_T and the ratio τ between propeller thrust and total thrust can approximately be calculated as a function of the angle of incidence of the nozzle profile in the way as described by Chen [7], [8].

The radial velocity u_r, induced by the propeller at the nozzle, is principally a function of the actuator disk loading. The results given by Yim and Chen [9] enable the calculation of the mean value of the radially induced velocity along the duct $\bar{u}_r$ as a function of the propeller thrust coefficient c_{T_p} and the ratio between the nozzle chord length c and the propeller radius R.

$$\frac{\bar{u}_r}{u} = g\left(c_{T_p}; \frac{c}{R}\right) \qquad (2.1\text{-}8)$$

The propeller may be considered as operating in open water with an equivalent uniform stream velocity $u + u_n = u + u_1 - \frac{u_2}{2}$. Therefore equation (2.1-8) becomes:

$$\frac{\bar{u}_r}{u + u_n} = g\left(c'_{T_p}; \frac{c}{R}\right) \qquad (2.1\text{-}9)$$

where u_n denotes the mean axial velocity induced by the nozzle at the propeller location.

The sectional lift of the nozzle is according to the two dimensional theory equal to (see for sign conventions Figure 4):

$$L = \frac{1}{2} \rho U^2 c C_{L_\alpha} \alpha \qquad (2.1-10)$$

where C_{L_α} and α denote the sectional lift coefficient and the angle of attack of the nozzle profile respectively. In the case of symmetrically loaded ducts there are no radial velocities induced by the nozzle in the mid plane of the nozzle. Consequently the thrust coefficient of the nozzle C_{T_n} can be readily obtained from equations (2.1-9) and (2.1-10).

$$C_{T_n} = \frac{T_n}{\frac{1}{2} \rho U^2 \pi R^2} = 2 \frac{c}{R} C_{L_\alpha} \alpha \, g\left(C_{T_p}'; \frac{c}{R}\right) \qquad (2.1-11)$$

Furthermore,

$$C_{T_n} = (1 - \tau) C_T \qquad (2.1-12)$$

From equations (2.1-9), (2.1-11) and (2.1-12) it follows that

$$\Theta = \operatorname{arctg} g\left(C_{T_p}'; \frac{c}{R}\right) - \frac{(1-\tau) C_T}{2 \frac{c}{R} C_{L_\alpha} \sin\left[\operatorname{arctg} g\left(C_{T_p}'; \frac{c}{R}\right)\right]} \qquad [illegible]$$

where Θ denotes the angle between the nozzle profile and the shaft line. The relation between the thrust coefficient C_T and the ratio $\tau = \frac{T_p}{T}$ is plotted in Figure 5 for some values of Θ and for the case $\frac{c}{R} = 1.2$ and $C_{L_\alpha} = 5.5$ Figure 5 shows that for a given nozzle shape, the thrust on the nozzle increases with increasing loading of the nozzle-propeller system.

2.2. Representation of ducted propellers by vortex distributions.

The calculations on the ducted propellers are based on the following assumptions. The ducted propeller moves steadily forward. The forward velocity was assumed to be sufficiently large, the nozzle loading and the propeller loading sufficiently low to permit the application of linearized theory.

The calculations on ducted propellers may be classified into two types:
(1) the direct problem, in which the propeller blade form and the shape of the duct are described,
(2) the inverse problem, in which a certain combination of blade forces and duct forces are given.
Notable with respect to the direct problem is the theoretical treatment of Morgan [6] .
The present investigation is concerned with the inverse problem.

The considered ducted system consists of an annular airfoil of finite length with an impeller having an infinite number of blades. The mathematical model of the geometrical configuration of the ducted propeller can be represented by vortex and source distributions as summarized in Figure 6.

The propeller is considered as an actuator disk which is set normal to the free stream. It is driven to rotate in its own plane at an angular velocity ω.

The propeller flow field consists of helical trailing vortices starting from the propeller disk at hub and nozzle diameter.
The strength of the trailing vortices is a function of the loading of the propeller disk γ and the advance coefficient $\Im$.

Each helical trailing vortex line lies on a cylinder of constant diameter (equal to hub or nozzle diameter) and has a constant pitch.
The radial component of the induced velocity exhibits a logarithmic singularity at the periphery of the propeller disk. Since logarithmic singularities are integrable, the stream line near the propeller tip is continuous but with infinite slope.

The flow around the nozzle is represented by a distribution of ring sources and a distribution of ring vortices along a cylinder of constant diameter. The annular airfoil is axisymmetrical, so that the nozzle has no trailing vortices. The nozzle is thus replaced by:

(1) A bound ring vortex distribution with a strength equal to zero at the leading edge of the nozzle and equal to the strength of the circumferential component of the helical trailing vortices at the propeller disk. The induced radial velocity due to this vortex distribution has a logarithmic singularity at the propeller plane at the tip diameter. The ring vortex distribution along the duct has been chosen in such a way that the logarithmic singularity of the radial velocity induced by this vortex distribution and the actuator disk compensate each other. Consequently the total radialy induced velocity has a smooth behaviour. This fact simplifies the numerical calculations.

(2) A source and sink distribution representing the thickness effect of the nozzle.

(3) Continuous bound ring vortex distributions with zero strength at the leading and trailing edges of the nozzle and with sinusoidal shapes. Other vortex distributions along the nozzle can be built up by Fourier synthesis.

The nozzle will have shock free entry because the total ring vortex strength at the leading edge equals zero.

The range of angles of attack within which this shock - free entry can be realized if the loading of a given ducted propeller system is varied largely depends on the shape of the leading edge of the nozzle profile. Shock-free entry occurs on thick profiles having rounded leading edges, over a larger range of angles of attack than on thin profiles having sharp leading edges.

The resulting mathematical model is summarized in Figure 6, where w_a ; w_T and w_r are the dimensionless velocities (in axial-, circumferential- and radial direction, respectively) induced by all the vortices and sources. The vortex strength per unit area of the actuator disk is denoted by γ . The amplitudes of the sinusoidal ring vortex distributions along the nozzle are denoted by γ_m . The source and sink distribution along the nozzle is given by $-q(x)$.

The total induced velocities can be calculated according to the law of Biot - Savart.

The propeller flow field is known now and the propeller thrust, the thrust of the nozzle, the propeller torque and the efficiency can be calculated for the chosen data of design parameters. At the same time the shape of the camber line of the nozzle and the static pressure along the nozzle can be calculated.

The details of the theory are not given here.

A numerical program for the N.S.M.B. - digital computer based on this theory was made.

Computations were carried out to select systematic series of nozzle shapes.

3. Calculation of systematic series of duct shapes.

The basic-design parameters of ducted propellers are (see Figure 7):

(1) the ratio between nozzle length and propeller diameter, $\frac{c}{D}$.

(2) the ratio between nozzle length in front of propeller disc and total nozzle length, $\frac{a}{c}$.

(3) the ratio between hub and propeller tip diameter, $\frac{d}{D}$.

(4) the thickness distribution and the maximum thickness of the nozzle profile.

(5) the advance coefficient J.

(6) the loading of the propeller.

(7) the loading of the nozzle.

Based on the theoretical analysis described in the previous section calculations were carried out to come to series of nozzle shapes. The data used for the design parameters are:

$\frac{c}{D} = 0.6$

$\frac{a}{c} = 0.5$

$\frac{d}{D} = 0.2$

The nozzle profile has a NASA 0015 basic thickness form.

The loading of the propeller, the loading of the nozzle and the advance coefficient were systematically varied.

The numerical results are presented in Figure 2 and graphically represented in the Figures 8 through 12.

The effect of the ratio τ between propeller thrust and total thrust on efficiency for some values of the thrust coefficient C_T and for $J=0$ is shown in Figure 2.
The ducted propeller corresponds for the case $J=0$ with an actuator disk enclosed by a nozzle and rotating at an infinite angular velocity.
The results of the momentum considerations described in section 2.1 are presented in Figure 2.

The efficiencies calculated by these two methods agree very well for small values of τ . The differences between the efficiencies for large values of τ can be explained by the thickness effect of the nozzle which is only taken into account in the vortex theory. The effect of the nozzle on the flow at the propeller is in that theory taken into account in a more thorough way.

The differences between the curves in Figure 2 show that for large ratios between propeller thrust and total thrust, thin nozzle profiles are more suitable with respect to efficiency.
The efficiency of the propulsion system always diminished with increasing ratio τ . However, it is noted that for lightly loaded systems, the decrease in efficiency is small.
The shape of the camber line of a nozzle $s(x)$ is completely determined by the strength of the vortices along the nozzle γ_1 the ratio between the vortex strength at the propeller plane γ and the advance coefficient J and by the geometry of the system ($\frac{c}{D}$; $\frac{a}{D}$; $\frac{d}{D}$; thickness distribution and maximum thickness of the nozzle).

$$s(x) = f\left(\gamma_1 ; \frac{\gamma}{J} ; \text{GEOMETRY}\right).$$

The propeller is represented by an actuator disk rotating at an <u>infinite</u> angular velocity if the undisturbed stream velocity u is assumed to be constant and the advance coefficient J becomes zero.

The ratio $\frac{\gamma}{J}$ is kept constant, thus the vortex strength at the propeller goes in the same way to zero as the advance coefficient J.

The total thrust coefficient C_T and the ratio between propeller thrust and total thrust τ are denoted by C_{T_0} and τ_0 if $J=0$. Thus the shape of a nozzle is also completely determined by C_{T_0} ; τ_0 and the geometry of the ducted propeller system.

$$S(x) = f\,(C_{T_0} ;\ \tau_0 ;\ \text{GEOMETRY})$$

Calculations of the efficiency η_i, the total thrust coefficient K_T and the ratio between propeller thrust and total thrust at various advance coefficients J, were made for a number of nozzle shapes determined by C_{T_0} and τ_0.
In addition, the mean value of the static pressure at the propeller plane p_{mean} and the minimum static pressure at the exterior surface of the nozzles p_{min} were calculated for the nozzles considered.
The following non-dimensional pressure coefficients are introduced.

$$C_{p_{mean}} = \frac{p_{mean} - p_0}{\frac{1}{2}\rho U^2}$$

$$C_{p_{min}} = \frac{p_{min} - p_0}{\frac{1}{2}\rho U^2}$$

where p_0 and $\frac{1}{2}\rho U^2$ are the static pressure and the dynamic pressure of the undisturbed stream respectively.

The numerical results are presented in the Figures 8 through 12. The nozzle shapes considered are tabulated below.

Table

Figure number	Nozzle shapes determined by				
	τ_o	c_{T_o}			
8	0.6	0.25	0.50	1.00	2.00
9	0.8	"	"	"	"
10	1.0	"	"	"	"
11	1.2	"	"	"	"
12	1.4	"	"	"	"

It appears that the efficiency η_i of a ducted propeller decreases for increasing advance coefficient λ.
This phenomenon can be explained by the losses due to rotation. The kinetic energy in the propeller slip stream, which is lost, may be split up into the losses due to the axial acceleration of the fluid and those due to the rotation of the fluid. The losses due to the axial acceleration are independent of the advance coefficient λ, those due to the rotation of the fluid are equal to zero for $\lambda=0$ and increase with increasing λ.
Application of <u>pre-turning</u> vanes becomes important in the case of heavily loaded systems if the gain in rotational efficiency is larger than the efficiency loss due to friction.

The thrust coefficient c_T of the ducted propeller always diminishes with increasing advance coefficient λ. This phenomenon can also be explained by the rotation of the fluid.

The minimum static pressure at the exterior surface of the nozzle is almost independent of the total thrust coefficient c_T. With increasing ratio τ between propeller thrust and total thrust, the minimum static pressure decreases. Consequently the risk of cavitation at the exterior surface of the nozzle increases in that case.

The shape of the nozzles for the experiments were selected in such a way that "ram pressures" are expected at the propeller plane. Thus the ratio $\tau = \frac{T_P}{T}$ should be above 1.0. The nozzles are determined for relatively high ship speeds.

The data used for the nozzles are:

nozzle	(30)	$C_{T_o} = 0.92$	$\tau_o = 1.04$
	(31)	$= 0.92$	1.18
	(32)	$= 0.92$	1.36

The nozzle shapes are presented in Figure 13 and tabulated in table 1.

The ideal efficiency η_i, the thrust coefficient K_T, and the ratio $\tau = \frac{T_P}{T}$ at various advance coefficients J are presented in Figure 14. In addition the pressure coefficients $C_{p_{mean}}$ and $C_{p_{min}}$ are given.

4. Experiments on a systematic series of ducted propellers.

The experiments were carried out in the N.S.M.B. cavitation tunnel no. 1 having a 90 cm x 90 cm closed test section and a uniform flow. Five different screw models were tested in combination with the nozzles (19) (26) (30) (31) and (32)

The results of earlier investigations by Van Manen into screws in nozzles are given in the N.S.M.B. publications [4] [5]

Nozzle No. (19) is recommended by the N.S.M.B. for practical purposes. This nozzle increases the flow rate through the propeller disk.

Later on it was tried to build up a ram pressure inside the nozzle by a suitable choise of the camber of the nozzle profile. A practical shape of a nozzle was designed, indicated by No. (26). Nozzle No. (26) has a cylindrical inner wall so that the screw can arbitrarily be located in the nozzle with a constant clearance between blade tip and nozzle.

Nozzle No. (30) (31) and (32) are calculated with the aid of the theoretical analysis described in the previous sections.

The mean lines and the thickness distributions of all the mentioned nozzle shapes are presented in Figure 13. and tabulated in table 1.

The experiments were all carried out with a series of five bladed Kaplan type screws. The most important characteristics are presented in the table below. Further particulars of the screw models are given in the Figures 15 through 19.

table		
Diameter	D	240 mm
Number of blades	Z	5
Pitch ratio	P/D	1.0-1.2-1.4-1.6-1.8
Pitch distribution		uniform near the tip, decreasing to the hub.
Blade area ratio	B.A.R.	100 %
Blade outline		Kaplan type
Blade section		NASA 16 - parabolic camber line - flat face.
Total number of screws		5
Propellers indicated by		3527, 3528, 3529, 3530, 3531.

The screws were designed in combination with nozzle No. (19)
The pitch distribution depends on the nozzle induced velocities at the location of the screw and on the radial load distribution on the screw.

The screws were located in the nozzles with a uniform tip clearance of 1 mm.

Cavitation tunnel experiments were carried out at constant rpm of the screw models, at speeds of advance covering a slip range from 40 - 100 % and at various cavitation numbers. The torque and thrust on the screw and the thrust on the nozzle were recorded by means of strain gauges.

The total thrust coefficient K_T , the torque coefficient K_Q the efficiency η and the ratio τ between propeller thrust and total thrust were all calculated as functions of the advance coefficient J. For the nozzles (19) , (26) , (30) , (31) and (32) the experimental results are presented in the Figures 20 through 24 respectively.

In addition, the mean static pressure coefficient $c_{p_{mean}}$ was derived from the measured thrust coefficient c_T and the ratio τ with the aid of Figure 3. The result is also presented in the Figures 20 through 24.

The relation between the thrust coefficient c_T and the ratio τ for the various nozzle shapes is given in Figure 5.

The results of the experiments are synthesized in a B_p-δ diagram. (see Figure 25). The parameters B_p and δ are defined by:

$$B_p = 33.08 \frac{K_Q^{1/2}}{J^{5/2}}$$

$$\delta = \frac{101.27}{J}$$

Cavitation observations were made during all the experiments. Figure 26 shows the inception lines for bubble cavitation at the exterior surface of the nozzles.
The cavitation number σ_o is plotted to a base of total thrust coefficient c_T. The cavitation number σ_o is defined by

$$\sigma_o = \frac{p_\infty - p_v}{\frac{1}{2}\rho u^2}$$

where p_v denotes the vapour pressure of the water.

The pressure coefficient $c_{p_{min.}}$, determining the minimum static pressure at the exterior surface of the nozzle, was calculated for the various nozzles.
The numerical results are presented in Figure 26.

It is noted that the results of the thrust, torque and velocity measurements were not corrected for the wall effects of the cavitation tunnel.

5. Discussion of theoretical and experimental results.

Certain simplifying assumptions were made in the development of the theory for the numerical calculations of nozzle shapes. The validity of the method must be tested by a comparison with measurements.

The experimentally obtained relation between the thrust coefficient K_T and the advance coefficient J for the nozzles No. (30), (31) and (32) in combination with the various screws, is given in the Figures 22 through 24 respectively. The theoretically obtained relations between K_T and τ for which the nozzles No. (30), (31) and (32) were designed are presented in Figure 14. A nozzle screw combination meets the requirements of the theory if the theoretical design curve of the nozzle and the measured thrust curve of the nozzle - screw combination intersect at the design J.

The point of intersection of the various nozzle - screw systems are given in the following table.
The measured torque coefficient K_Q, the efficiency η and the ratio τ are tabulated aswell.

Nozzle No.	screw	P/D	K_T	J	K_Q	η	τ
(30)	3527	1.0	0.193	0.75	0.0379	0.60	1.05
	3528	1.2	0.262	0.88	0.0588	0.63	1.05
	3529	1.4	0.337	1.00	0.0834	0.65	1.05
	3530	1.6	0.409	1.11	0.1101	0.67	1.03
	3531	1.8	0.490	1.24	0.1398	0.69	1.01
(31)	3527	1.0	0.209	0.79	0.0430	0.61	1.19
	3528	1.2	0.279	0.92	0.0672	0.61	1.21
	3529	1.4	0.342	1.03	0.0941	0.60	1.22
	3530	1.6	0.404	1.13	0.1244	0.59	1.23
	3531	1.8	0.464	1.23	0.1596	0.58	1.25
(32)	3527	1.0	0.223	0.82	0.0558	0.53	1.17
	3528	1.2	0.300	0.97	0.0823	0.56	1.18
	3529	1.4	0.360	1.10	0.1126	0.57	1.18
	3530	1.6	0.420	1.22	0.1462	0.55	1.24
	3531	1.8	0.456	1.30	0.1836	0.51	1.20

The above results afford the possibility of comparison with the predicted performance.

The overall efficiency of the ducted propeller may be expressed as a product of the ideal efficiency η_i and the efficiency factor η_f due to profile drag and frictional drag of the propeller blades and the nozzle.

$$\eta = \eta_i \cdot \eta_f$$

For low advance coefficients J , the screw is represented in the theory by an actuator disk rotating at a high angular velocity. Consequently the efficiency loss of the screw due to friction becomes large and the efficiency factor η_f tends to zero. The frictional losses decrease with increasing J.

Figure 14 shows that the agreement between the calculated values of η and those obtained by the tests is good if the above considerations with respect to the frictional losses are taken into account.

It is also seen from Figure 14 that the calculated values of the ratio τ between propeller thrust and total thrust agree very well with the test results.

Flow observations were performed during the cavitation tunnel experiments. Separation phenomena at the exterior or the interior surface of the nozzles No. (30) , (31) and (32) were not observed over the range of considered water speeds.

The shapes of the cambers of nozzles No. (26) and No. (30) are geometrically almost equal. (see Figure 13). The cambers are only different at the leading edges of the nozzle profiles. Flow separation was observed at the interior surface of nozzle No. (26) during the cavitation tunnel tests. This phenomenon can be explained by the unfavourable shape of the nozzle at the leading edge.

The slope of a streamline passing through the propeller tip of a propeller in open water is directly proportional to the propeller thrust coefficient C_{T_p} . The thrust coefficient C_{T_n} is primarily determined by the thrust coefficient of the propeller C_{T_p} and the nozzle geometry.

Hence it is expected that there exists a fixed relation between the thrust coefficient C_T and the ratio $\tau = \frac{T_p}{T}$ of a nozzle which relation is independent of the advance coefficient J or of the screw considered.

The experimentally obtained relations between C_T and τ for the nozzles No. (19), (26), (30), (31) and (32), in combination with the various screws are given in Figure 5. The results confirm the above supposition.

The thrust coefficient C_T and the ratio τ between propeller thrust and total thrust are approximately calculated as a function of the angle θ between the nozzle profile and the propeller shaft line in section 2.1. The numerical results are also presented in Figure 5.

The agreement between the calculated relations of C_T and $\tau = \frac{T_P}{T}$ and those obtained by the tests is good in the neighbourhood of the design points of the various nozzles.

Inception lines for bubble cavitation at the exterior surface of the nozzles are presented in Figure 26.
A comparison between the inception lines of the various nozzles shows that for equal thrust coefficients C_T, the inception of cavitation shifts to higher σ_o at increasing negative loading on the duct or at correspondingly increasing ratio $\tau = \frac{T_P}{T}$.
The numerically obtained maximum cavitation numbers are also presented in Figure 26 for the various nozzles.
The calculated cavitation numbers show the same tendency as the measured inception lines.
The differences between the calculated and the measured cavitation numbers may be explained by the lack of exact data on cavitation inception.

Thus far, no remarks were made on the cavitation characteristics of the screw series considered. The screws were designed in combination with nozzle (19). The pitch distribution depends on the nozzle induced velocities at the propeller plane and on the radial load distribution of the screw. The distribution of the nozzle induced velocities at the propeller plane is rather different for the nozzles (30), (31), (32), and (19). Consequently the screws have bad characteristics with respect to cavitation inception if these are tested in combination with the nozzles (30), (31) and (32). Therefore no cavitation observations of the screws are reported.

6. Conclusions.

1. The ideal efficiency η_i of a ducted propeller system decreases with increasing ratio τ between propeller thrust and total thrust. However, it is noted that for lightly loaded systems, the decrease in efficiency is small.

2. Especially in the case of decelerating nozzles, it is recommendable to choose thin nozzle profiles due to the unfavourable effect of thickness of the nozzle on efficiency.

3. The mean static pressure at the propeller plane increases with increasing ratio τ between propeller thrust and total thrust. "Ram pressures" at the propeller plane are only built up if τ becomes larger than 1.0, consequently a negative thrust is produced by the duct in that case.

4. The method of calculation for the performance characteristics of a nozzle propeller system developed in this study gives results which compare favourably with the experimental results. It is recommended for a possible extension of the research to determine in the first instance the effects of the various design parameters ($\frac{d}{D}$; $\frac{c}{D}$ and so on) on the performance characteristics, with the aid of the theory.

5. The application of pre-turning vanes becomes important if the gain in rotational efficiency is larger than the efficiency loss due to friction of the vanes. This will be the case if the ducted propeller system is heavily loaded and the angular velocity of the propeller is relatively small. The losses due to the rotation of the fluid can be isolated with the aid of the theory. Hence, the losses due to rotation and the loss due to the friction of pre-turning vanes may be easily compared.

6. The static pressure at the exterior surface of the nozzle decreases if the static pressure at the propeller plane increases. However, the reduction in static pressure at the exterior nozzle surface is small in comparison with the gain in pressure at the propeller plane.

7. It follows from theory and experiment that there exists a fixed relation between the thrust coefficient C_T and the ratio $\tau = \frac{T_e}{T}$ of a nozzle, which relation depends neither on the advance coefficient J nor on the screw considered. This fact gives in an easy way information on the range of application of the nozzle.

References.

[1] Horn, F.: "Beitrag zur Theorie ummantelter Schiffsschrauben". Jahrbuch der Schiffbautechnischen Gesellschaft, Band 41 (1940).

[2] Dickmann, H.E. and Weissinger, J.: "Beitrag zur Theorie optimaler Düsenschrauben (Kortdüsen)" Jahrbuch der Schiffbautechnischen Gesellschaft, Band 49 (1955).

[3] Weissinger, J.: "The influence of profile thickness on ring airfoils in steady, incompressible flow". ARDC, AF 61(514)-904 (1957).

[4] van Manen, J.D.: "Open-water test series with propellers in nozzles." International Shipbuilding Progress, Vol. 1-no. 2 (1954).

[5] van Manen, J.D.: "Recent research on propellers in nozzles". International Shipbuilding Progress, Vol. 4-no. 36 (1957).

[6] Morgan, W.B.: "A theory of the ducted propeller with a finite number of blades." Report of the University of California Series No. 82, Issue no. 19 (1961).

[7] Chen, C.F.: "Feasibility study of supercavitating propellers in Kort nozzles - Phase 1 and Phase 2". Hydronautics Inc. Technical Report 005-3, Technical Report 005-4 (1961).

[8] Bohyun Yim; Chen C.F.:
"The flow field of an infinitely bladed propeller with radially non-uniform loading".
Hydronautics Inc. Technical Report 005-2.

Wageningen, May 1965.

Prof.Dr.Ir. J.D. van Manen
Principal Investigator.

x/L	nozzle 30 S(x)/L	nozzle 31 S(x)/L	nozzle 32 S(x)/L
0	+ 0.0112	- 0.0073	- 0.0232
0.083	+ 0.0130	+ 0.0008	- 0.0096
0.167	+ 0.0139	+ 0.0067	+ 0.0006
0.250	+ 0.0128	+ 0.0093	+ 0.0057
0.333	+ 0.0102	+ 0.0091	+ 0.0085
0.417	+ 0.0059	+ 0.0060	+ 0.0063
0.500	+ 0	+ 0	+ 0
0.583	- 0.0081	- 0.0096	- 0.0112
0.667	- 0.0186	- 0.0229	- 0.0276
0.750	- 0.0316	- 0.0404	- 0.0496
0.833	- 0.0476	- 0.0622	- 0.0773
0.917	- 0.0661	- 0.0881	- 0.1106
1.000	- 0.0874	- 0.1182	- 0.1498

Table 1

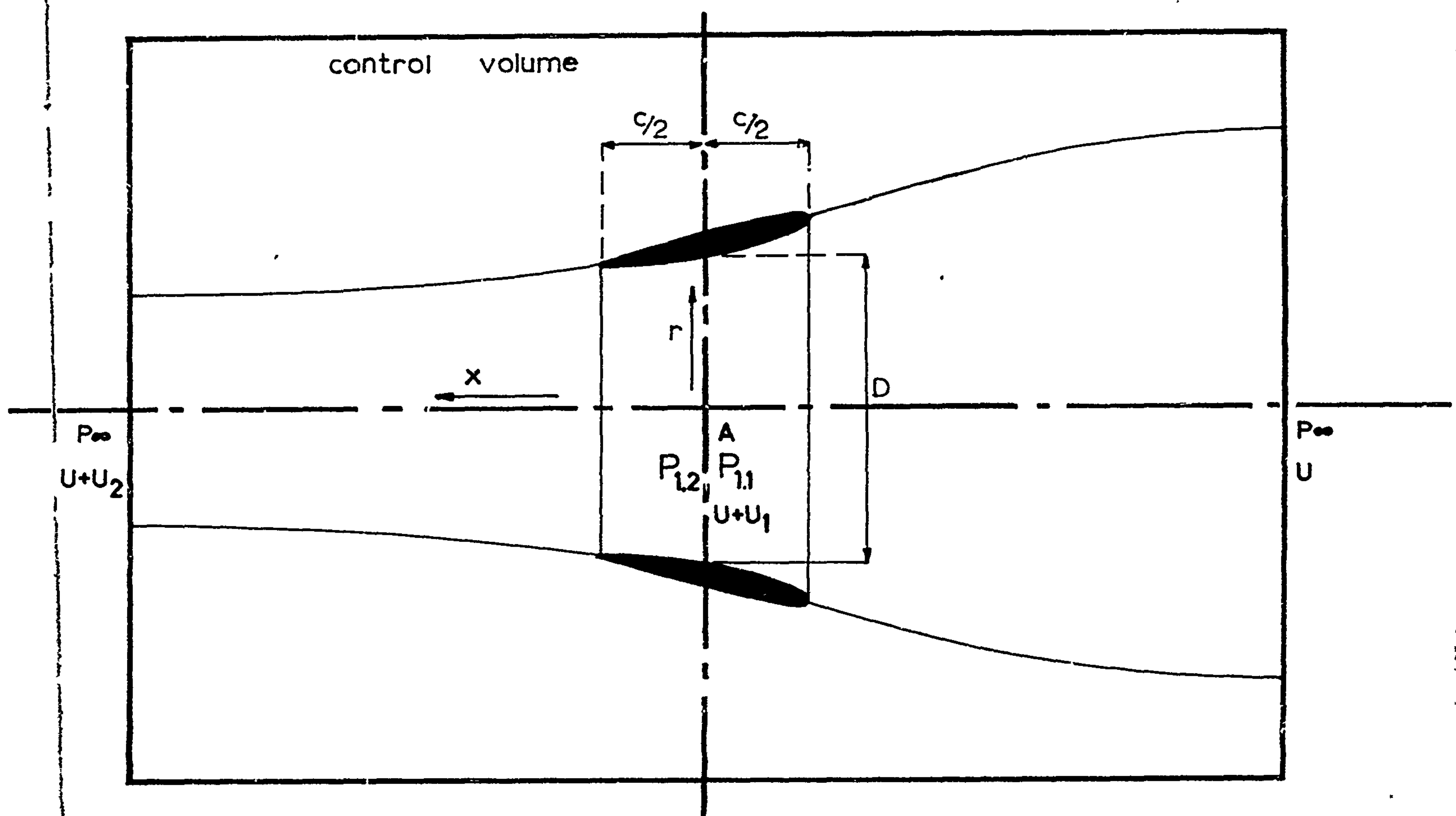

Figure 1. Control volume used for momentum consideration

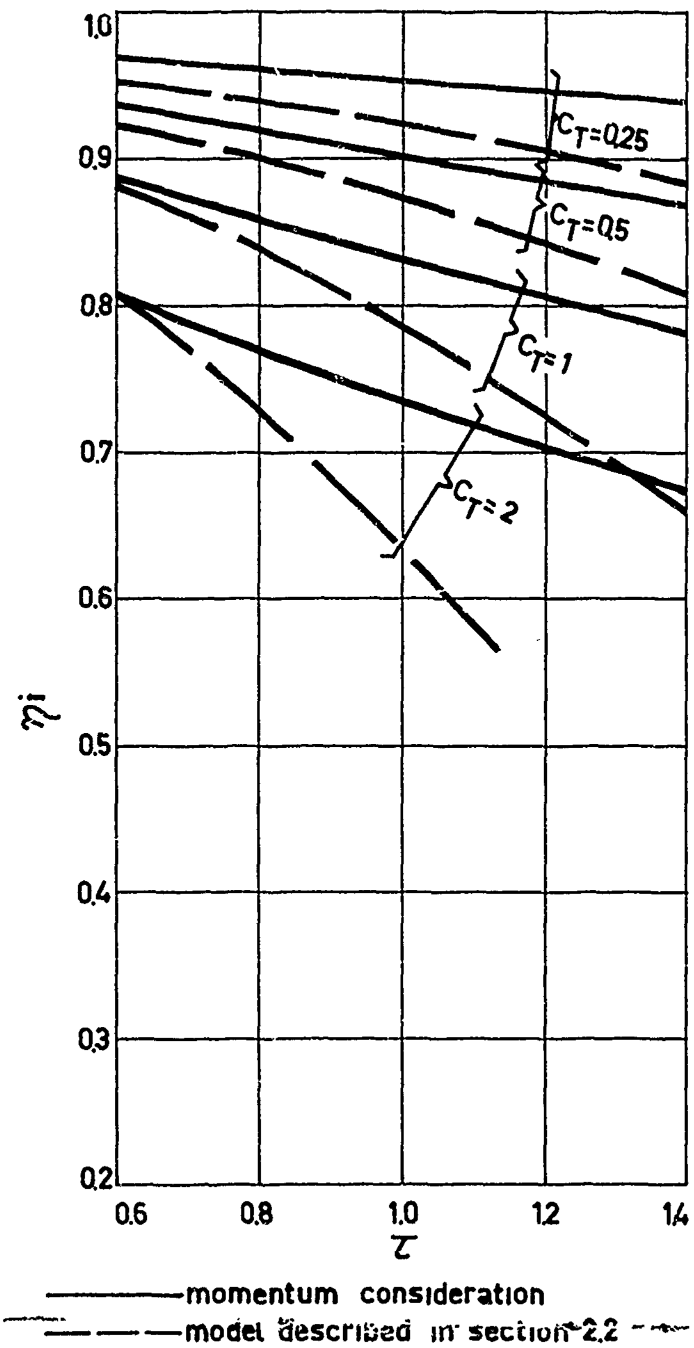

Figure 2. Ideal efficiency of propeller nozzle system.

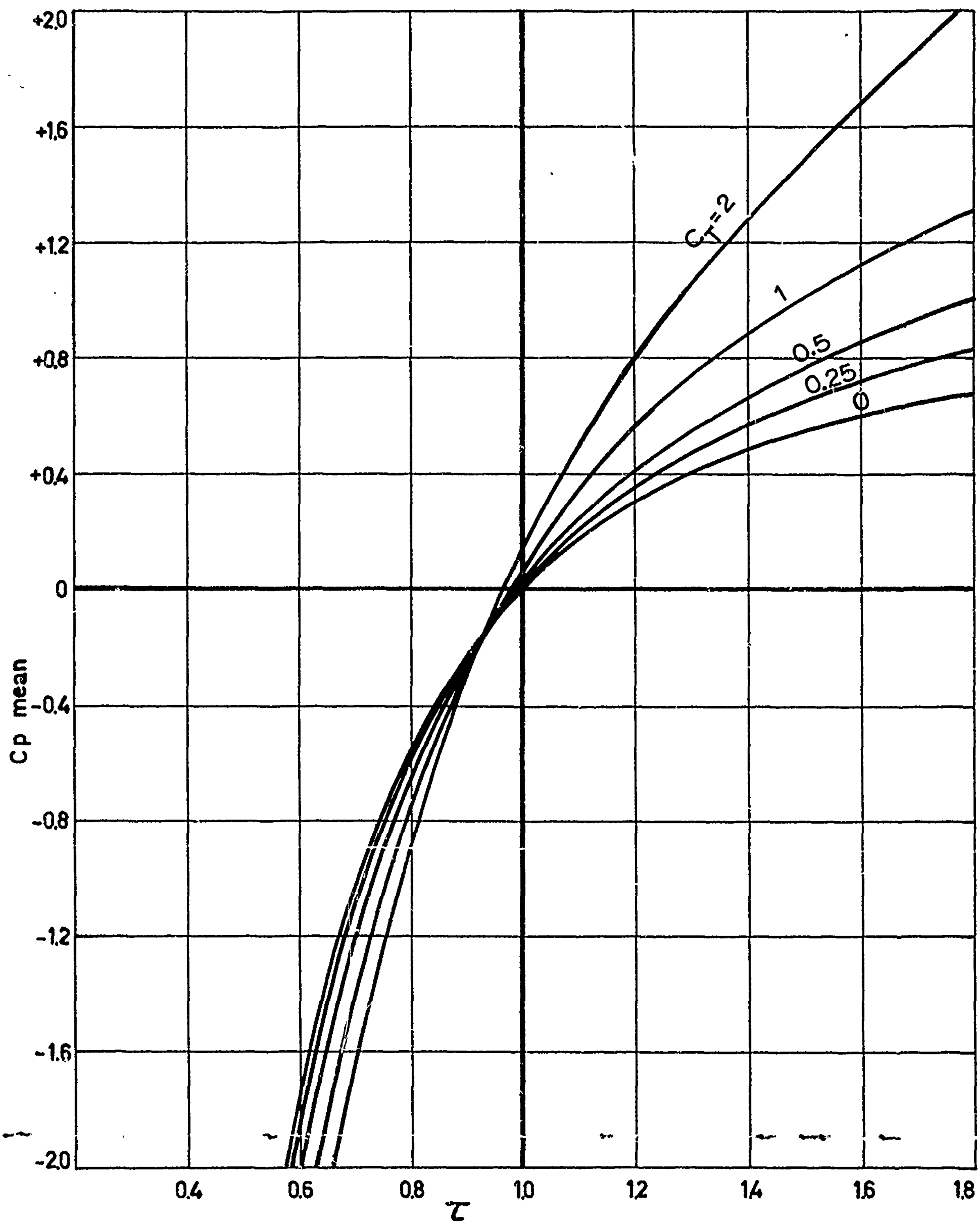

Figure 3. Mean static pressure at propeller plane of propeller nozzle system.

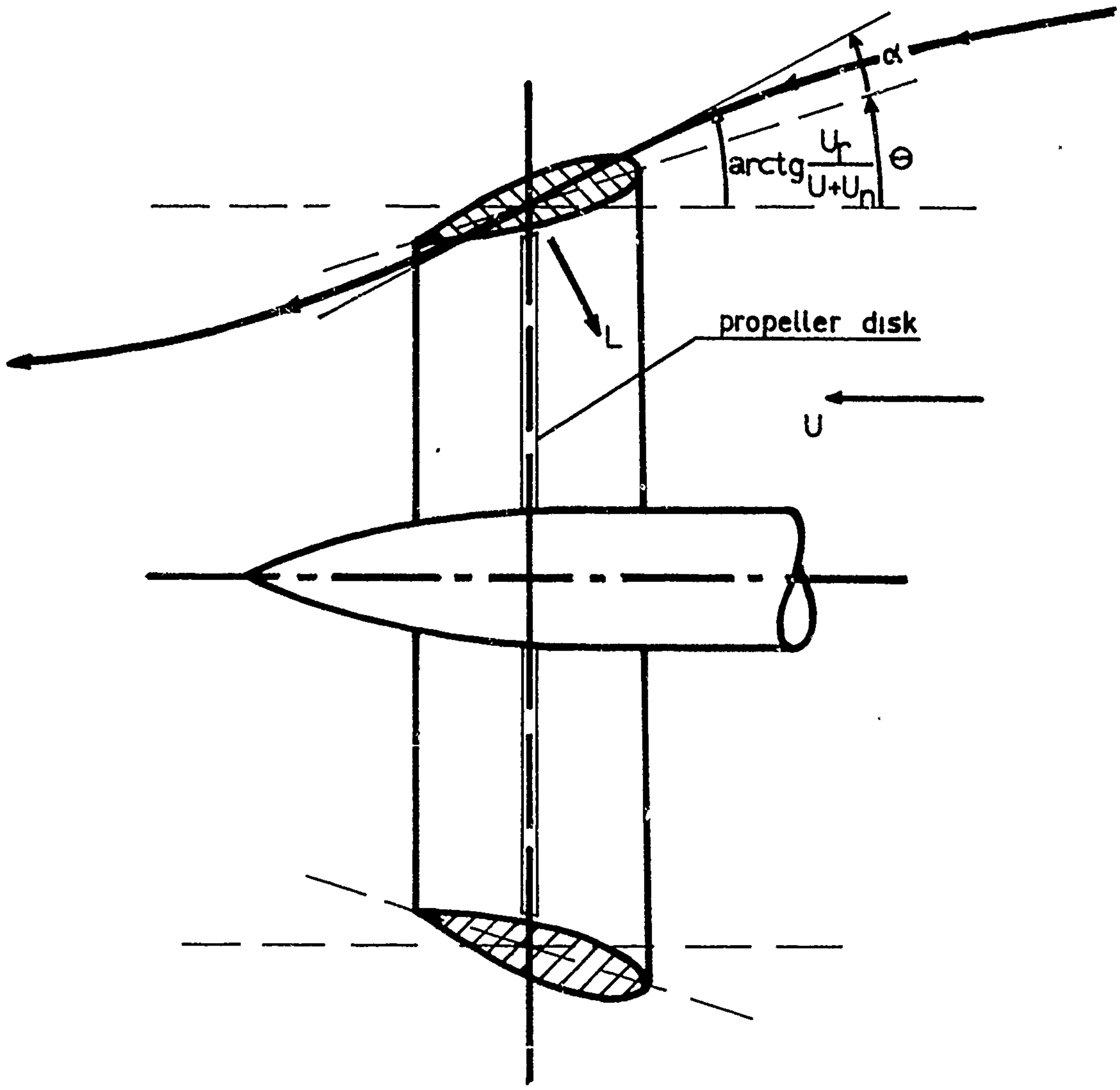

Figure 4. Schematic drawing of angle of attack of nozzle profile.

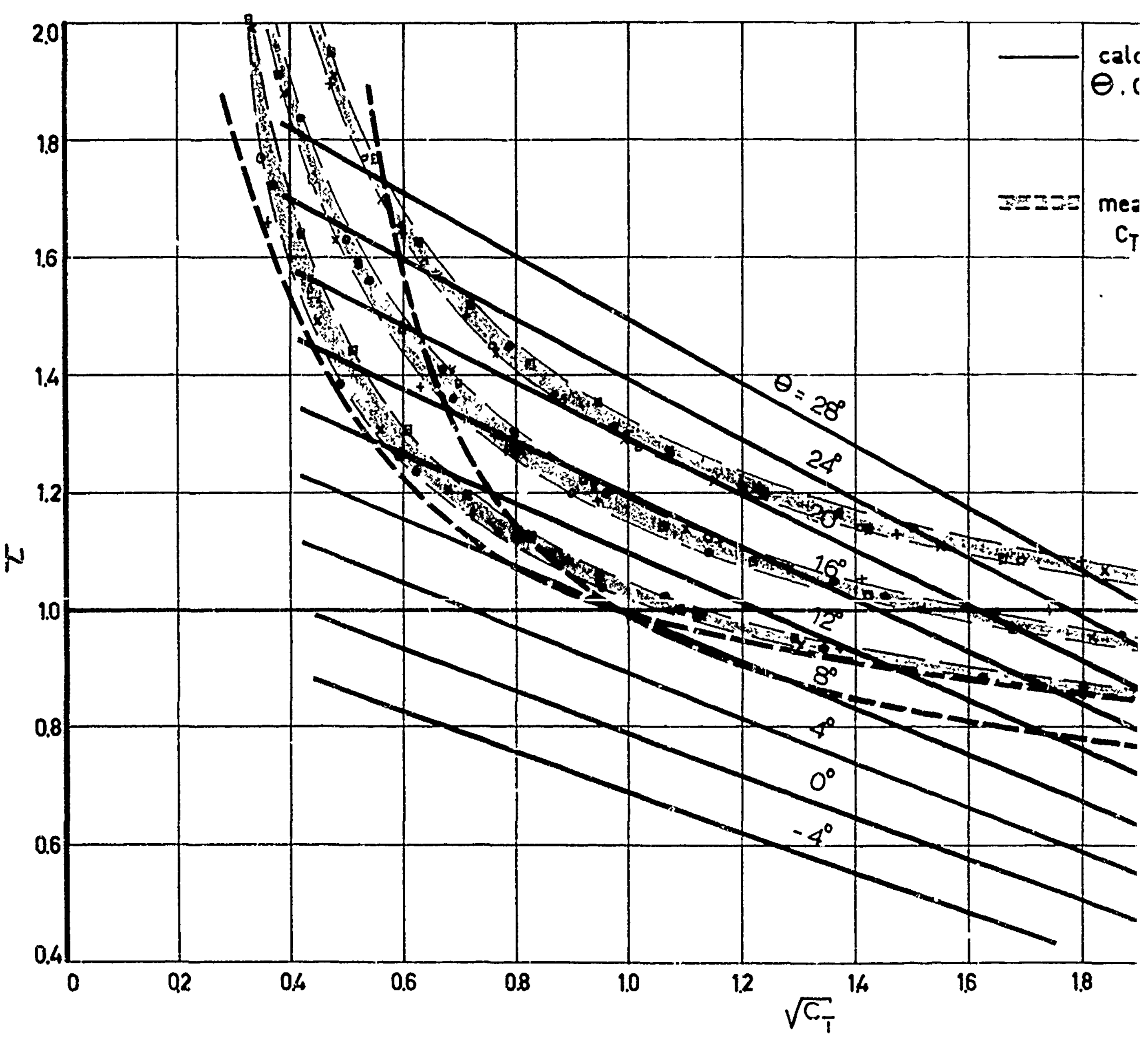

Figure 5. Estimated angle between nozzle profile and shaft line. Experimentally obtained relation between thrust coefficient C_T a between propeller thrust and total thrust of nozzle

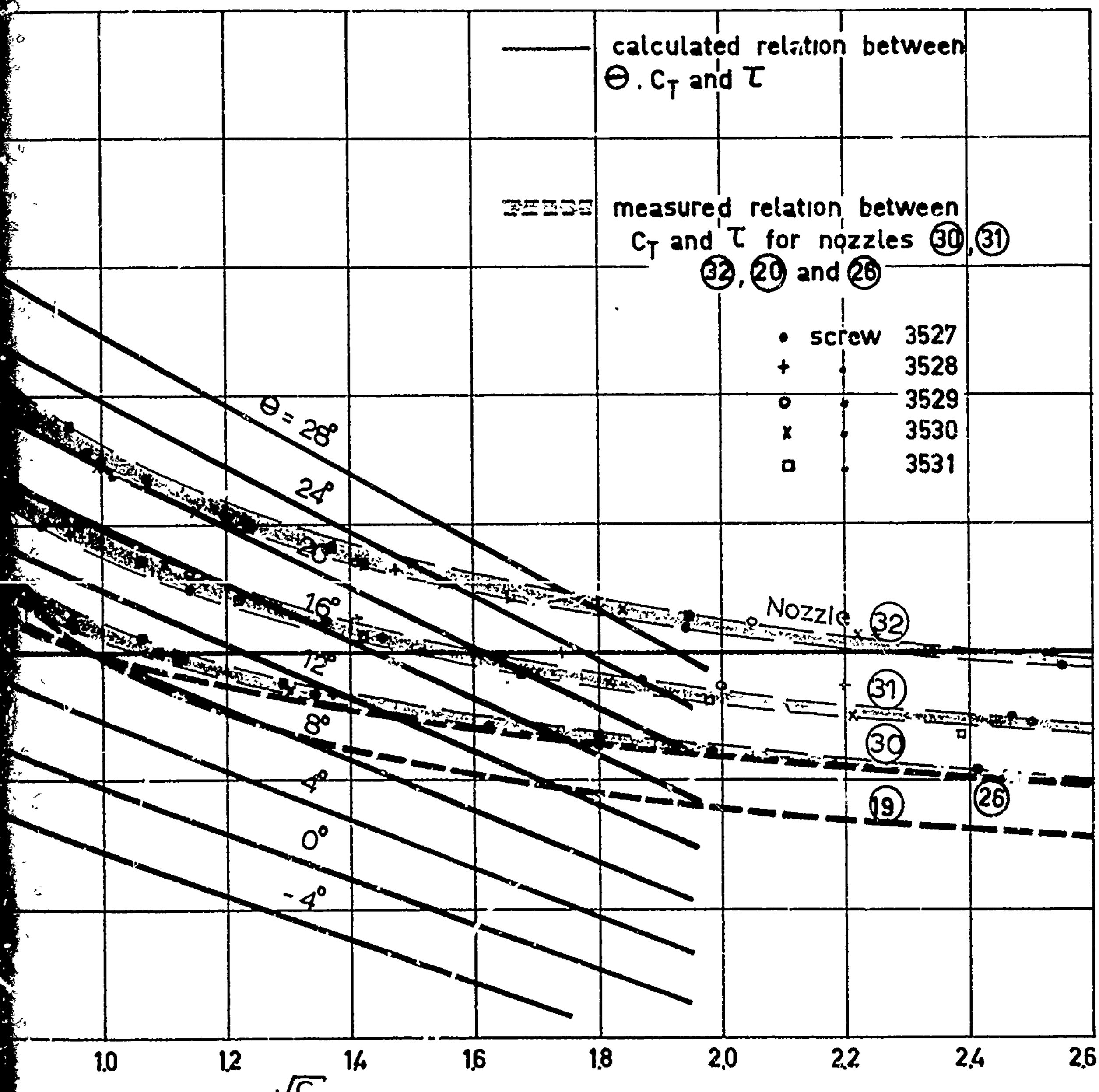

...e between nozzle profile and shaft line.
... obtained relation between thrust coefficient C_T and ratio τ
...ller thrust and total thrust of nozzle

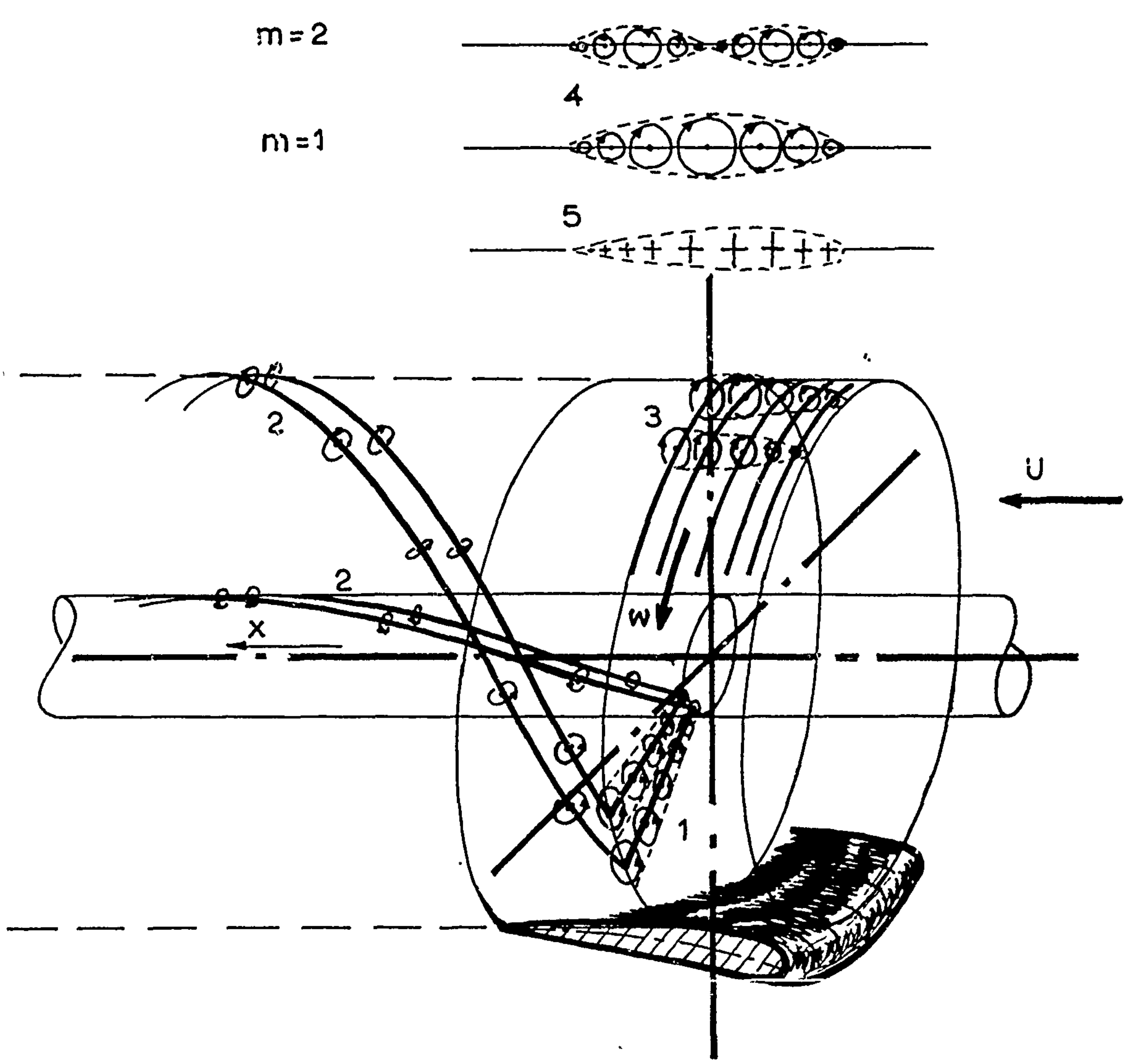

1. Screw disk with bound vortices.
2. Helical trailing vortices.
3. Discontinuous ring vortex distribution along nozzle.
4. Continuous ring vortex distribution along nozzle $[\gamma(x)=\gamma_m \sin m\theta]$.
5. Source and sink distribution along nozzle.

Figure 6. Mathematical model of ducted propeller with infinite number of blades.

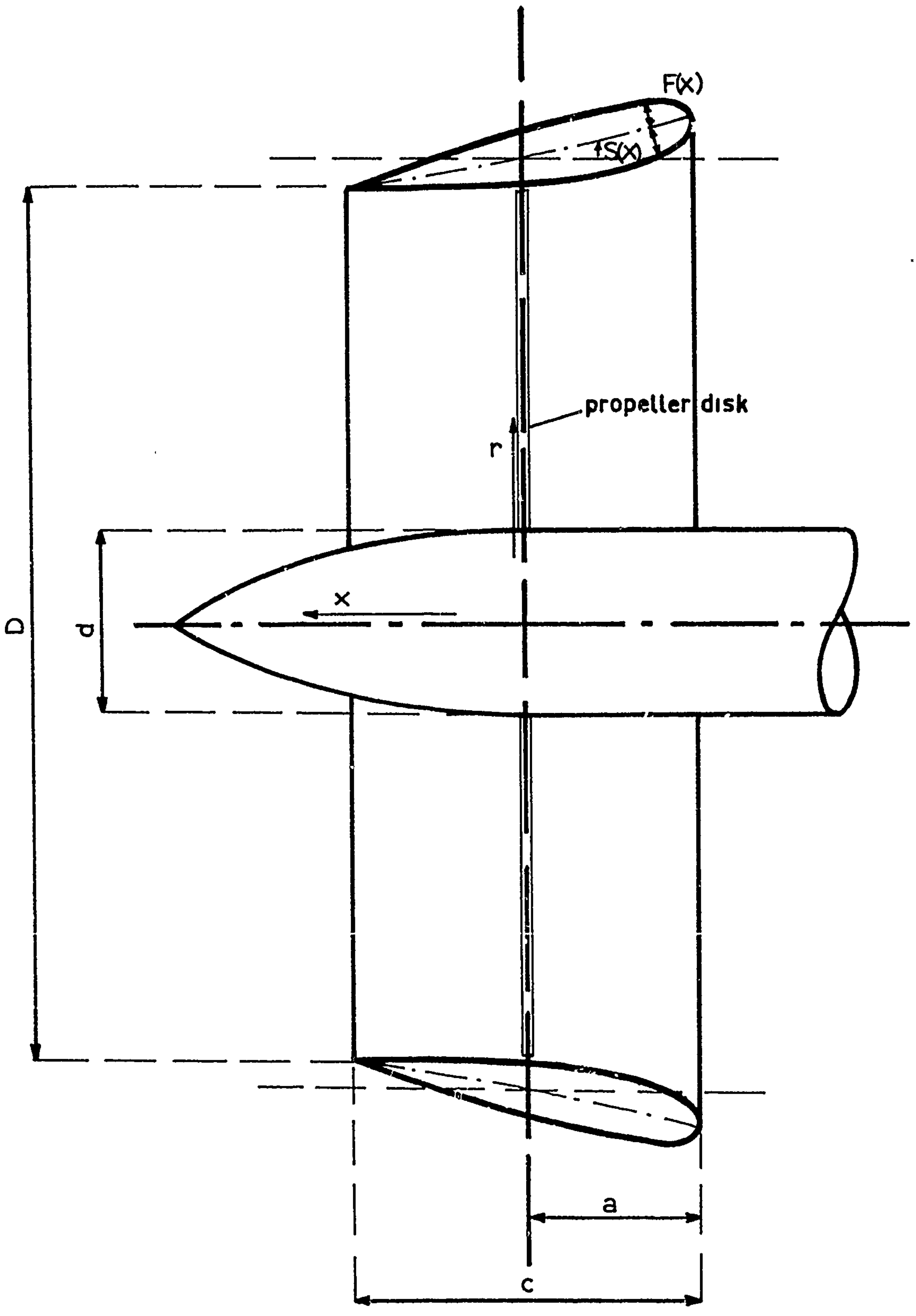

Figure 7. Ducted propeller.

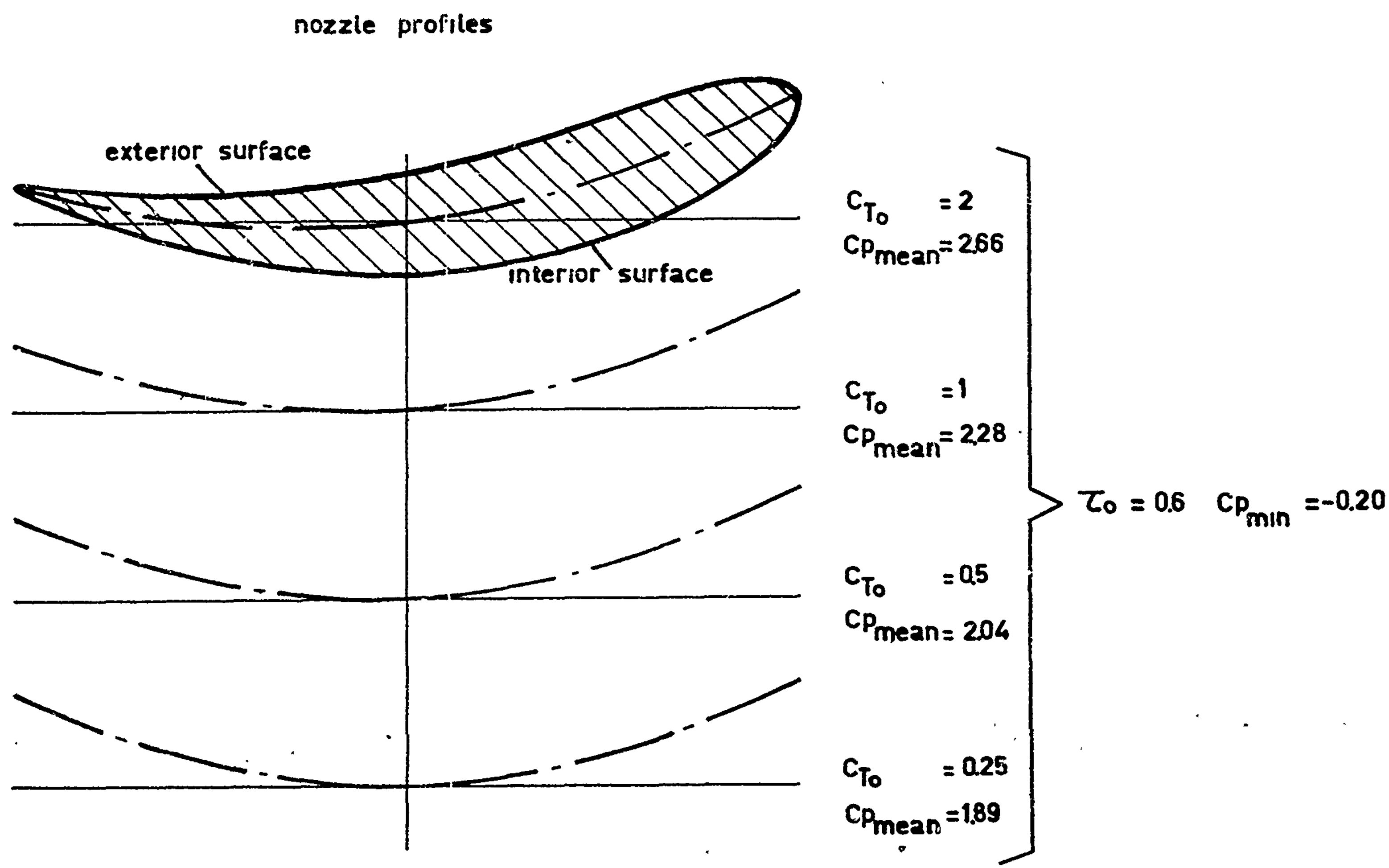
nozzle profiles
exterior surface
interior surface
$C_{T_o} = 2$
$Cp_{mean} = 2.66$
$C_{T_o} = 1$
$Cp_{mean} = 2.28$
$C_{T_o} = 0.5$
$Cp_{mean} = 2.04$
$C_{T_o} = 0.25$
$Cp_{mean} = 1.89$
$\tau_o = 0.6 \quad Cp_{min} = -0.20$

4.1

$C_{To} = 0.25$
$C_{P_{mean}} = 1.89$

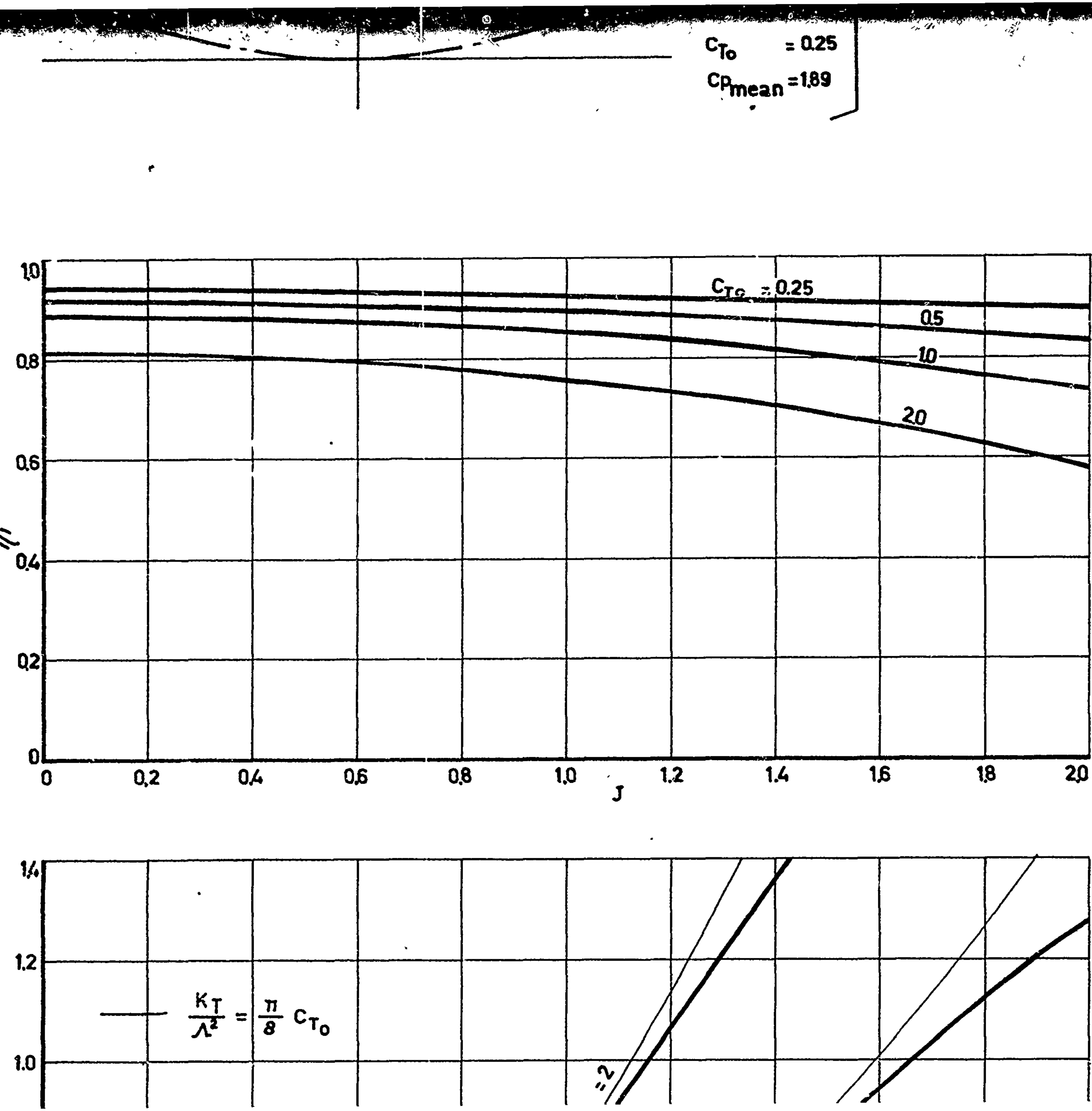

34.2

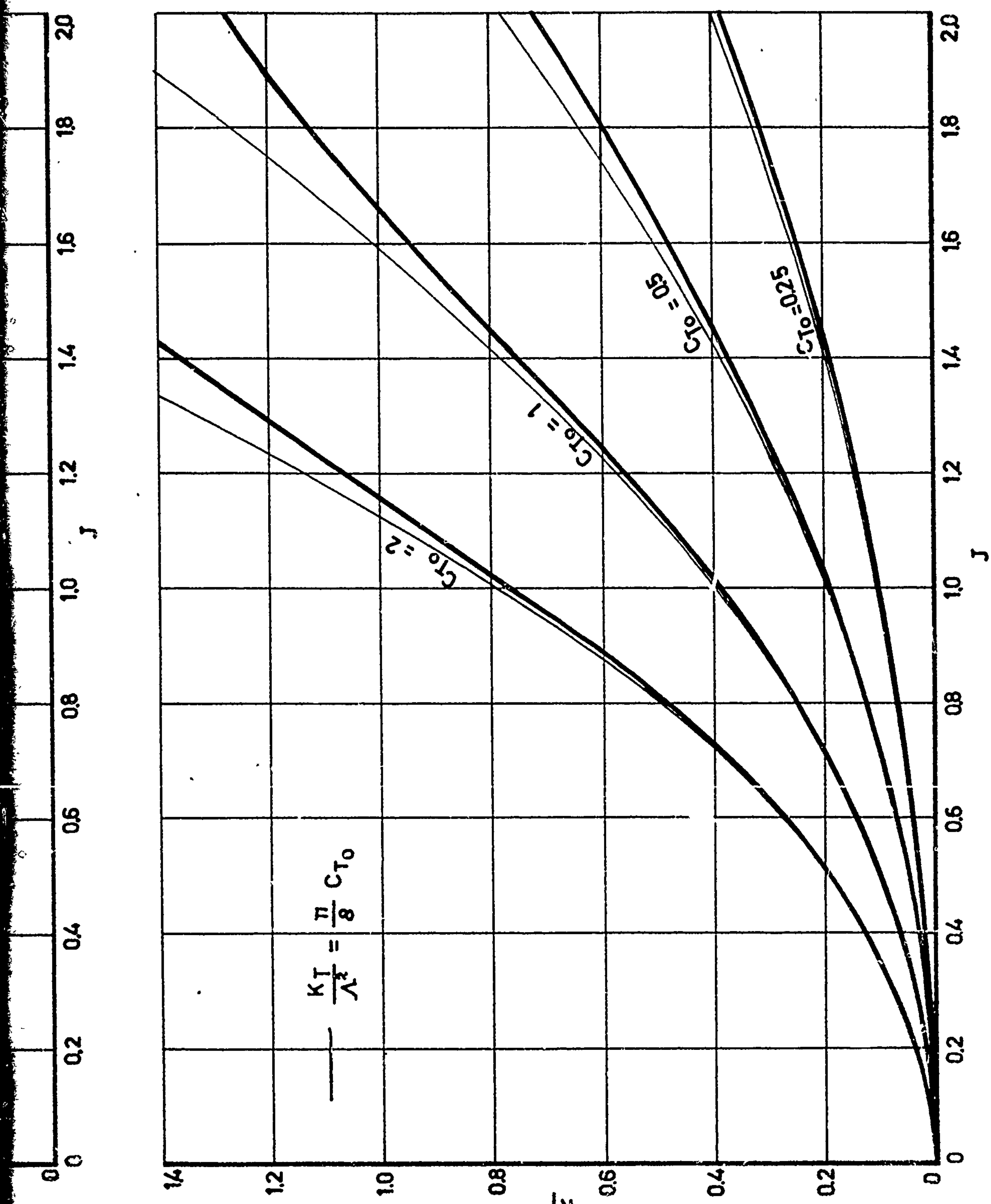

Figure 8. Characteristics of a systematic series of nozzle shapes.

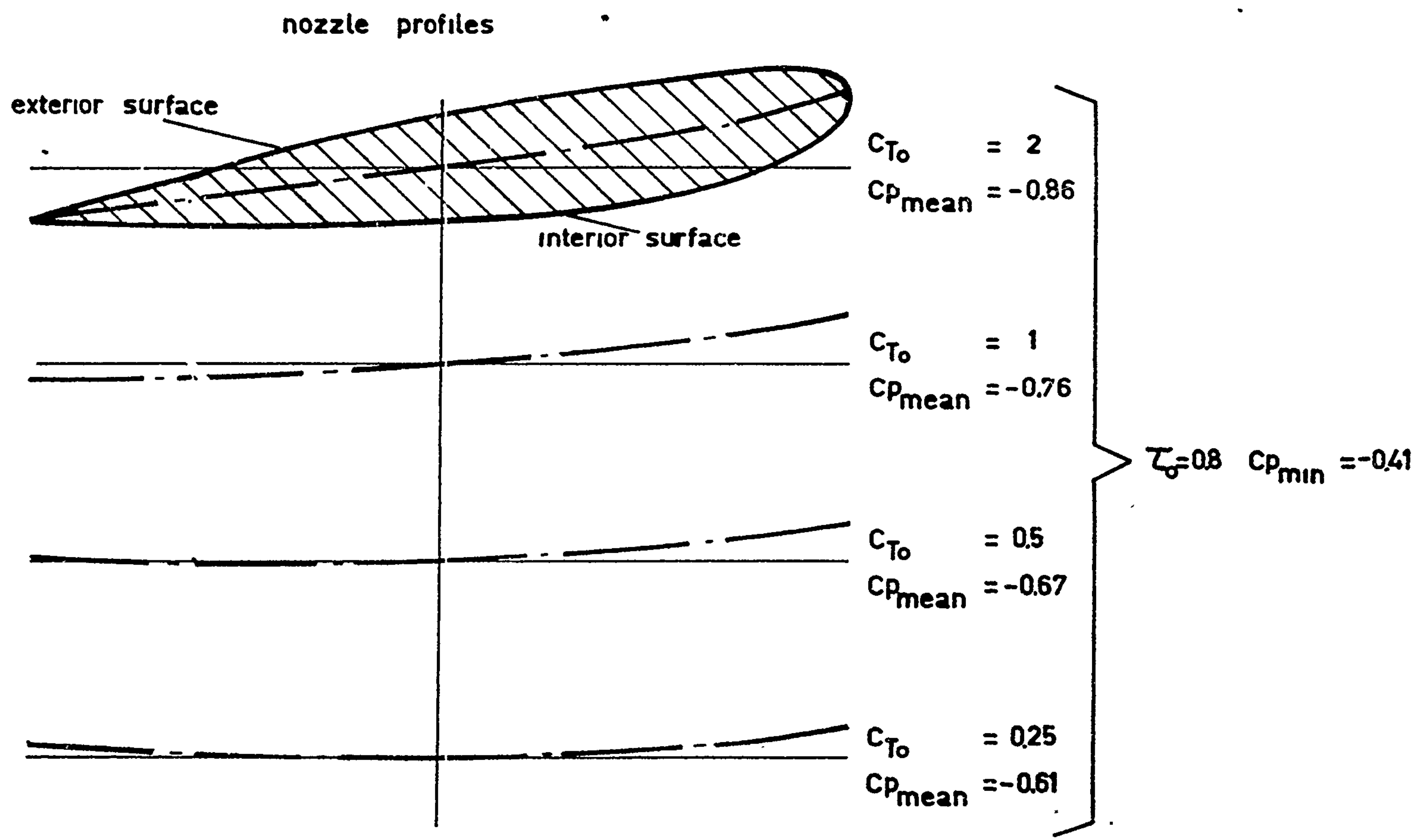
nozzle profiles
exterior surface
interior surface
C_{T_o} = 2
Cp_{mean} = -0.86
C_{T_o} = 1
Cp_{mean} = -0.76
C_{T_o} = 0.5
Cp_{mean} = -0.67
C_{T_o} = 0.25
Cp_{mean} = -0.61
τ_o = 0.8 Cp_{min} = -0.41

35.1

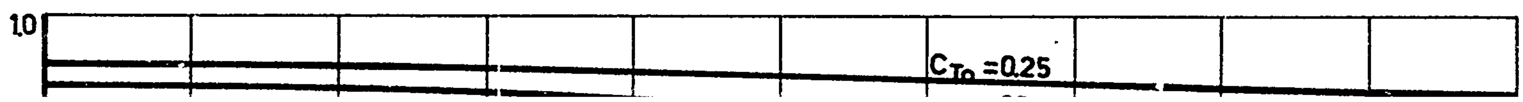
1.0
C_{T_o} = 0.25

$Cp_{mean} = -0.61$

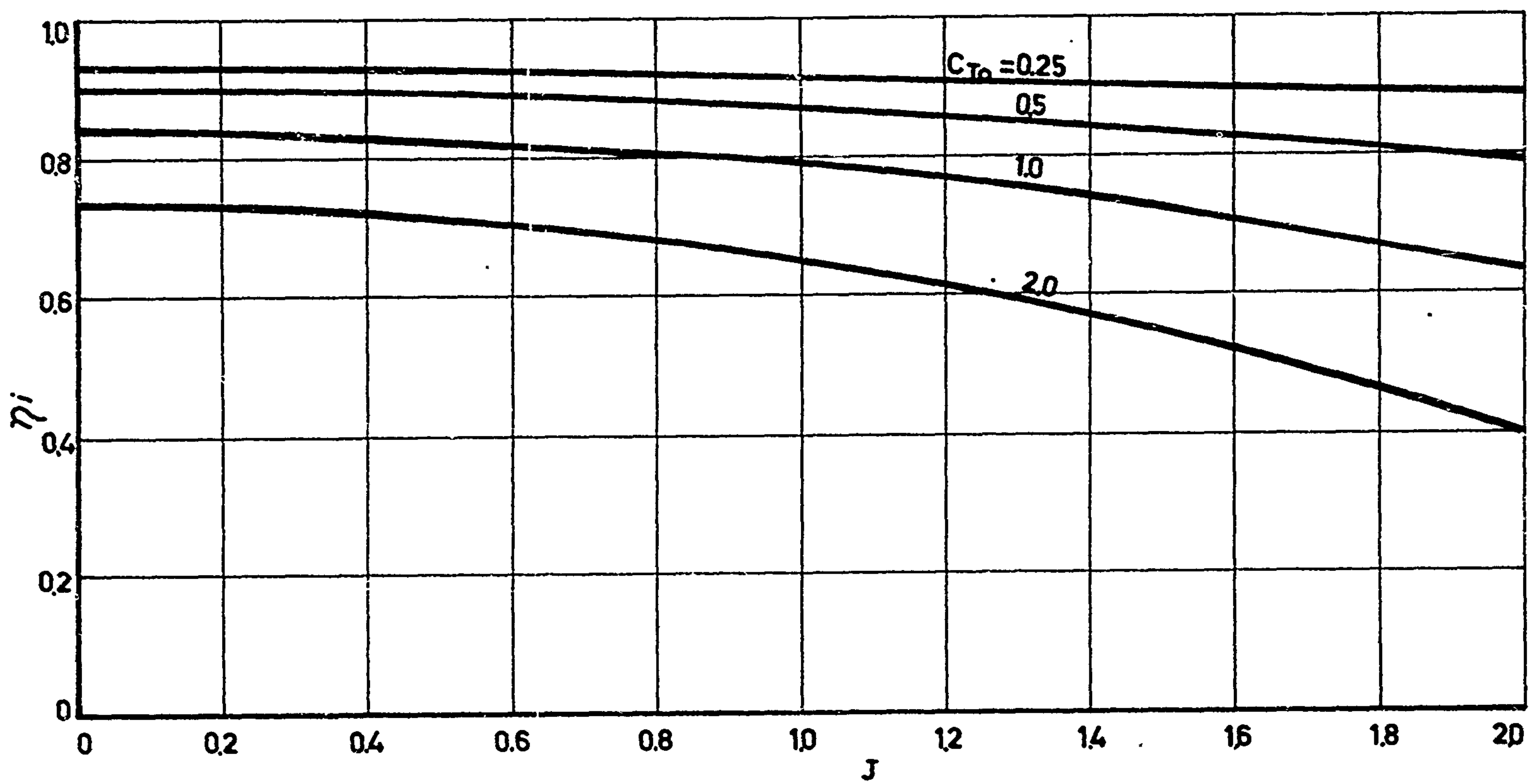

35.2

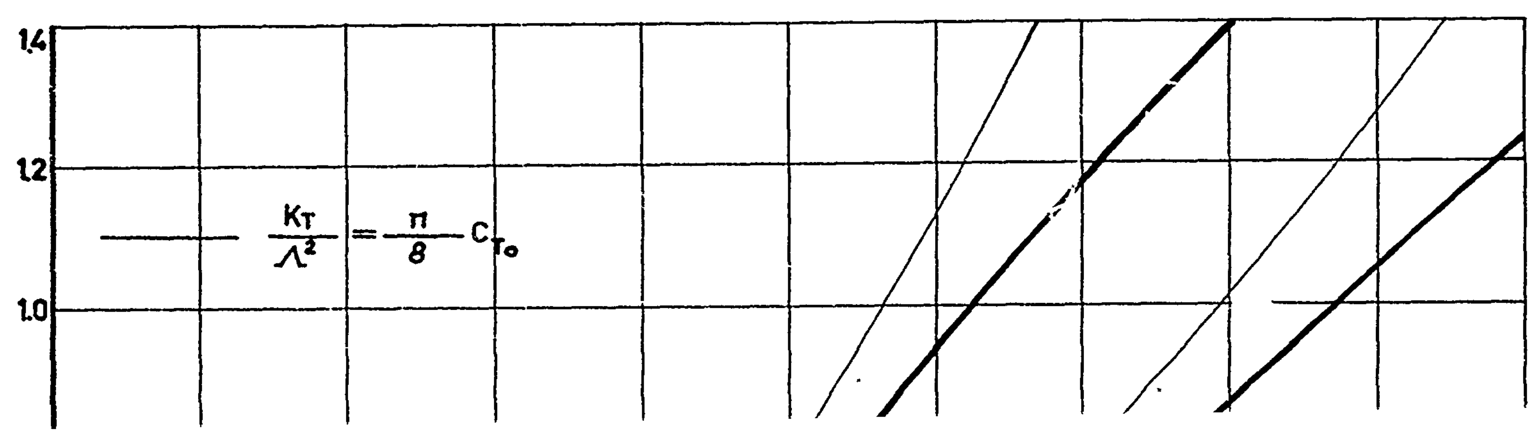

NEDERLANDSCH SCHEEP
PROEFSTATION

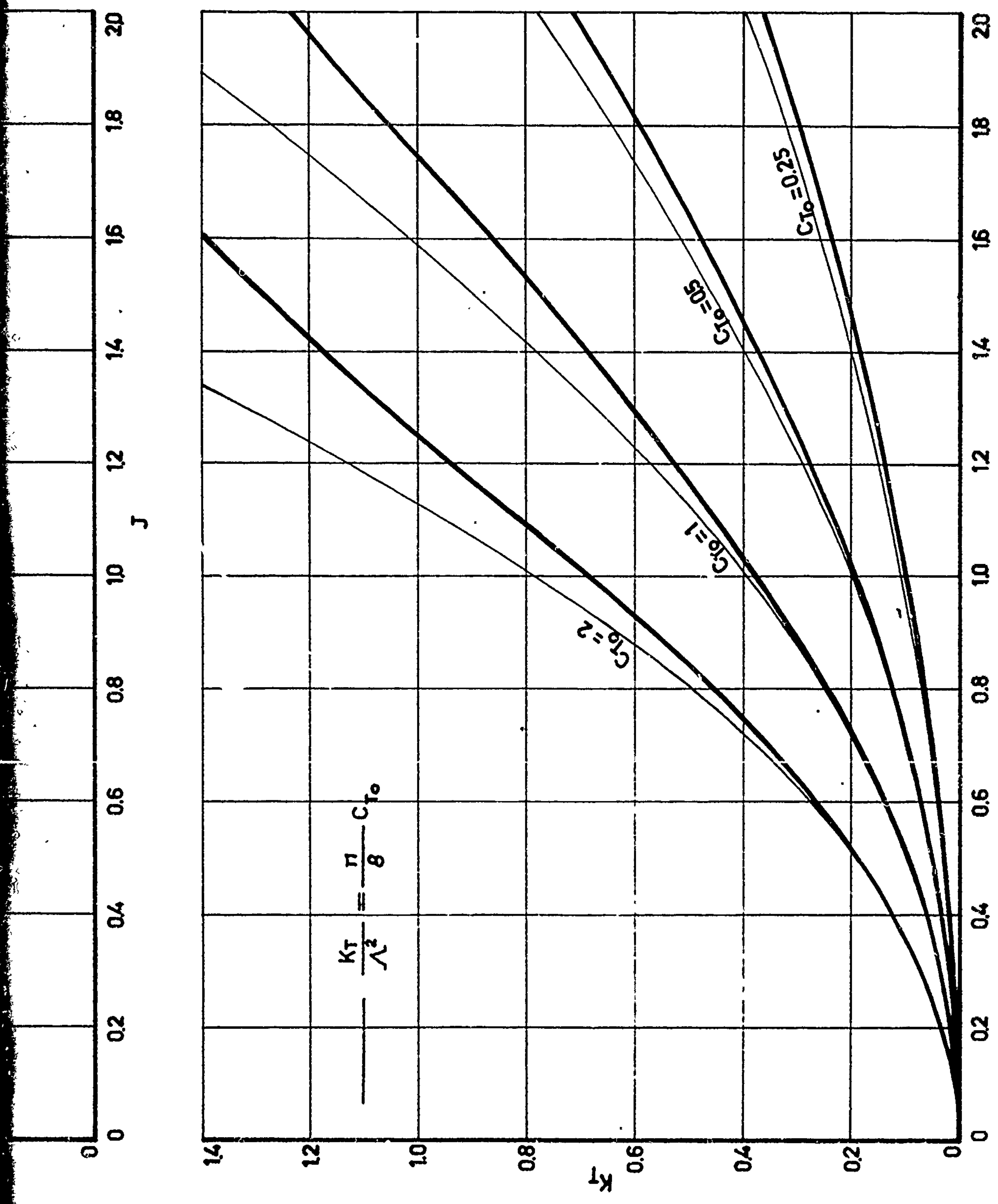

Figure 9. Characteristics of a systematic series of nozzle shapes.

5.2

35.3

36.1

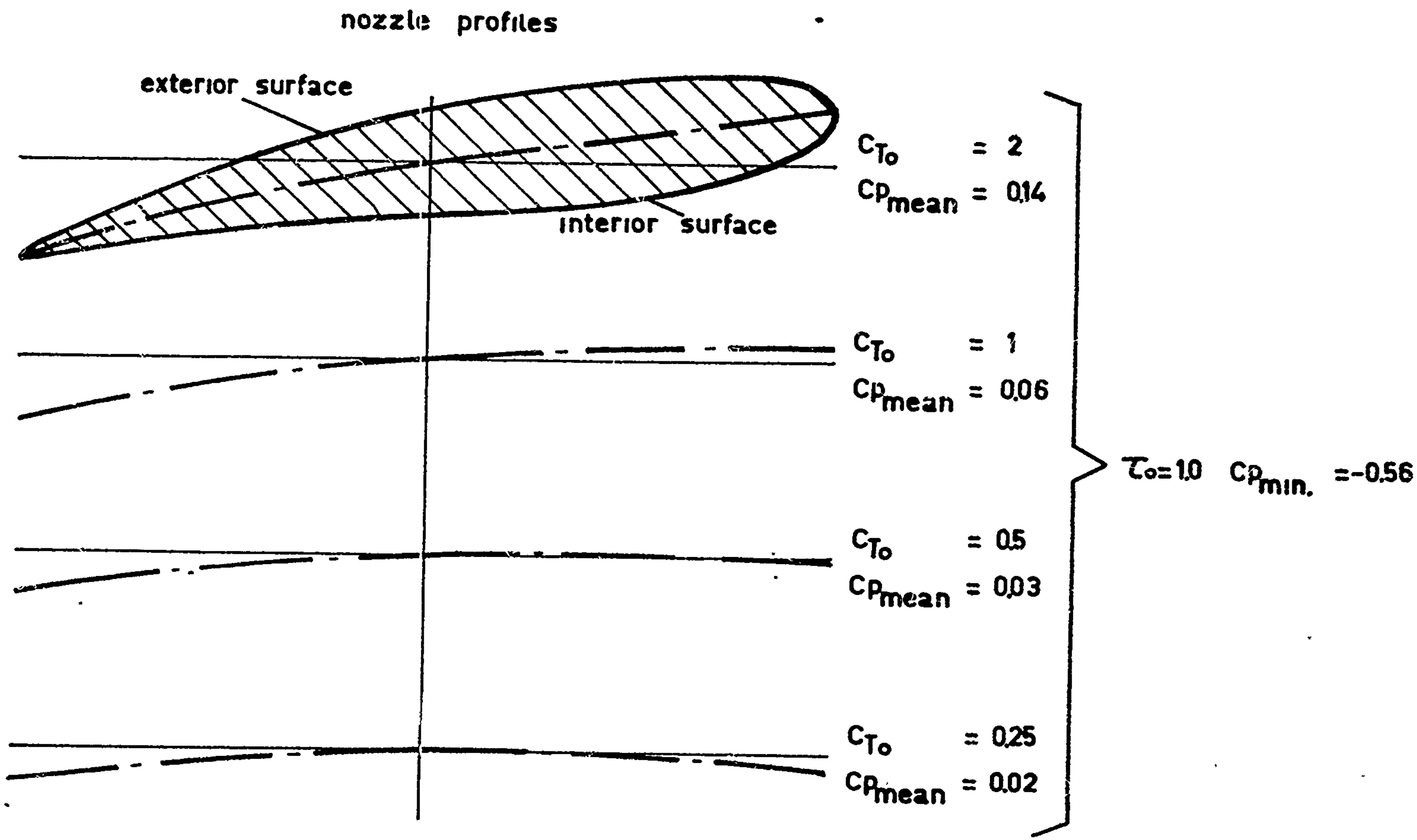
nozzle profiles
exterior surface
interior surface
C_{To} = 2
Cp_{mean} = 0.14
C_{To} = 1
Cp_{mean} = 0.06
C_{To} = 0.5
Cp_{mean} = 0.03
C_{To} = 0.25
Cp_{mean} = 0.02
τ_o = 1.0 $Cp_{min.}$ = -0.56

36.2

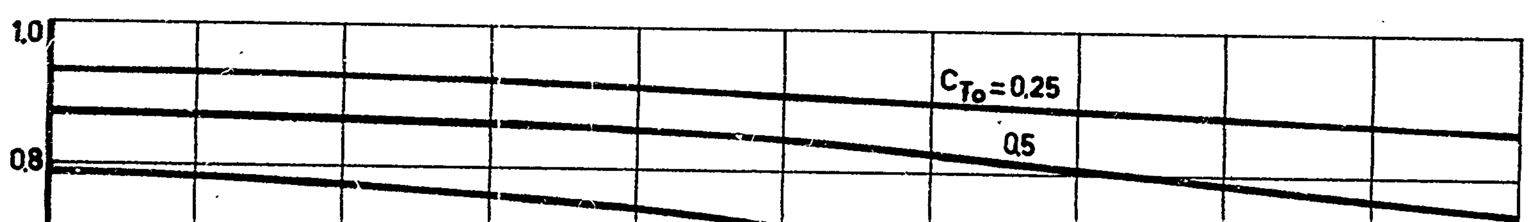
1.0
0.8
C_{To} = 0.25
0.5

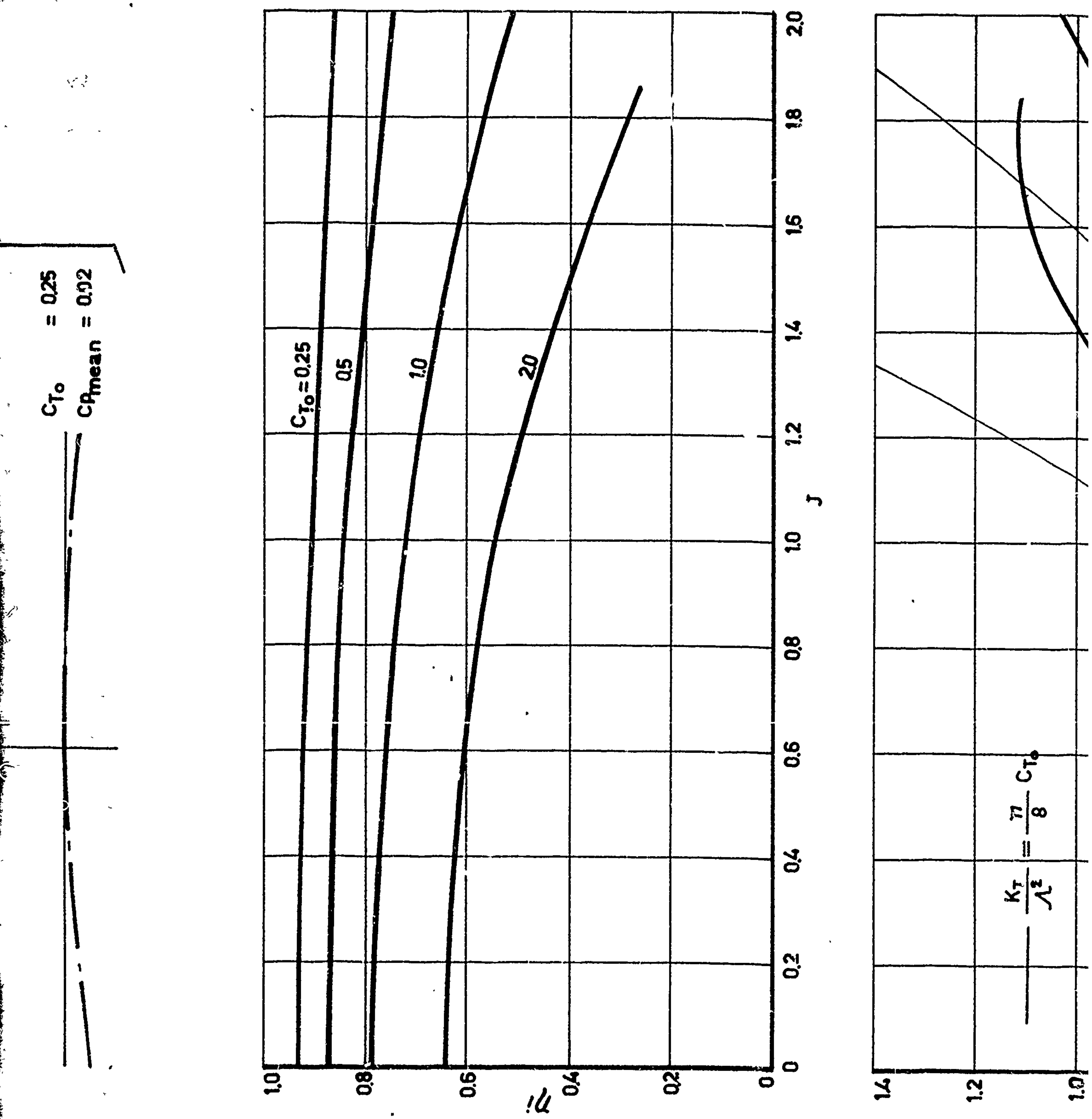
C_{To} = 0.25
$C_{P_{mean}}$ = 0.02
C_{To} = 0.25
0.5
1.0
2.0
J
η
0
0.2
0.4
0.6
0.8
1.0
1.2
1.4
1.6
1.8
2.0
$\frac{K_T}{\Lambda^2} = \frac{\pi}{8} C_{To}$

36.2.

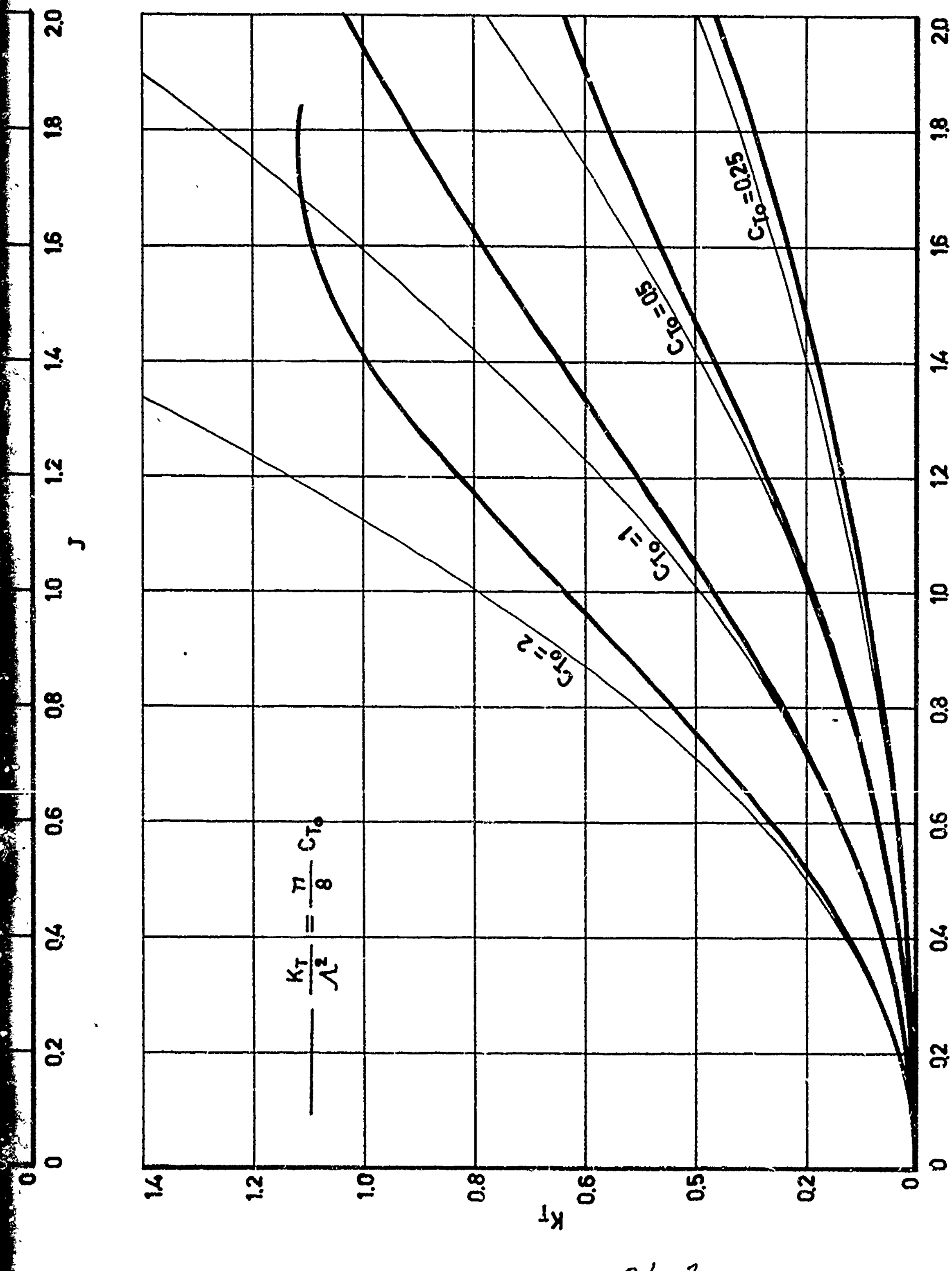

Figure 10. Characteristics of a systematic series of nozzle shapes.

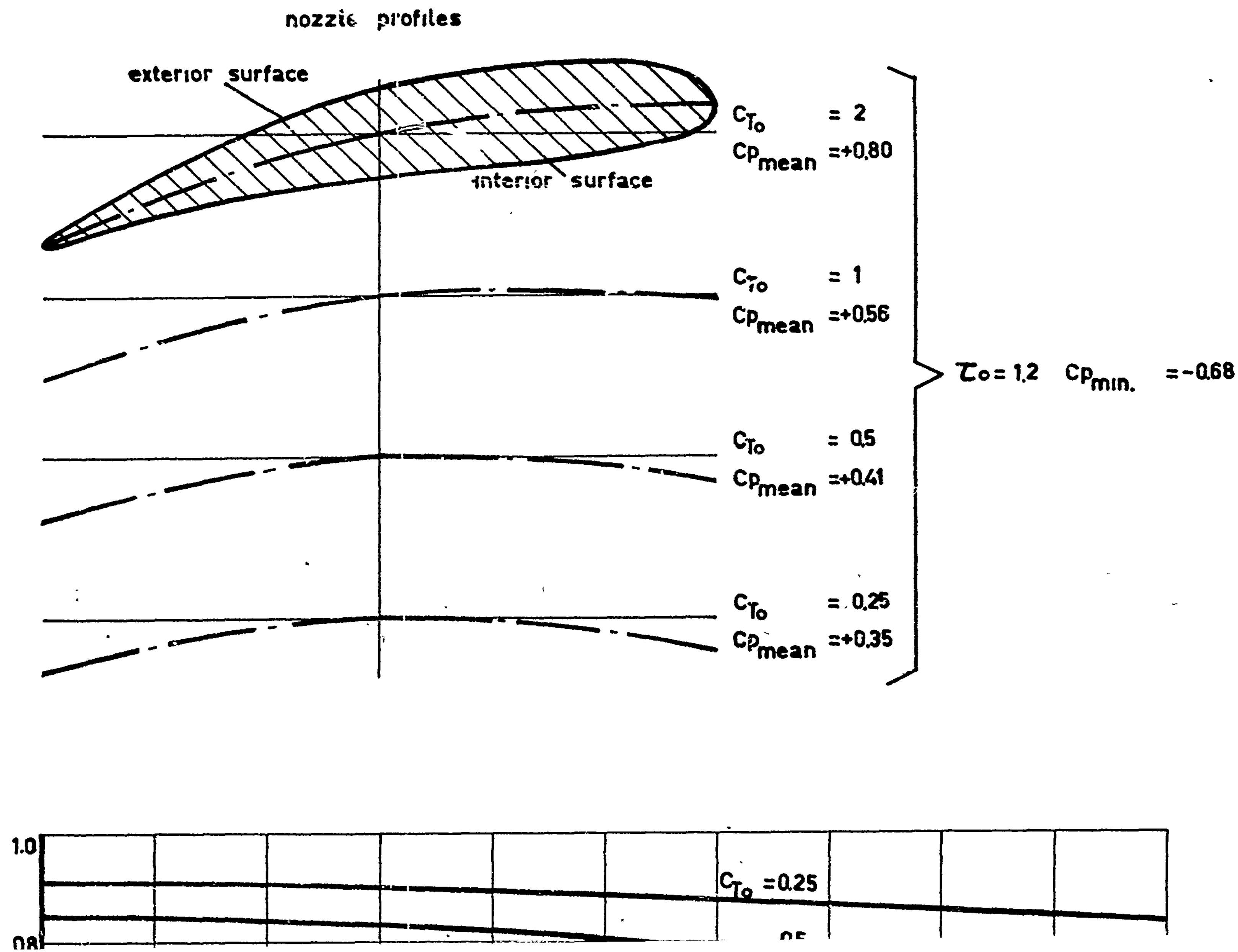

nozzle profiles
exterior surface
interior surface
C_{T_o} = 2
Cp_{mean} =+0,80
C_{T_o} = 1
Cp_{mean} =+0,56
C_{T_o} = 0,5
Cp_{mean} =+0,41
C_{T_o} = 0,25
Cp_{mean} =+0,35
τ_o = 1,2 $Cp_{min.}$ =-0,68
1.0
0.8
C_{T_o} =0.25

37.1

NEDERLANDSCH SCHEEPSBO[illegible]
PROEFSTATION WA[illegible]

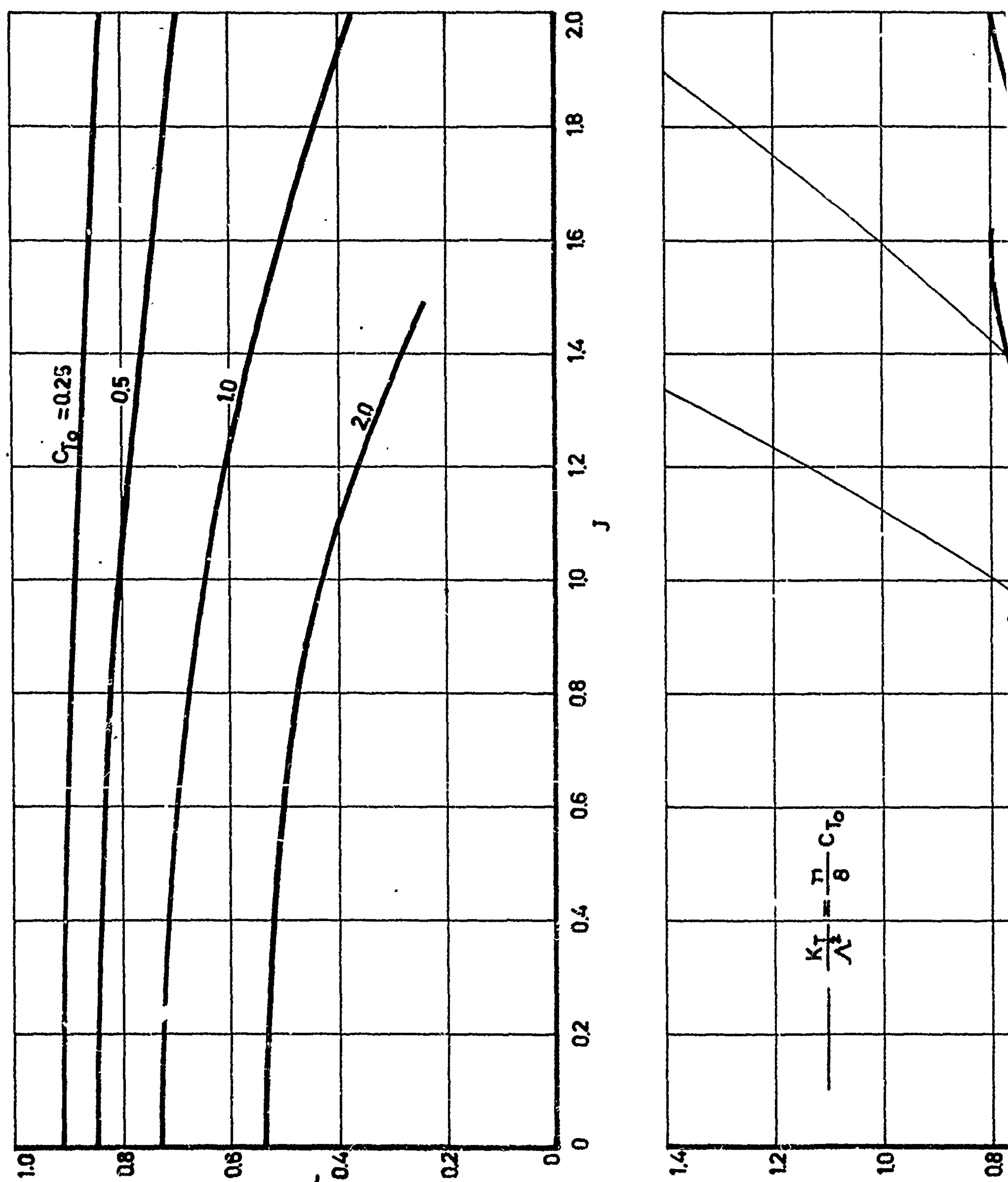

37.2

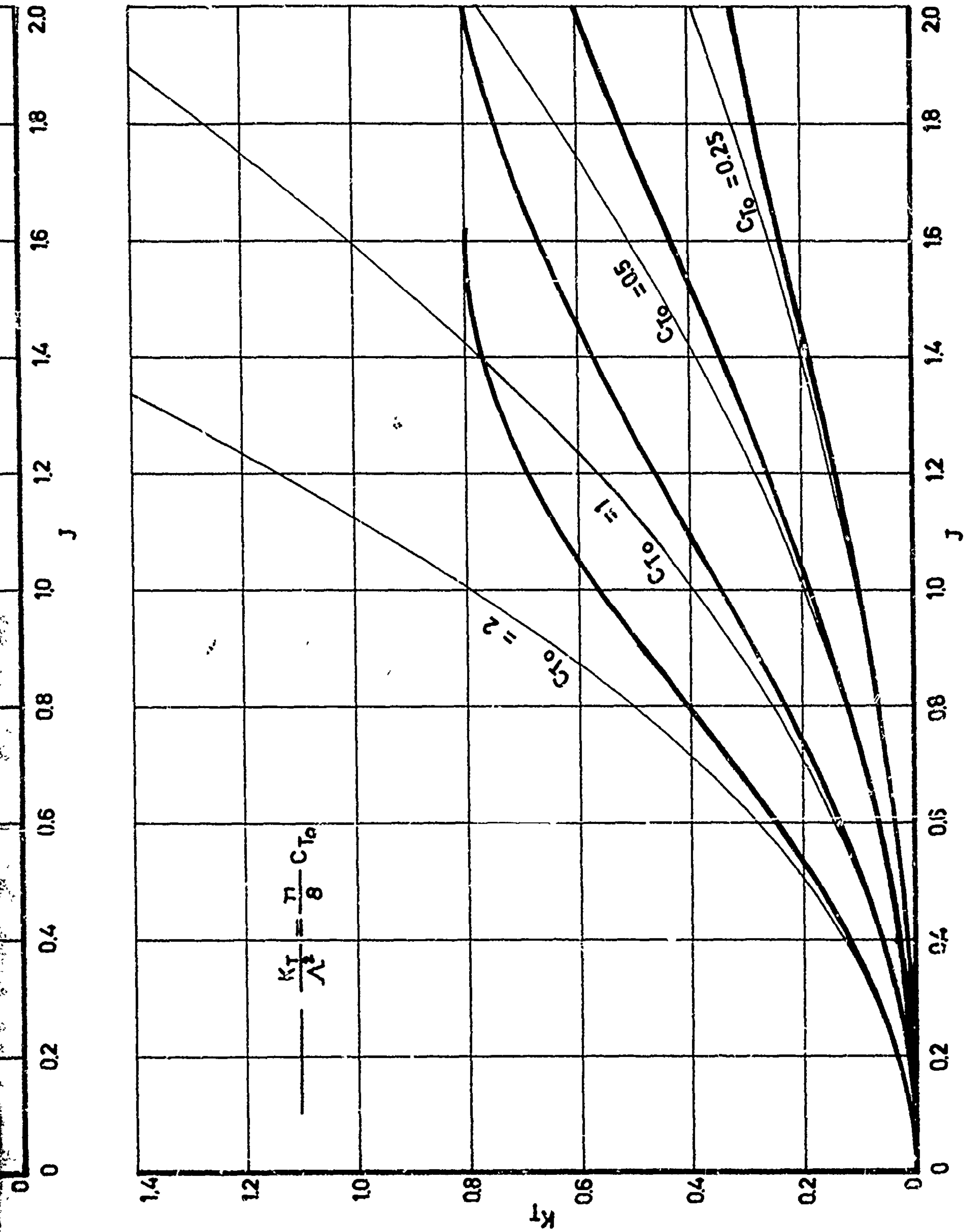

Figure 11. Characteristics of a systematic series of nozzle shapes.

38.1

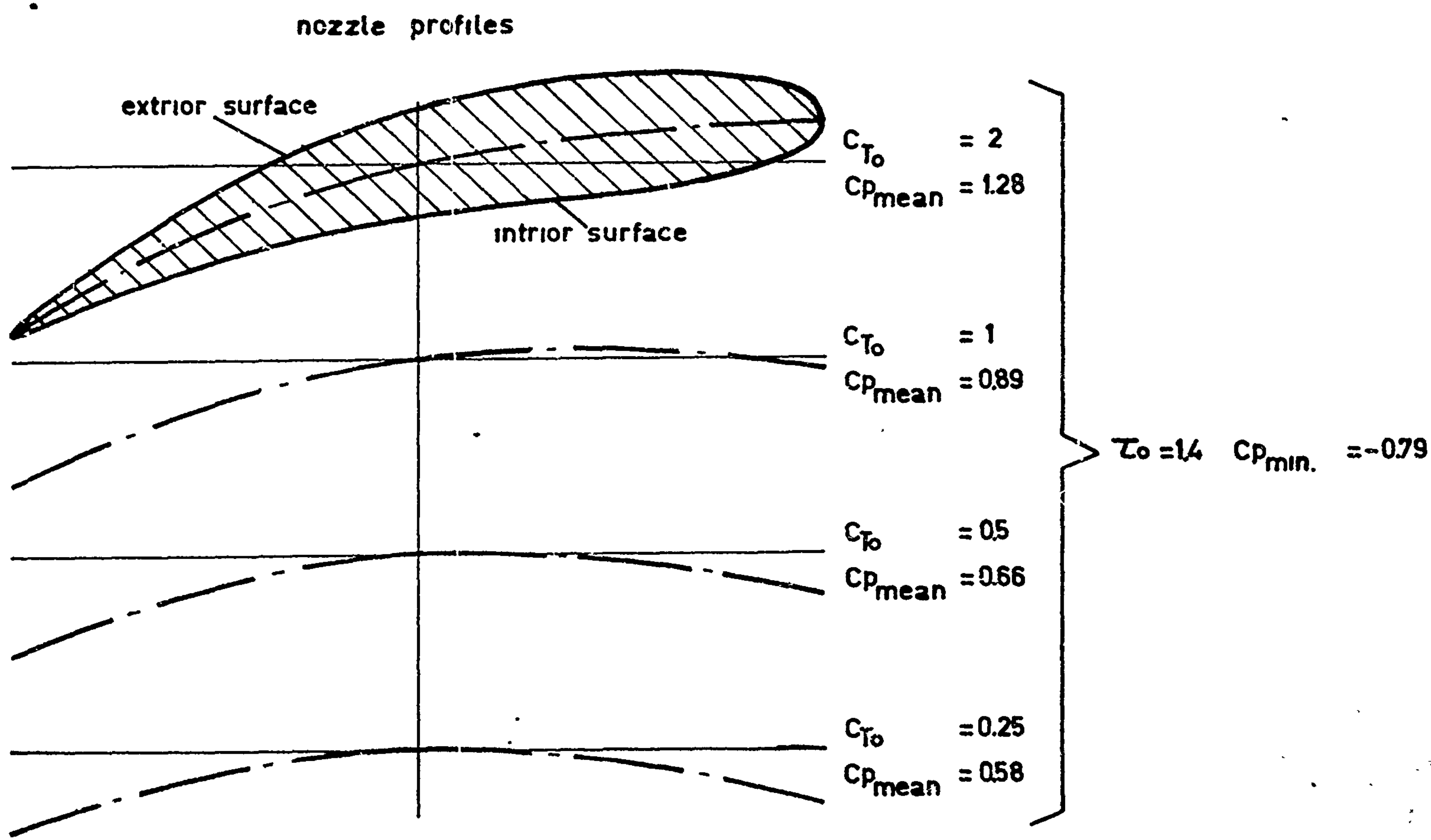

nozzle profiles
extrior surface
intrior surface
C_{To} = 2
Cp_{mean} = 1.28
C_{To} = 1
Cp_{mean} = 0.89
C_{To} = 0.5
Cp_{mean} = 0.66
C_{To} = 0.25
Cp_{mean} = 0.58
τ_o = 1.4 $Cp_{min.}$ = -0.79

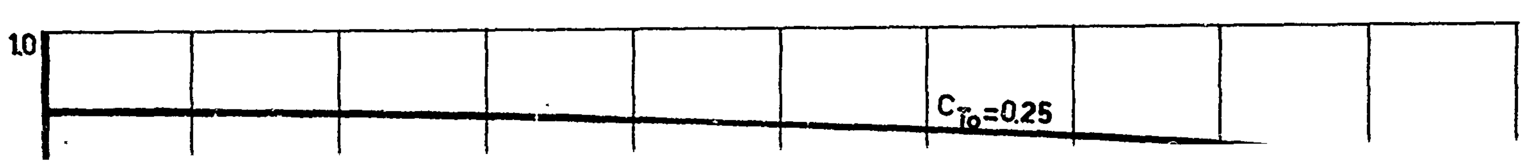

1.0
C_{To} = 0.25

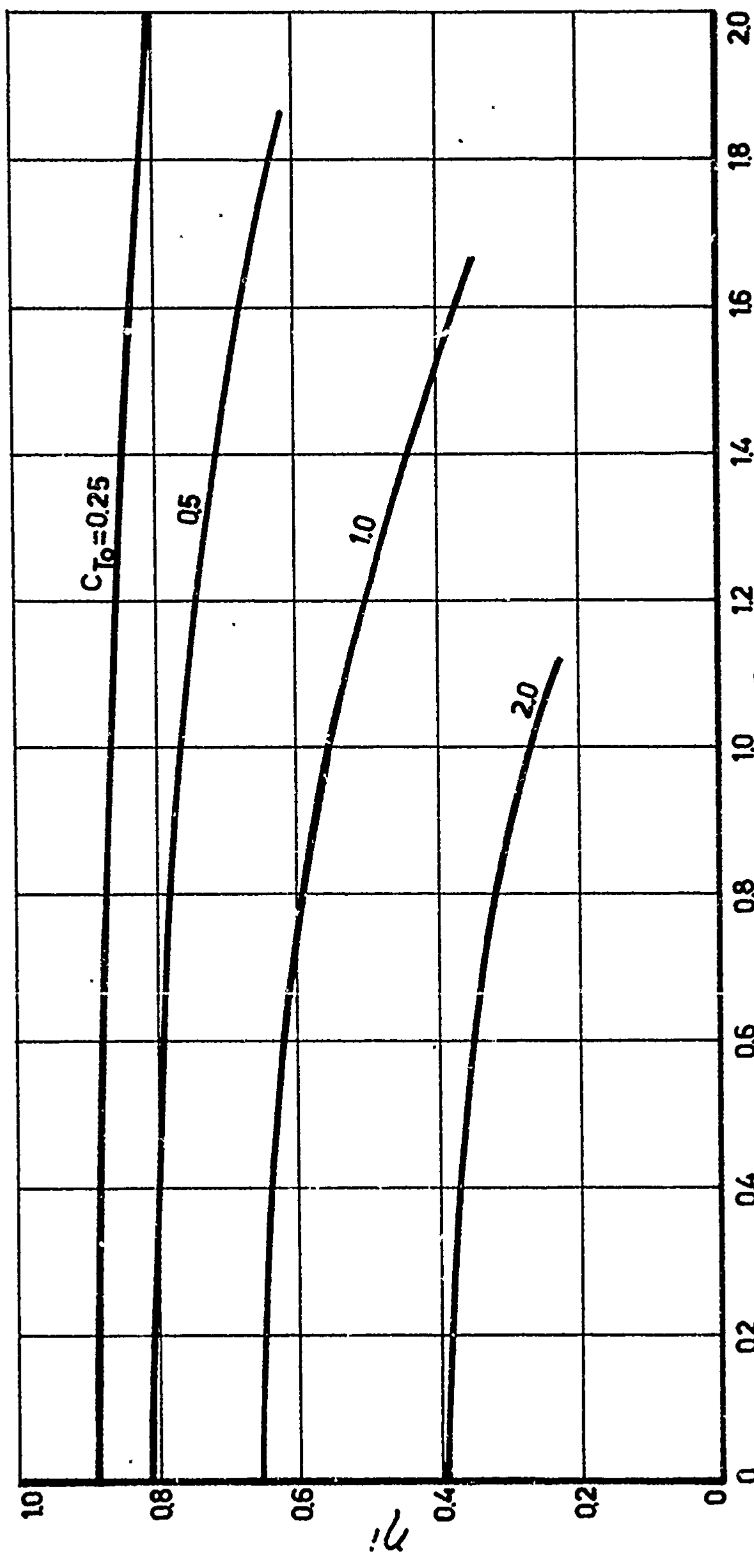
C_{T_0}=0.25
0.5
1.0
2.0
J
0 0.2 0.4 0.6 0.8 1.0 1.2 1.4 1.6 1.8 2.0
1.0 0.8 0.6 0.4 0.2 0
η_i

38·2

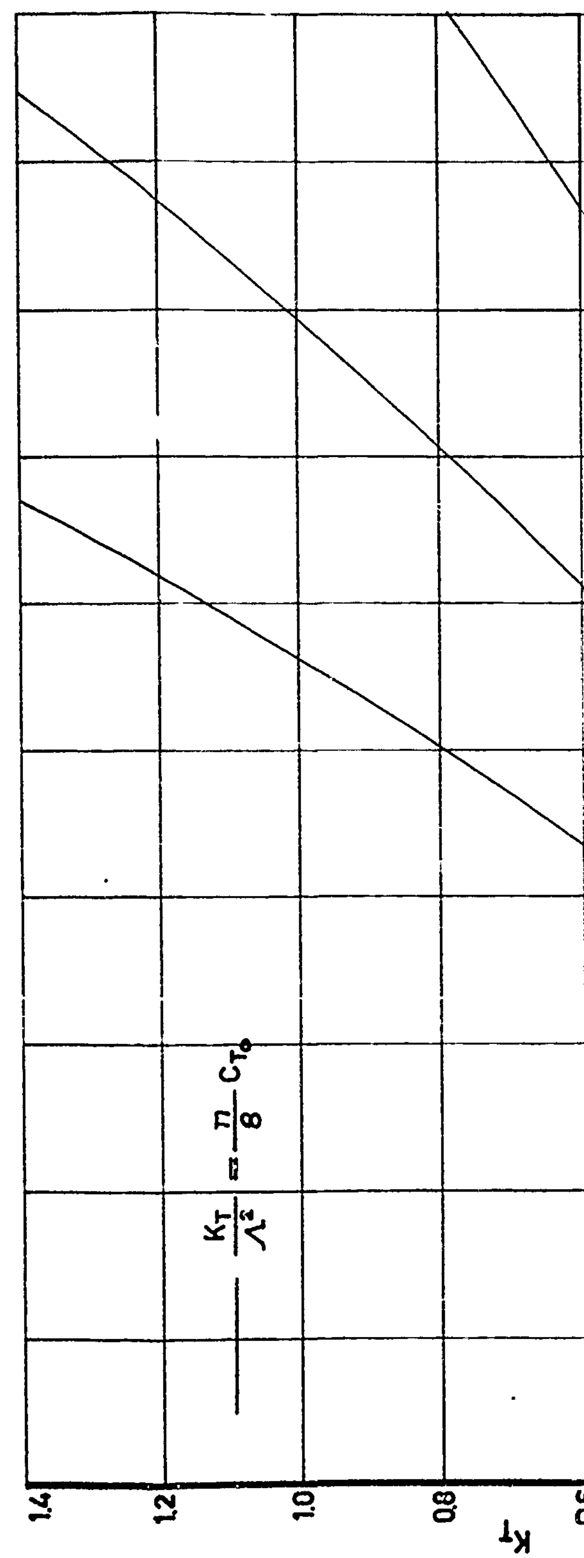
$\frac{K_T}{\Lambda^2} = \frac{\pi}{8} C_{T_0}$
1.4 1.2 1.0 0.8
K_T

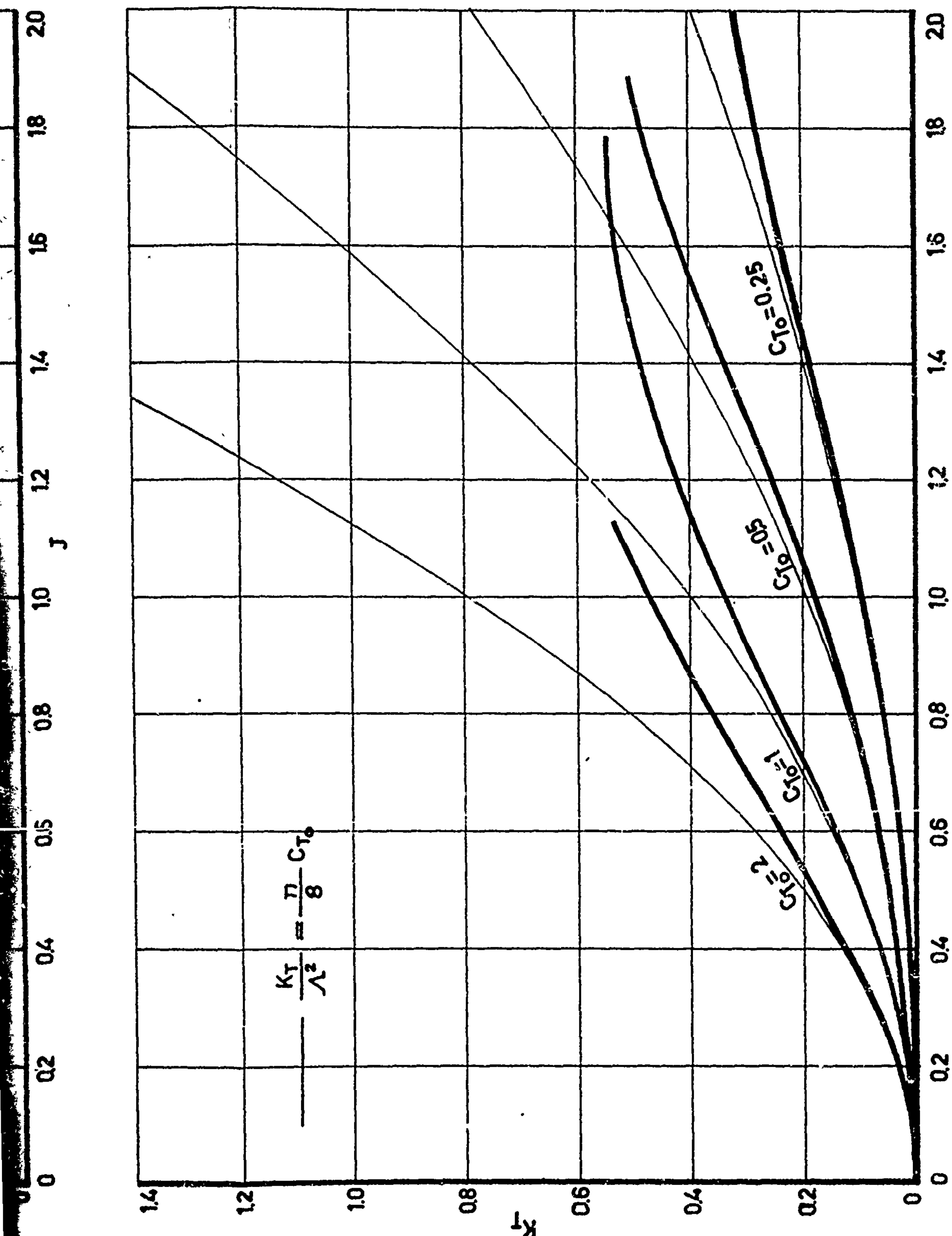

Figure 12. Characteristics of a systematic series of nozzle shapes

38.3

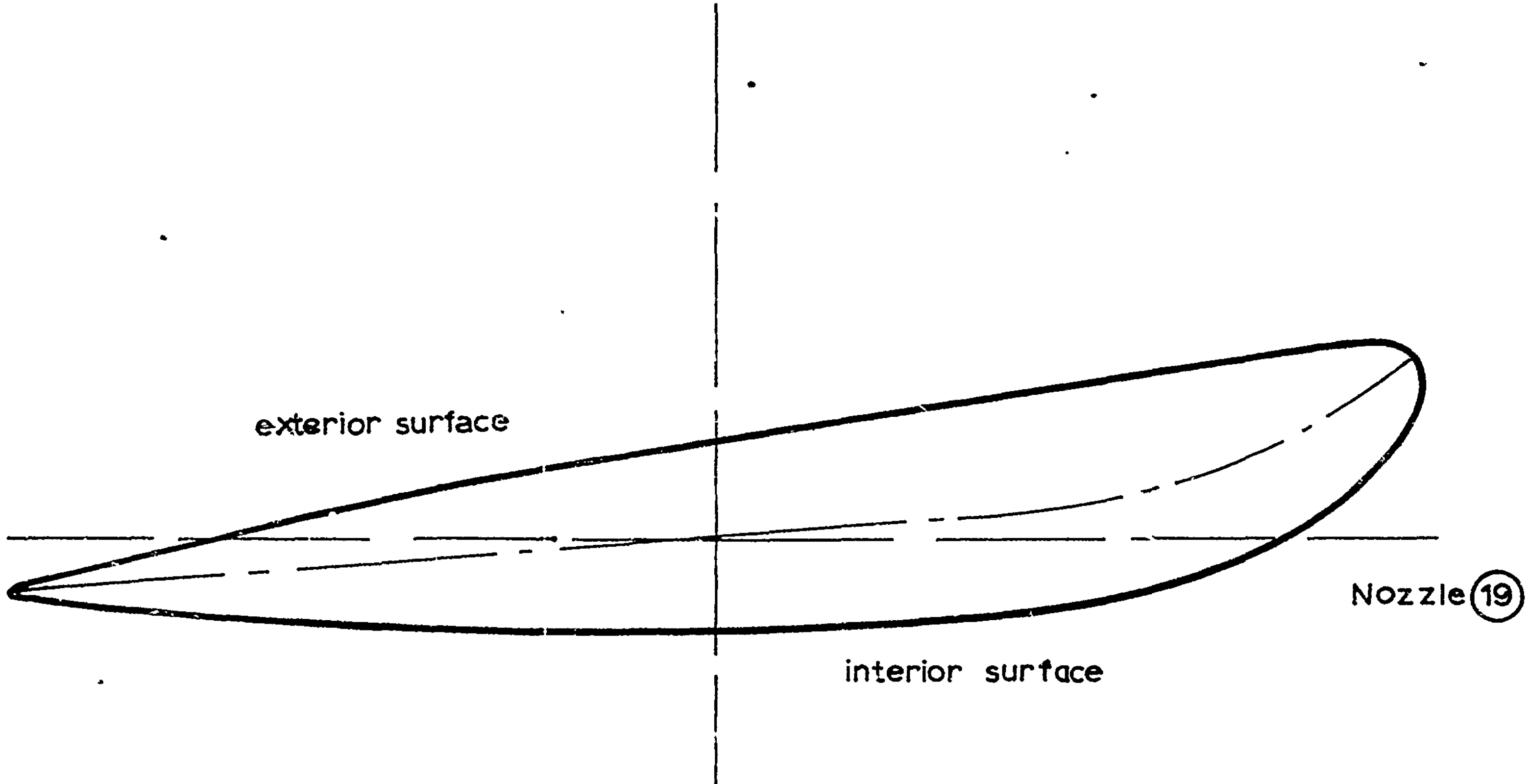

39.1

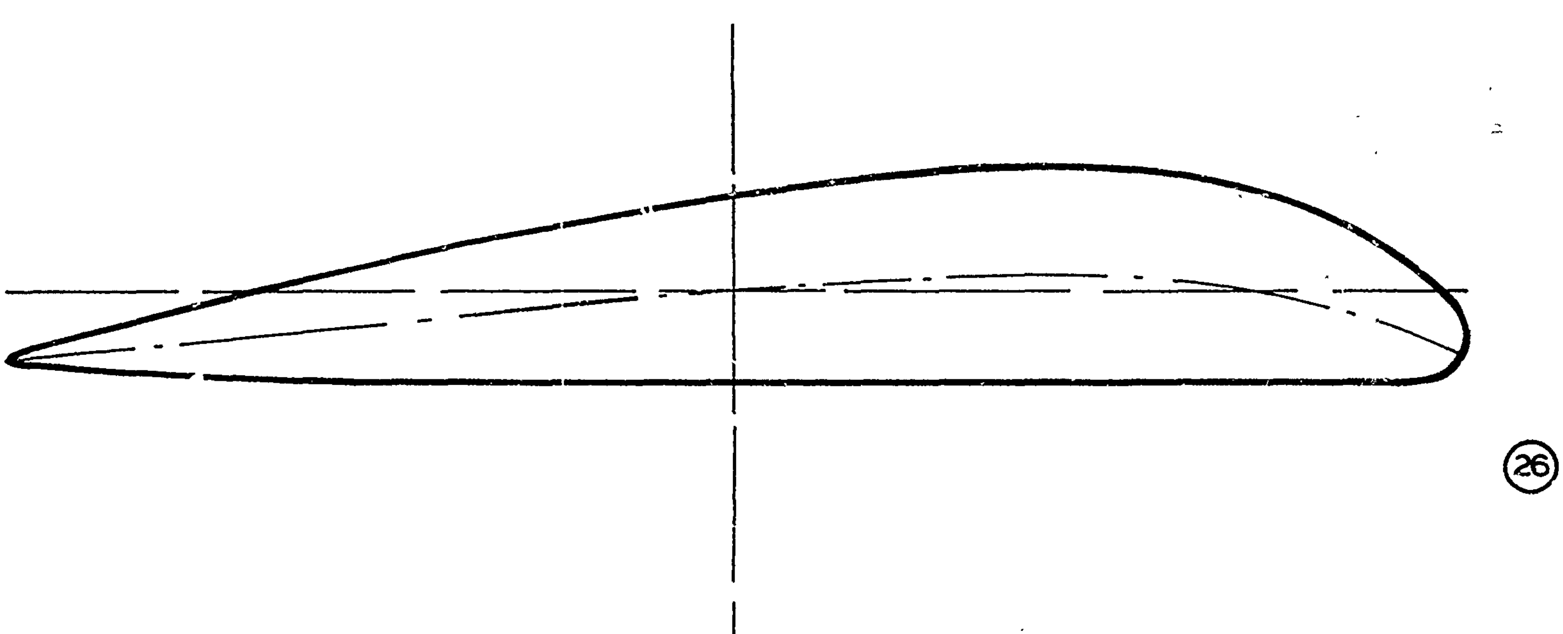

39.2

NEDERLANDSCH SCHEEPSBOU
PROEFSTATION WA

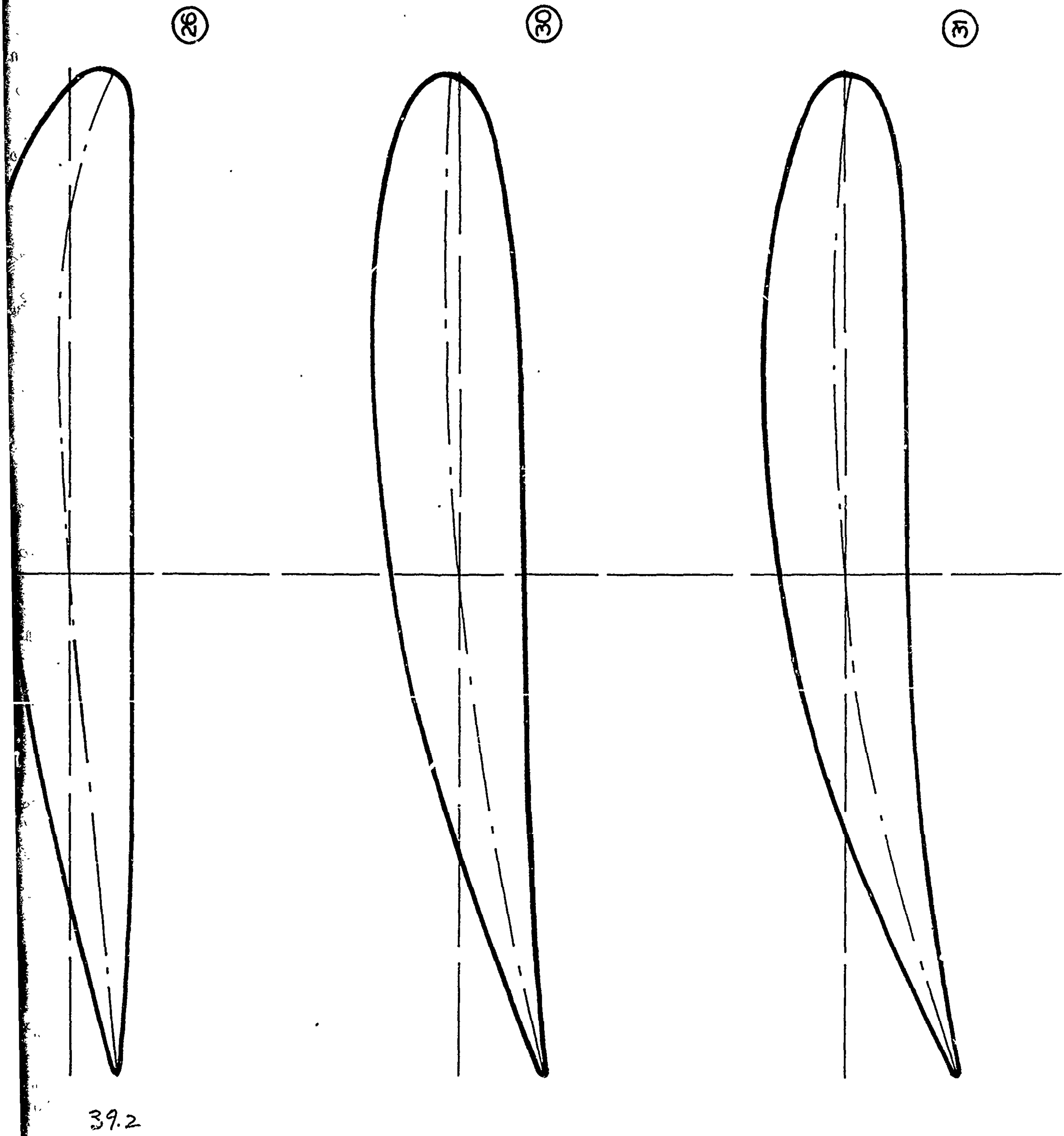

39.2

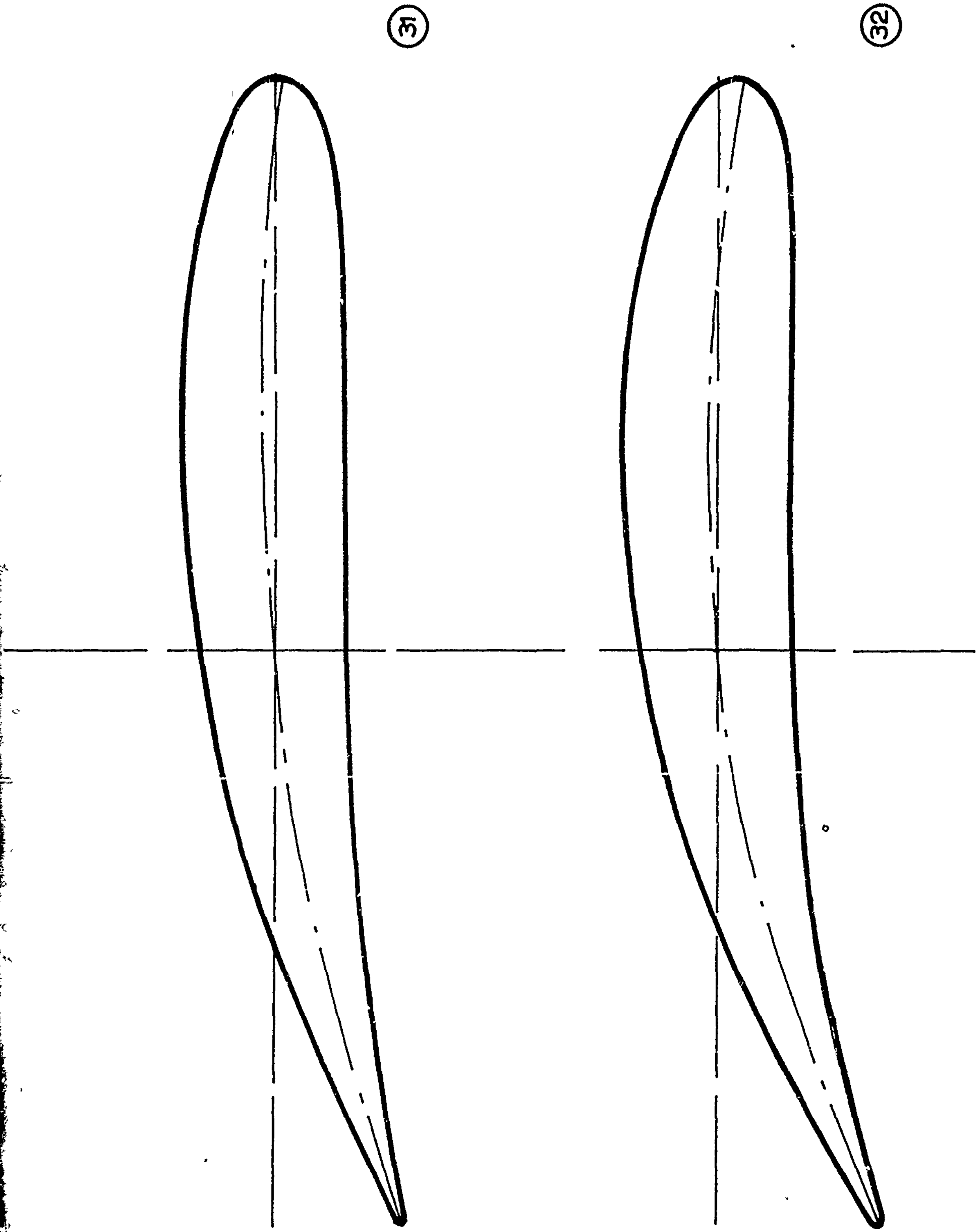

Figure 13. Camber and thickness distribution of nozzles selected for experiments

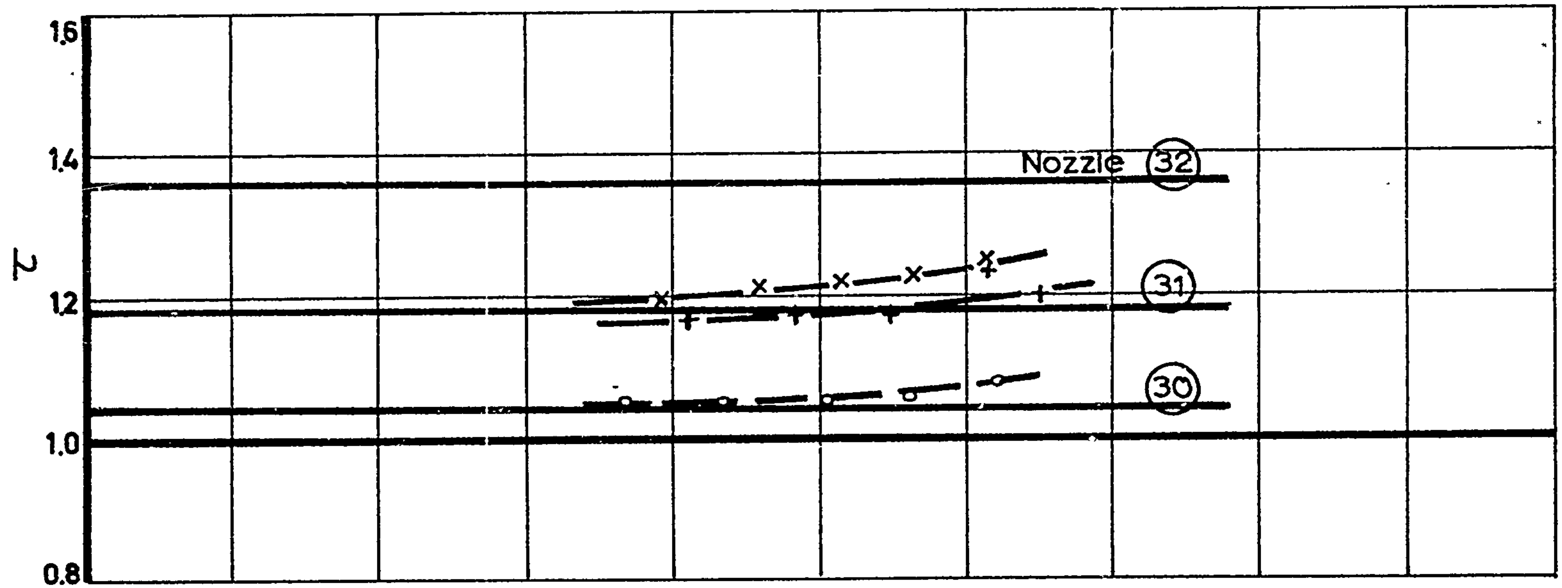

40.1

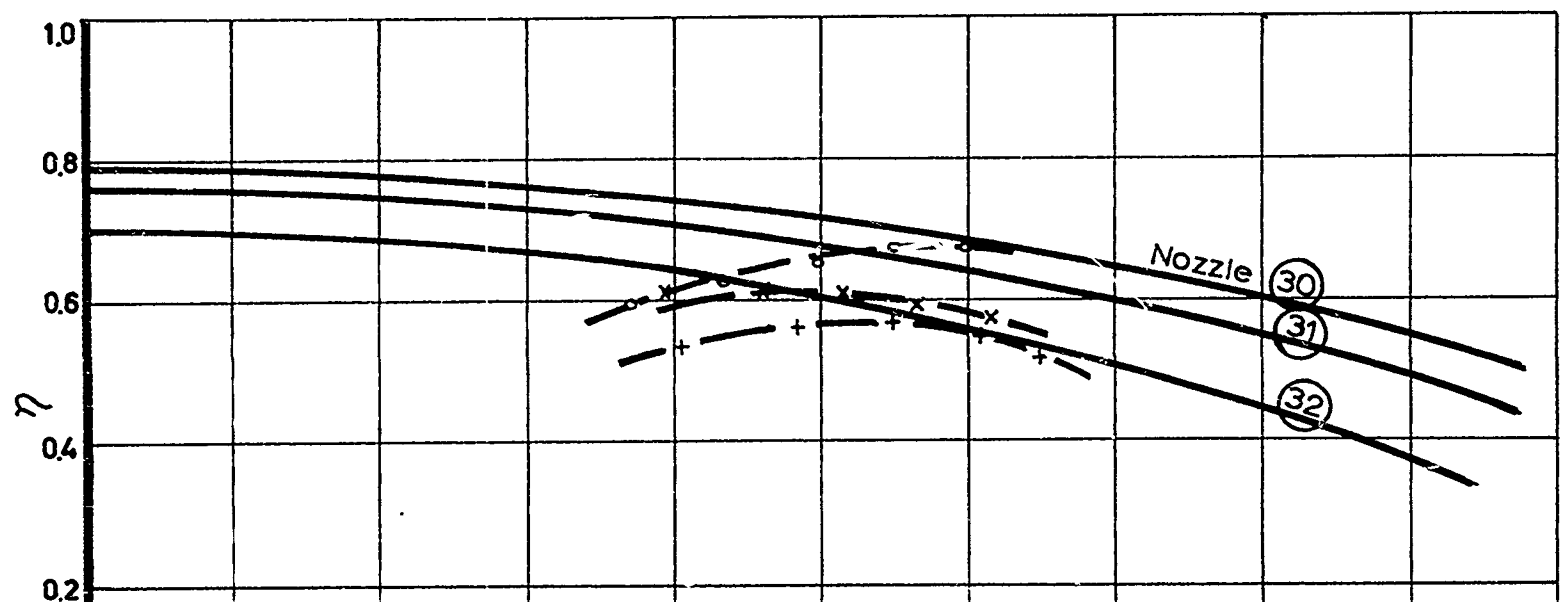

40.2

NEDERLANDSCH SCHEEPSBOUWKUNDIG
PROEFSTATION WAGENINGEN

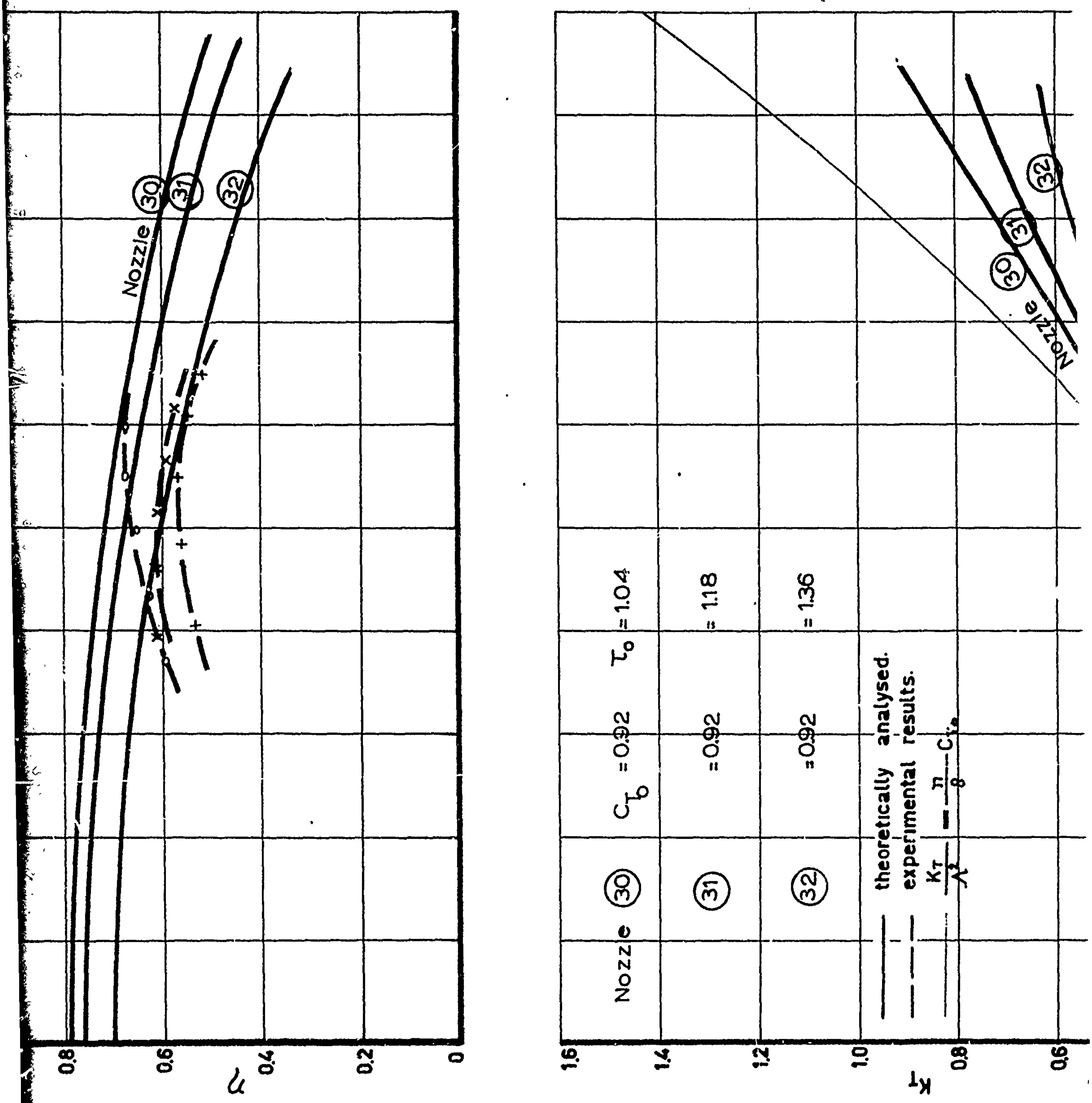

40.2

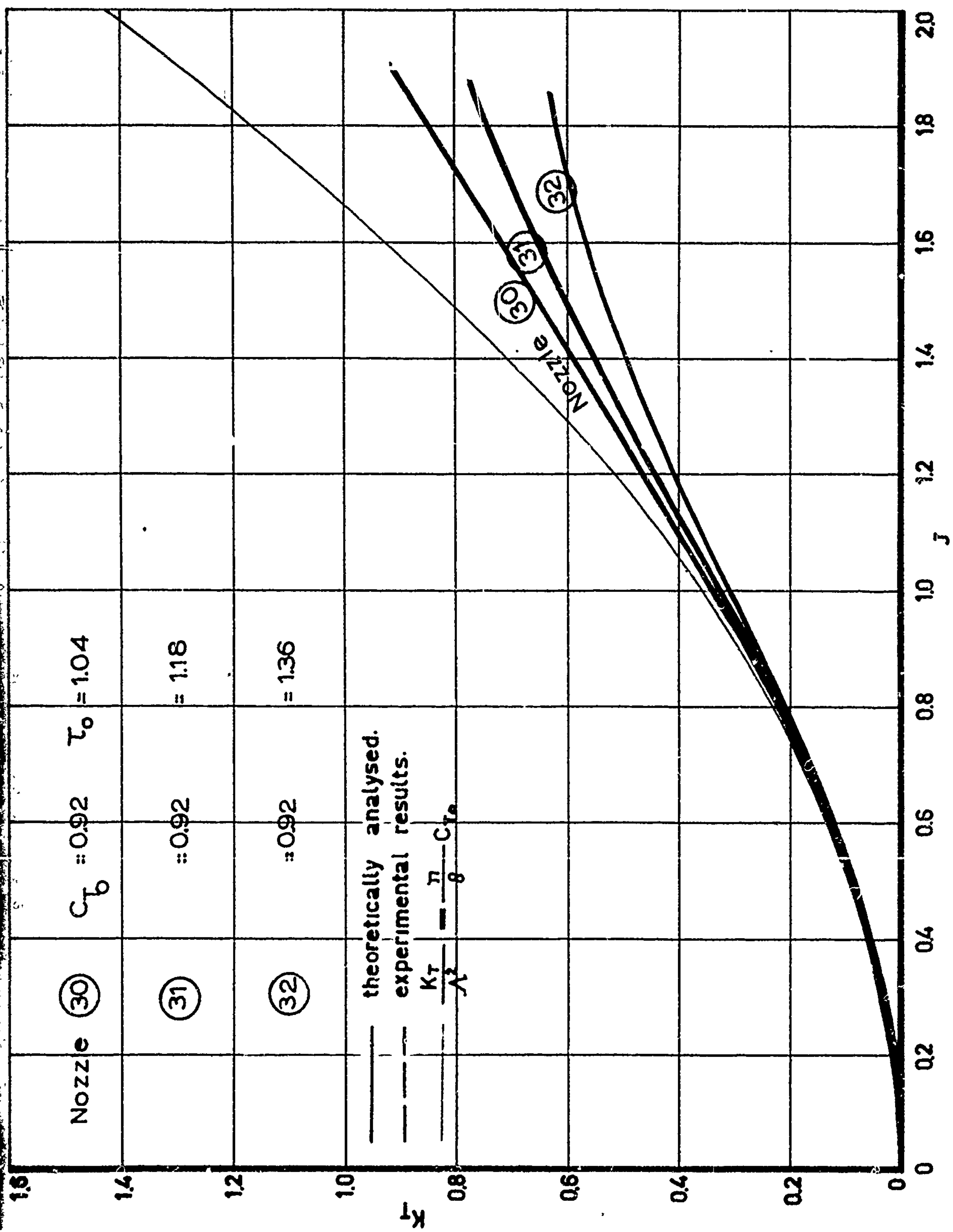

Figure 14. Characteristics of nozzles selected for experiments.

40.3

details of blade tip

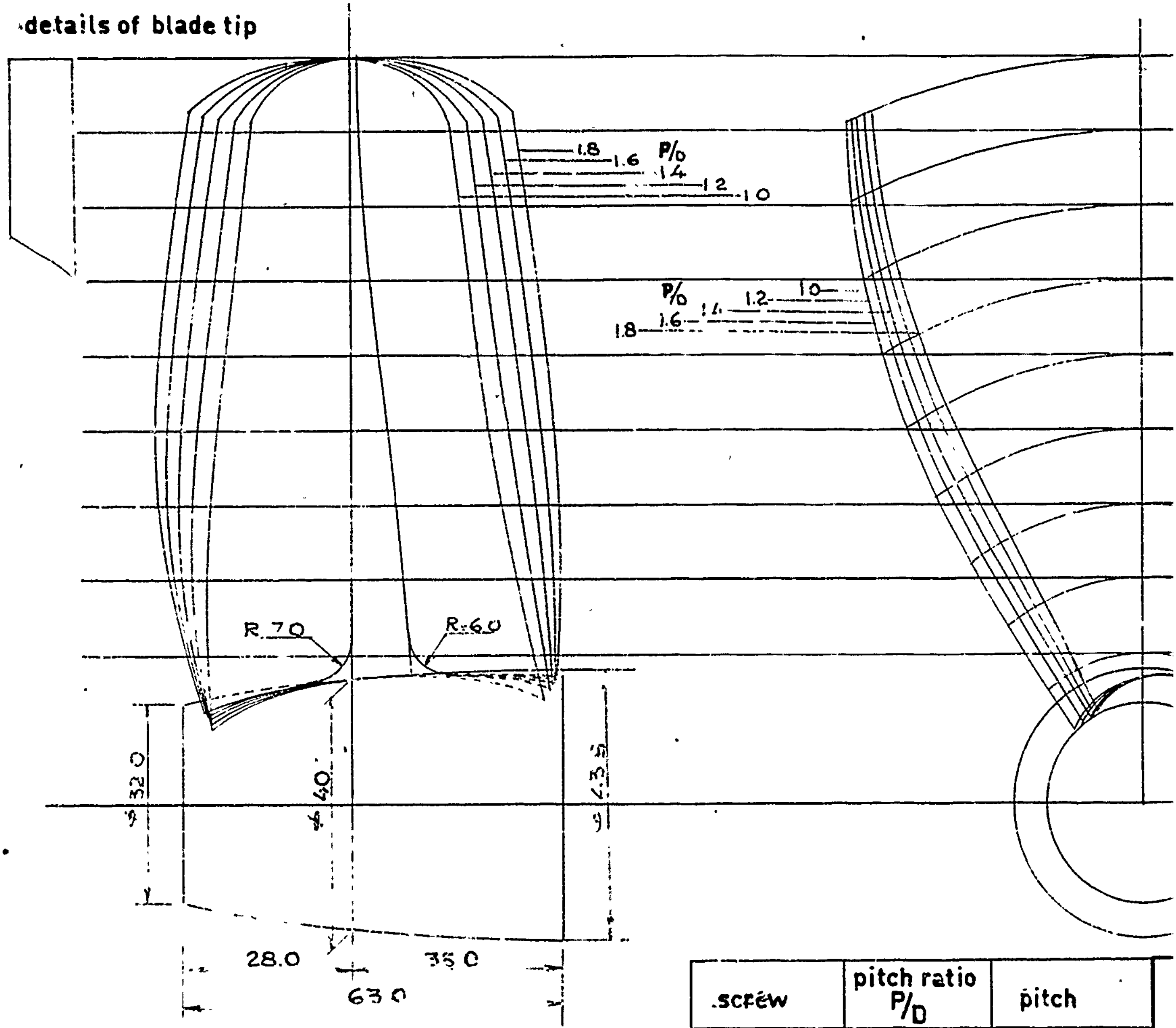

screw	pitch ratio P/D	pitch
3527	1.0	240.0 mm
3528	1.2	288.0 "
3529	1.4	336.0
3530	1.6	384.0
3531	1.8	432.0

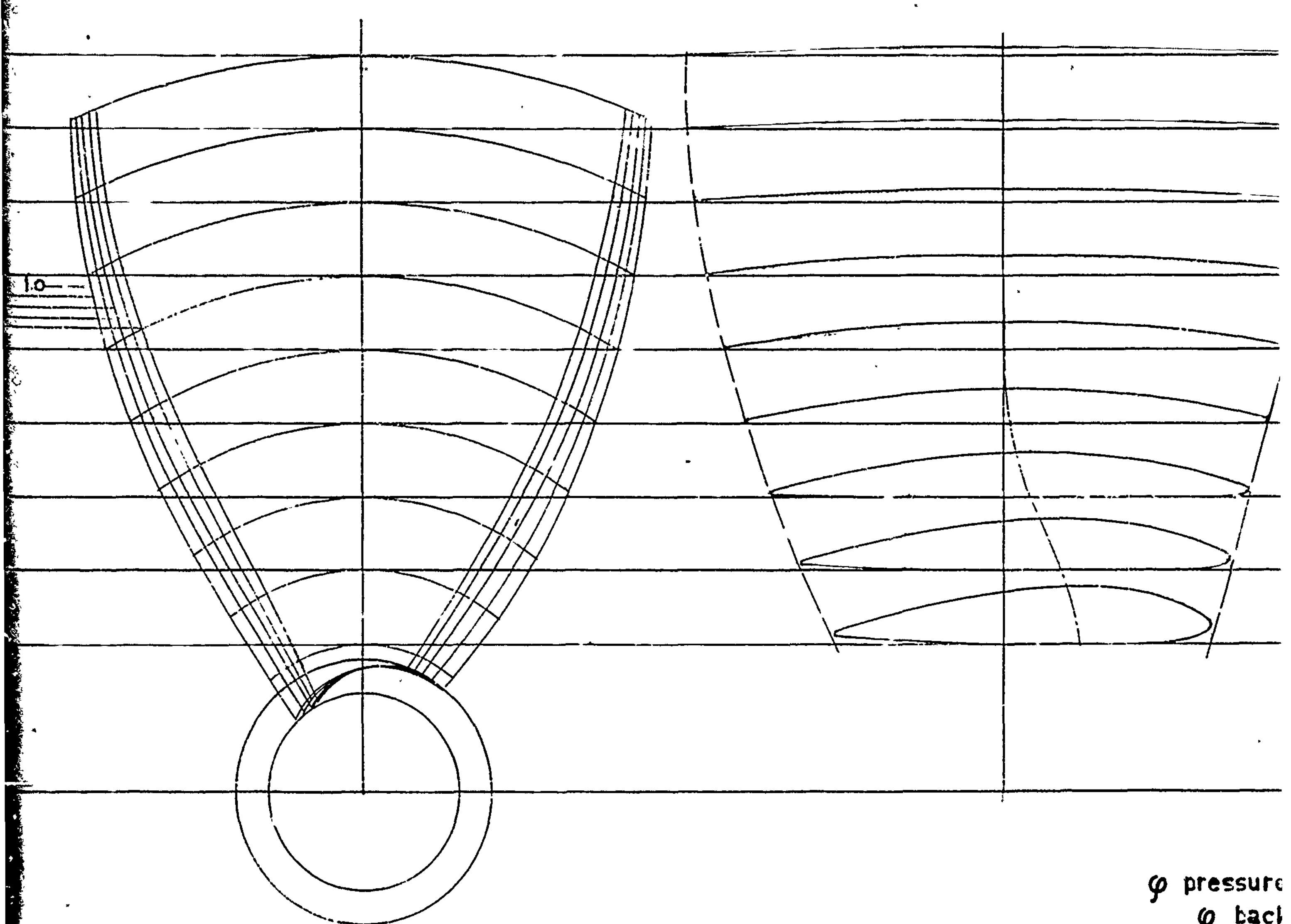

	pitch ratio P/D	pitch
	1.0	240.0 mm
	1.2	288.0 "
	1.4	336.0
	1.6	384.0
	1.8	432.0

diameter D = 240.0 mm.
number of blades z = 5
hub to diameter ratio $\frac{d}{D}$ = 0.167
blade area ratio $\frac{A_o}{A}$ = 1.0

Fig.15,16,17,18 and 19: Particulars of screw models 3527

NEDERLANDSCH SCHEEPSBOUWKUNDIG PROEFSTATION
WAGENINGEN

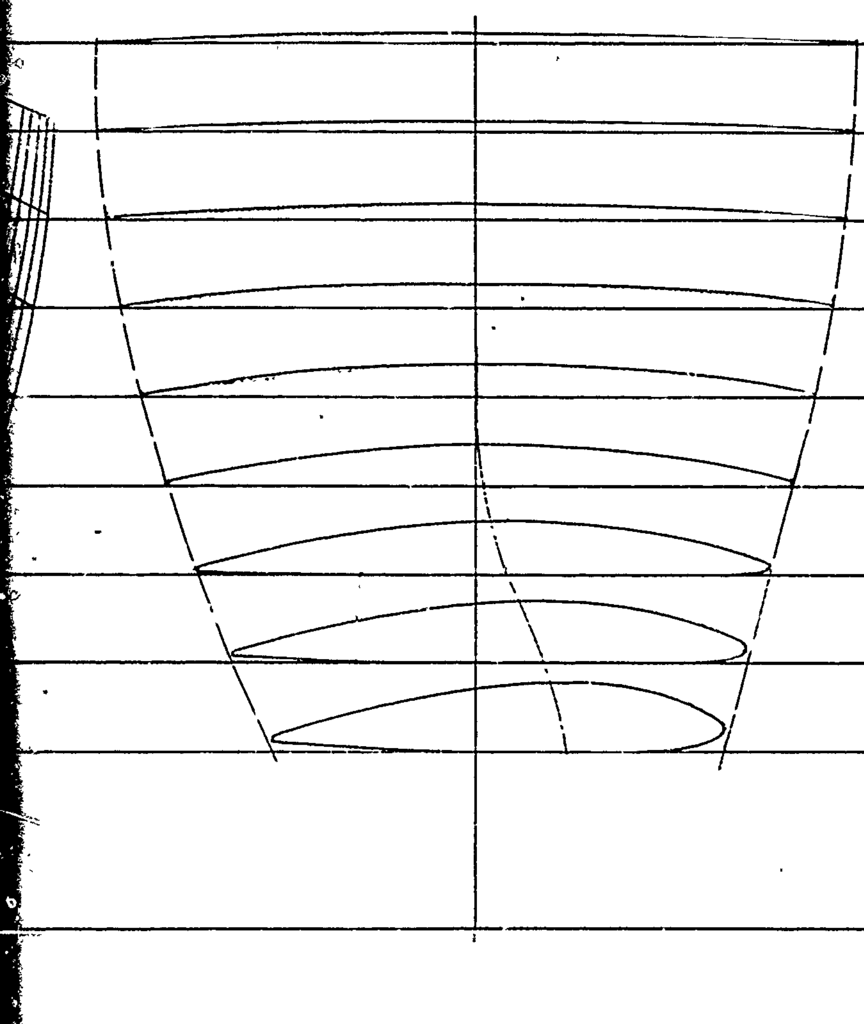

r/R	r	max. thickness
1.0	120.0	1.20
0.9	108.0	1.47
0.8	96.0	2.21
0.7	84.0	3.30
0.6	72.0	4.56
0.5	60.0	5.89
0.4	48.0	7.20
0.3	36.0	8.45
0.2	24.0	9.60

φ pressure side = 0° SIN φ =

φ back side = 5°12' SIN φ = 0.09101

D = 240.0 mm.

z = 5

ratio $\frac{d}{D}$ = 0.167

$\frac{A_o}{A}$ = 1.0

d 19. Particulars of screw models 3527 through 3531.

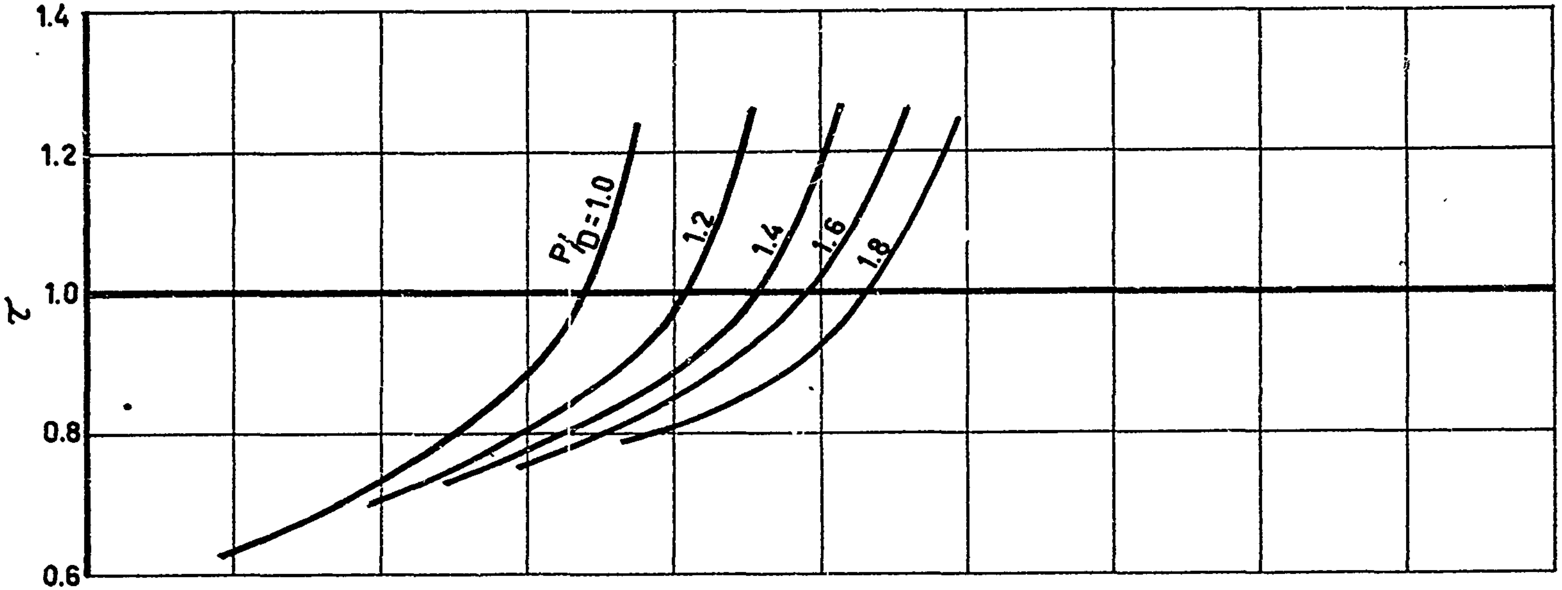
1.4
1.2
1.0
0.8
0.6
τ
P/D=1.0
1.2
1.4
1.6
1.8

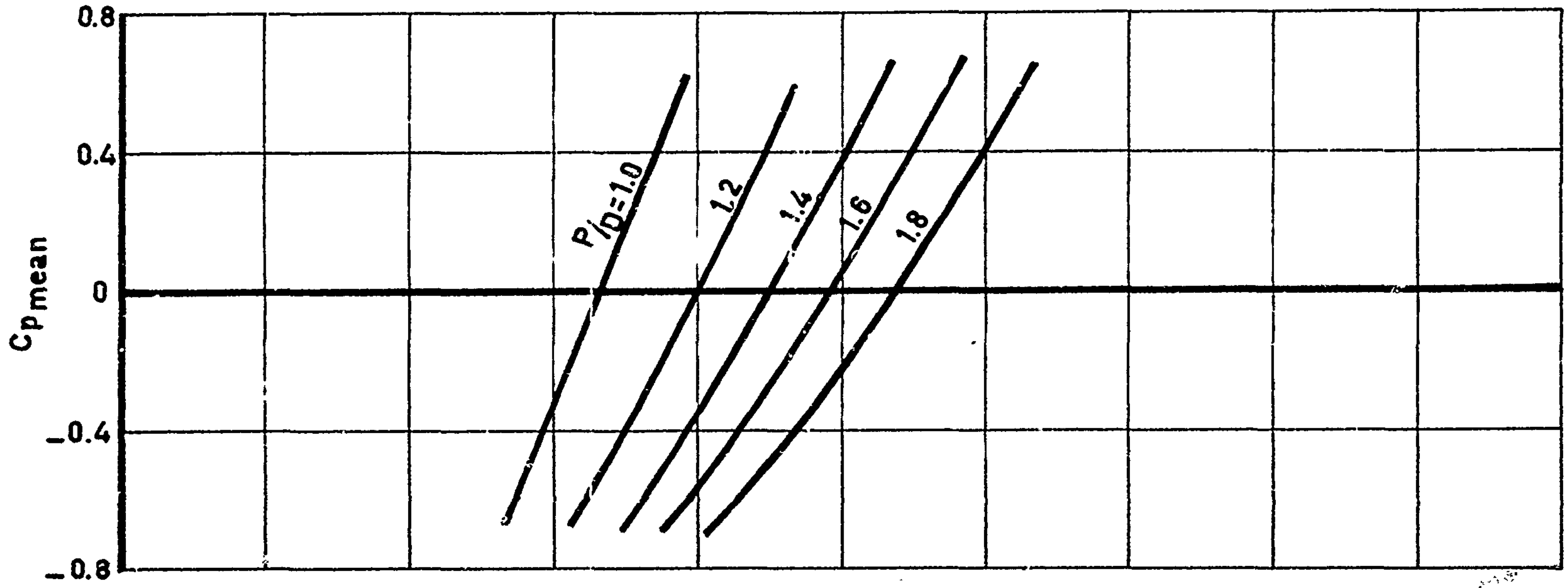
0.8
0.4
0
-0.4
-0.8
$C_{p\,mean}$
P/D=1.0
1.2
1.4
1.6
1.8

1.4

421

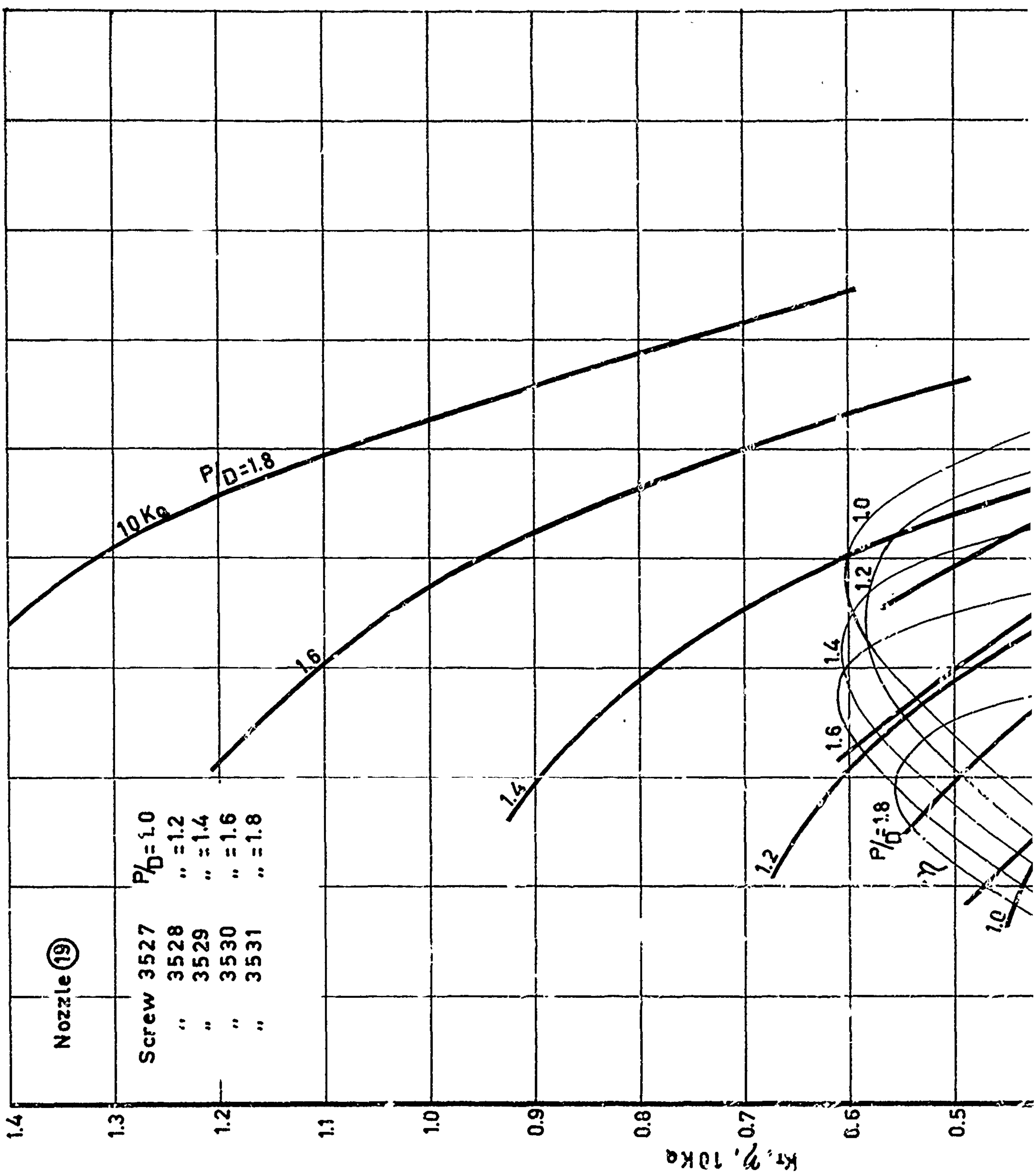
Nozzle (19)
Screw 3527 P/D = 1.0
" 3528 " = 1.2
" 3529 " = 1.4
" 3530 " = 1.6
" 3531 " = 1.8
10Kq
P/D = 1.8
1.6
1.4
1.2
1.0
P/D = 1.8
η
1.4
1.3
1.2
1.1
1.0
0.9
0.8
0.7
0.6
0.5
Kt, η, 10Kq

42 2

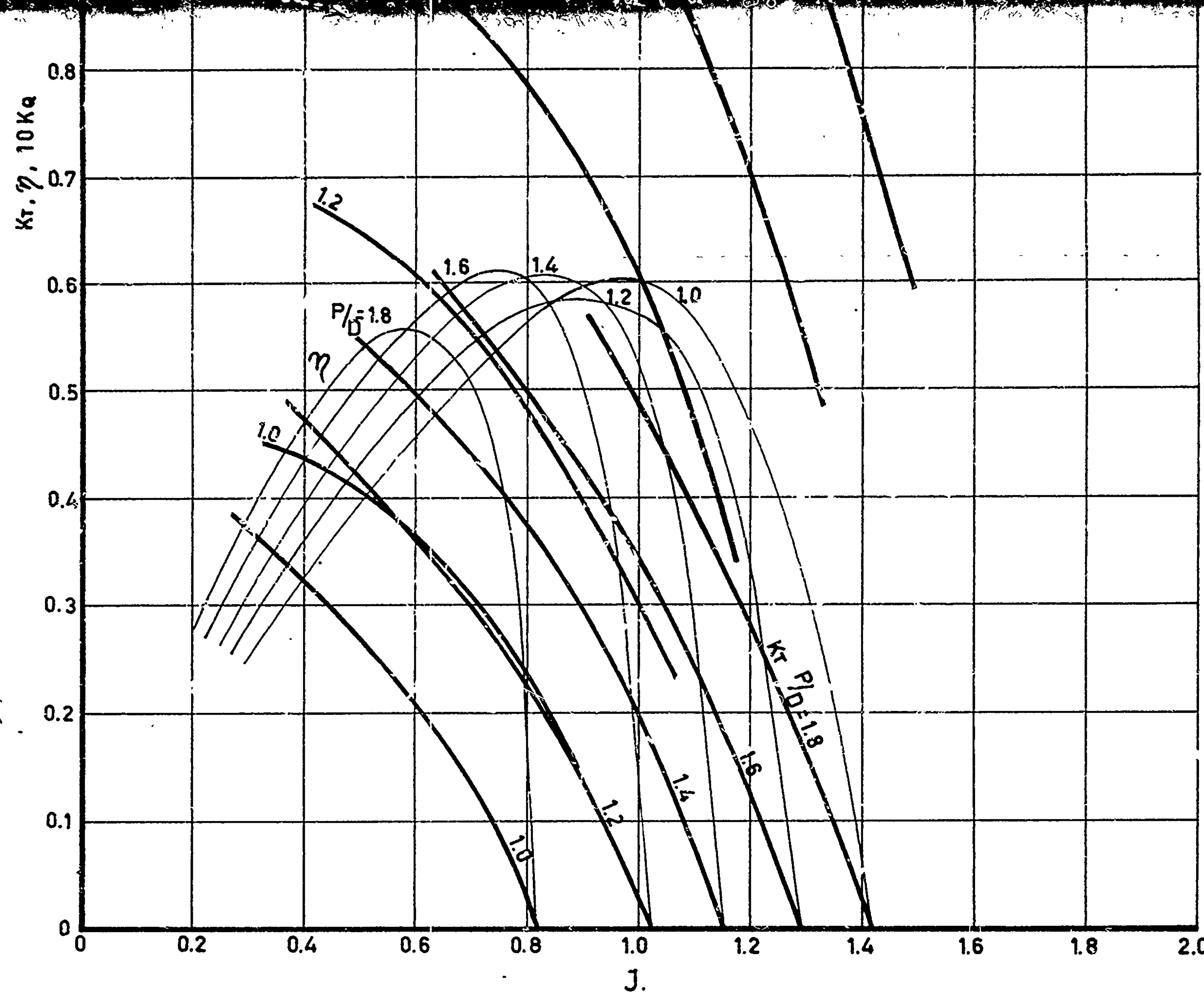

Figure 20. Experimentally obtained characteristics of nozzle № 19

42.3

43.1

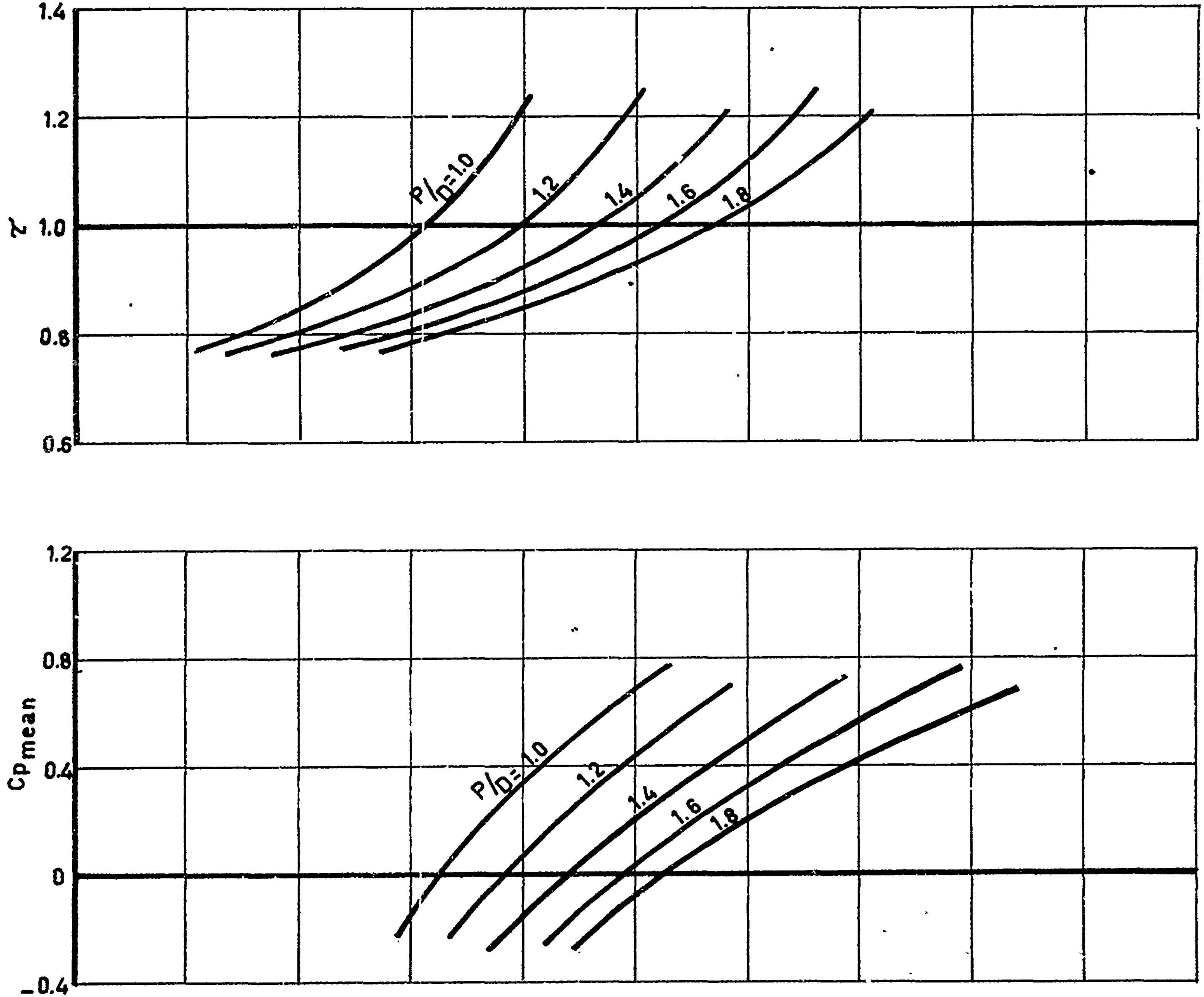

1.4
1.2
1.0
0.8
0.6
τ
P/D=1.0
1.2
1.4
1.6
1.8
1.2
0.8
0.4
0
-0.4
Cp mean
P/D=1.0
1.2
1.4
1.6
1.8

NEDERLANDSCH S
PROEFSTATION

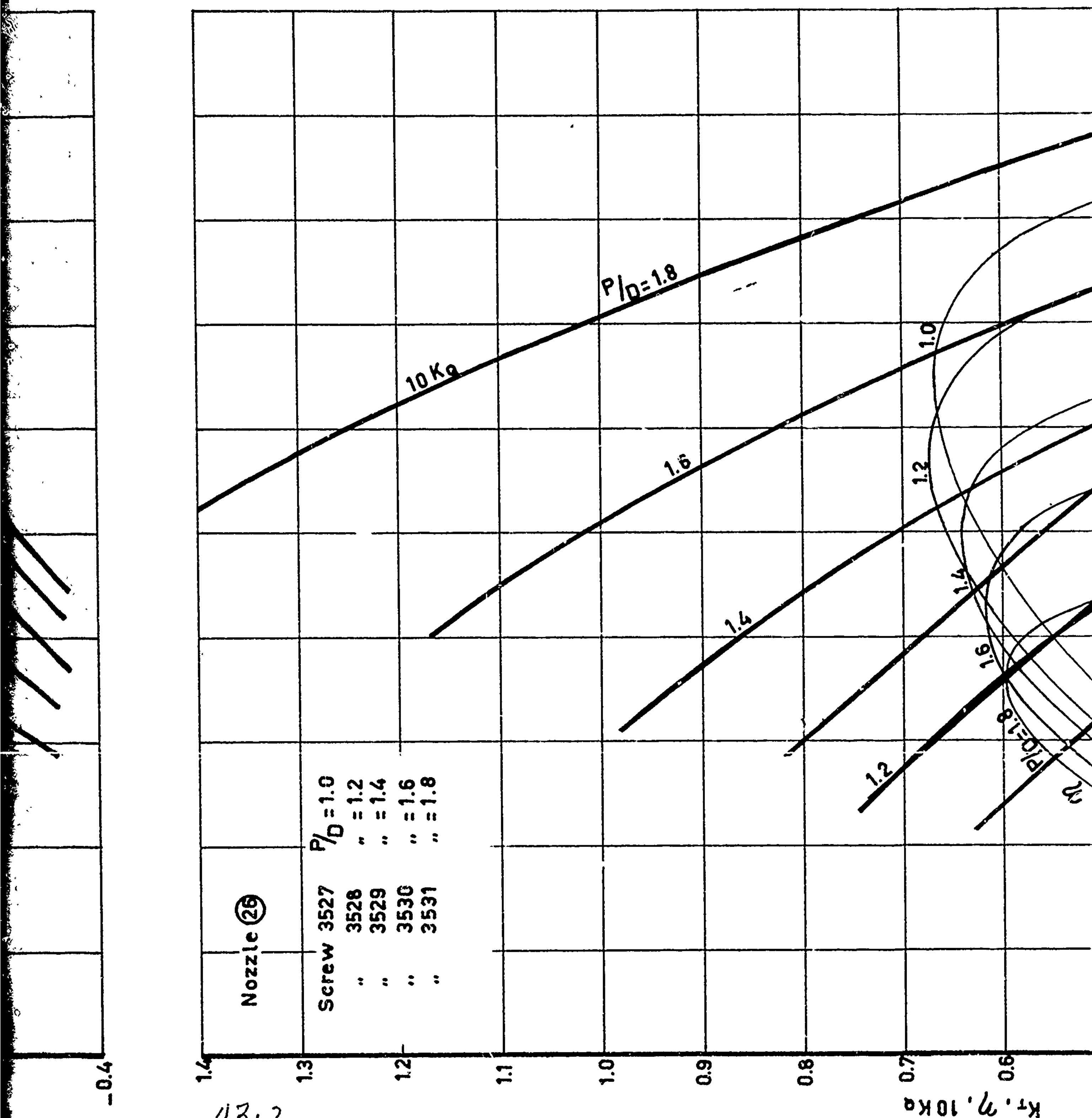

43.2

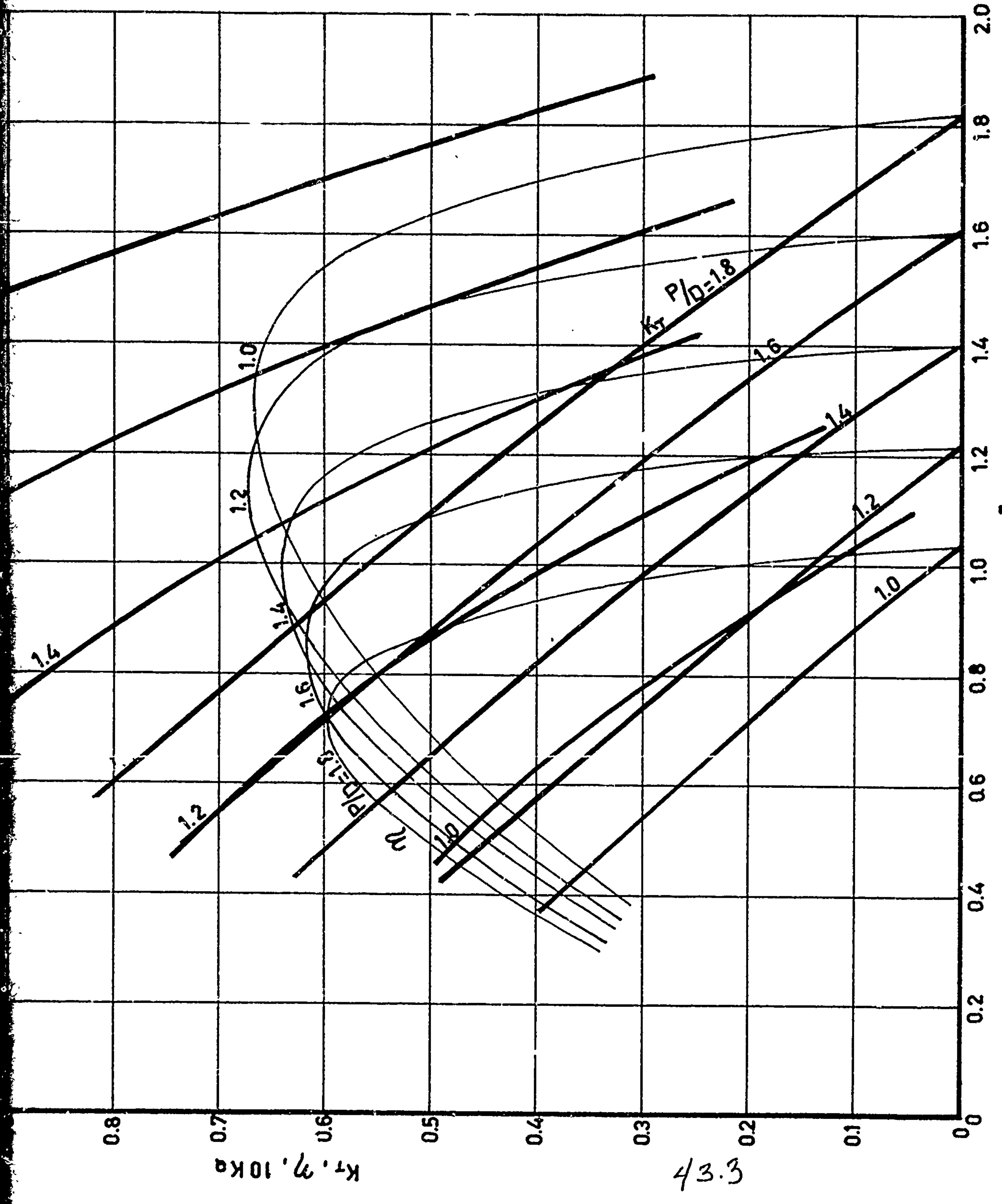

Figure 21. Experimentally obtained characteristics of nozzle Nº 26

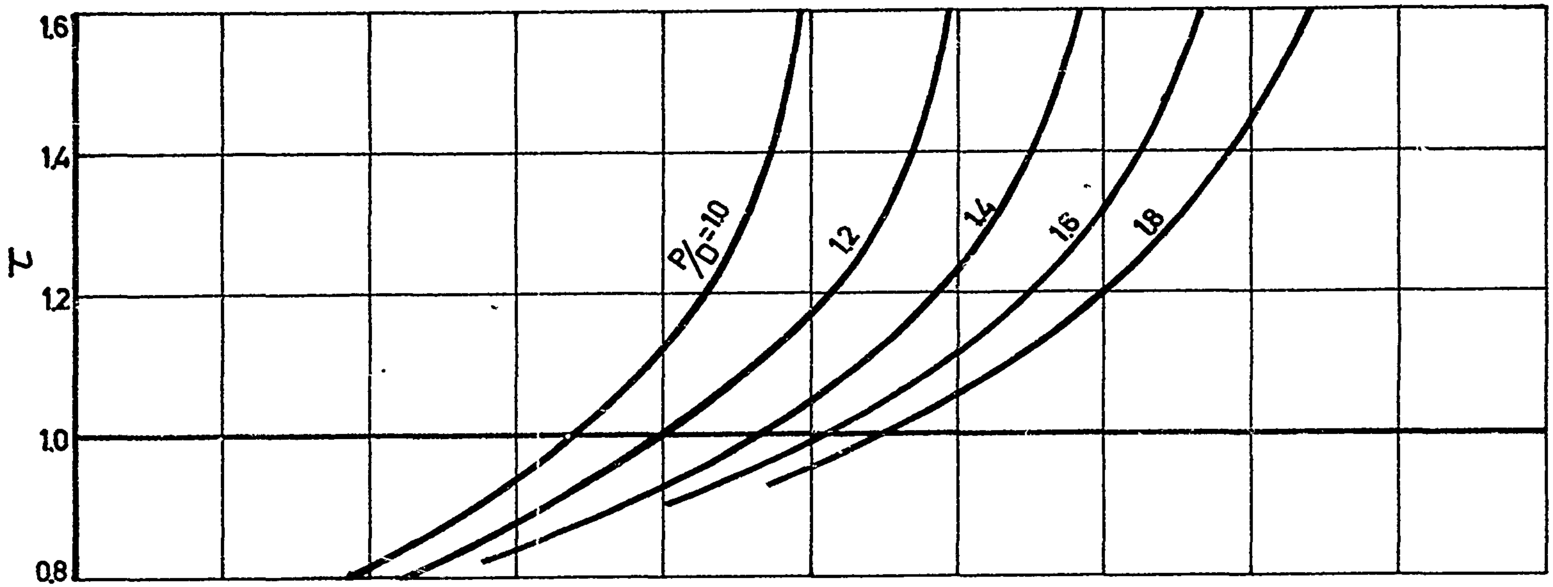
1.6
1.4
1.2
1.0
0.8
τ
P/D=1.0
1.2
1.4
1.6
1.8

44.1

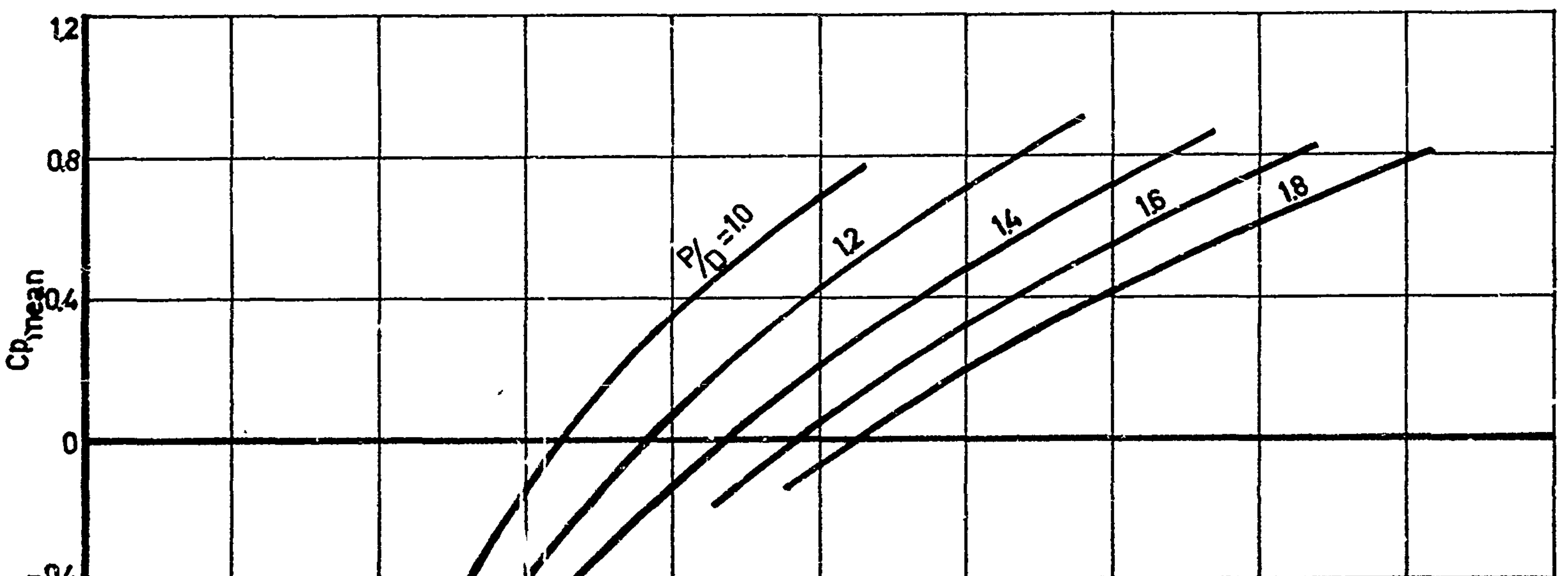
1.2
0.8
0.4
0
-0.4
Cp mean
P/D=1.0
1.2
1.4
1.6
1.8

44.2

NEDERLANDSCH SCHI
PROEFSTATION

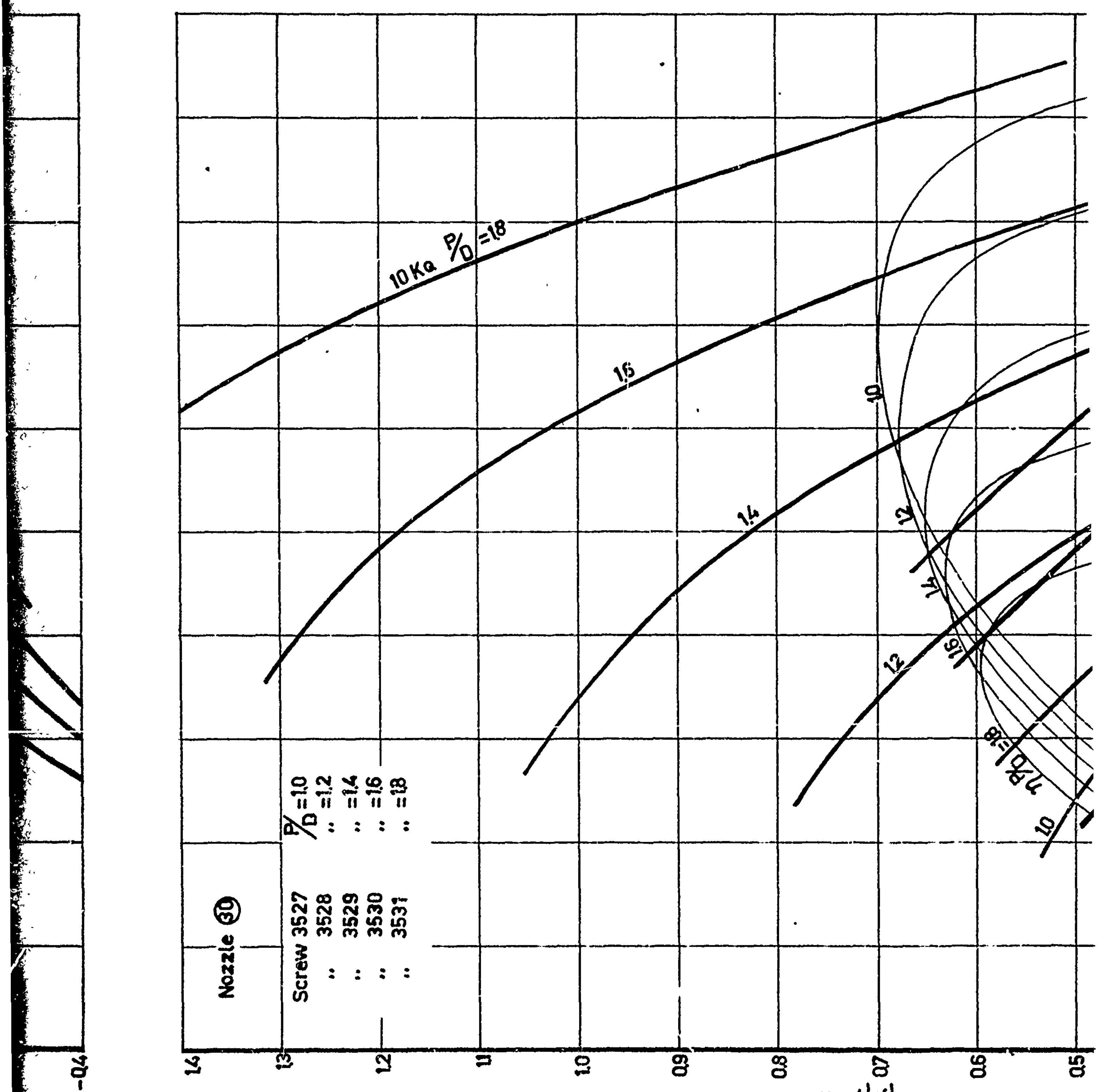

44·2

NEDERLANDSCH SCHEEPSBOUWKUNDIG PROEFSTATION WAGENINGEN	NO.	BLZ.

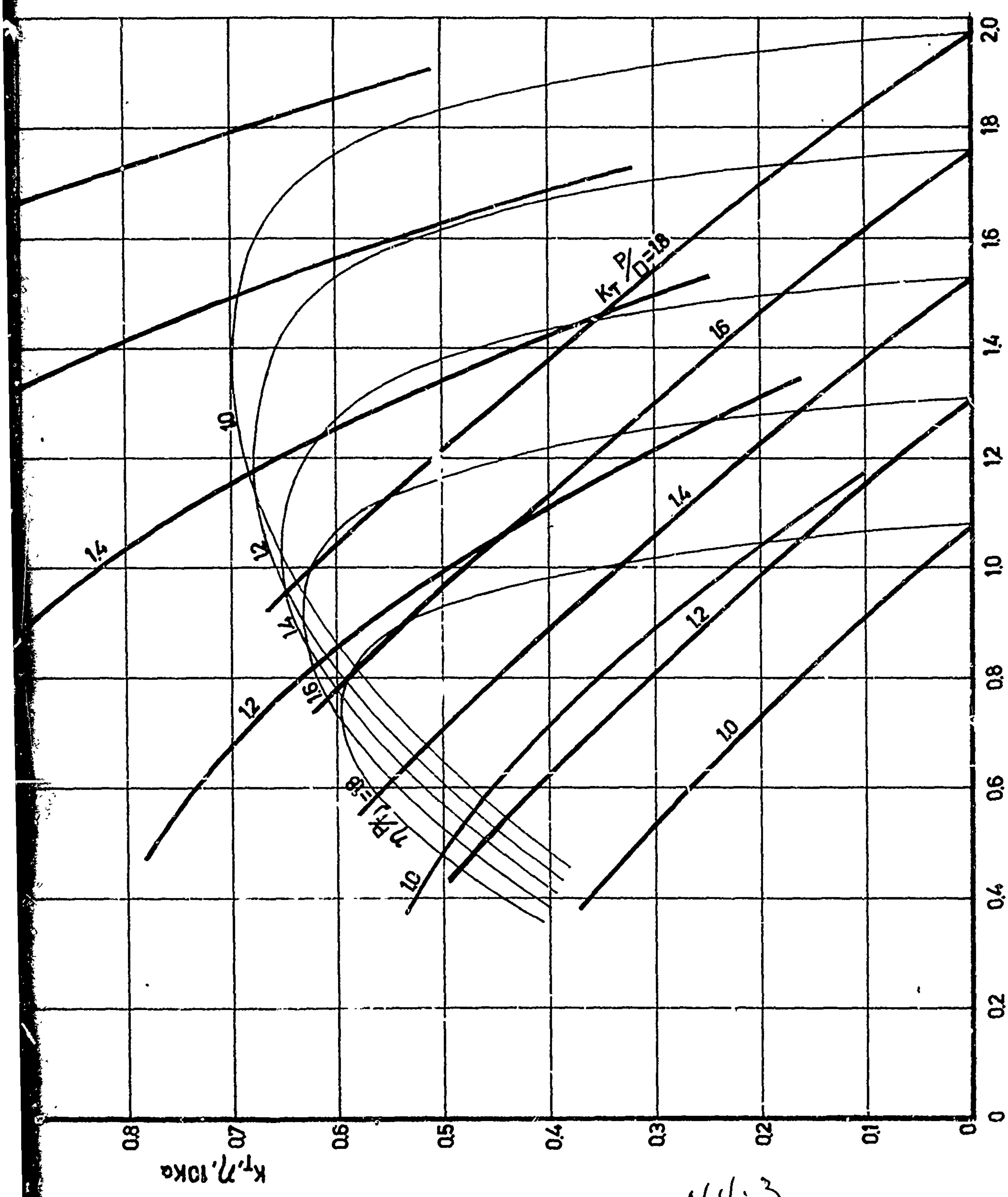

Figure 22. Experimentally obtained characteristics of nozzle No 30.

44.3

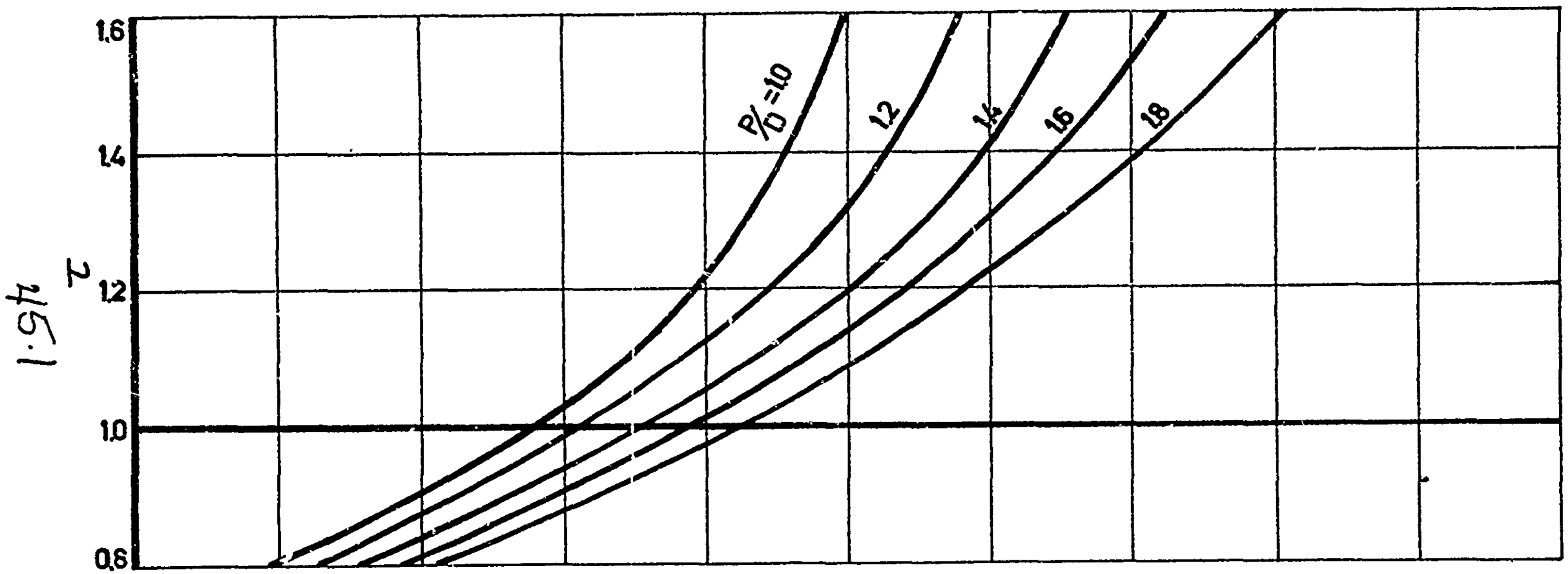
1.6
1.4
1.2
1.0
0.6
τ
P/D=1.0
1.2
1.4
1.6
1.8

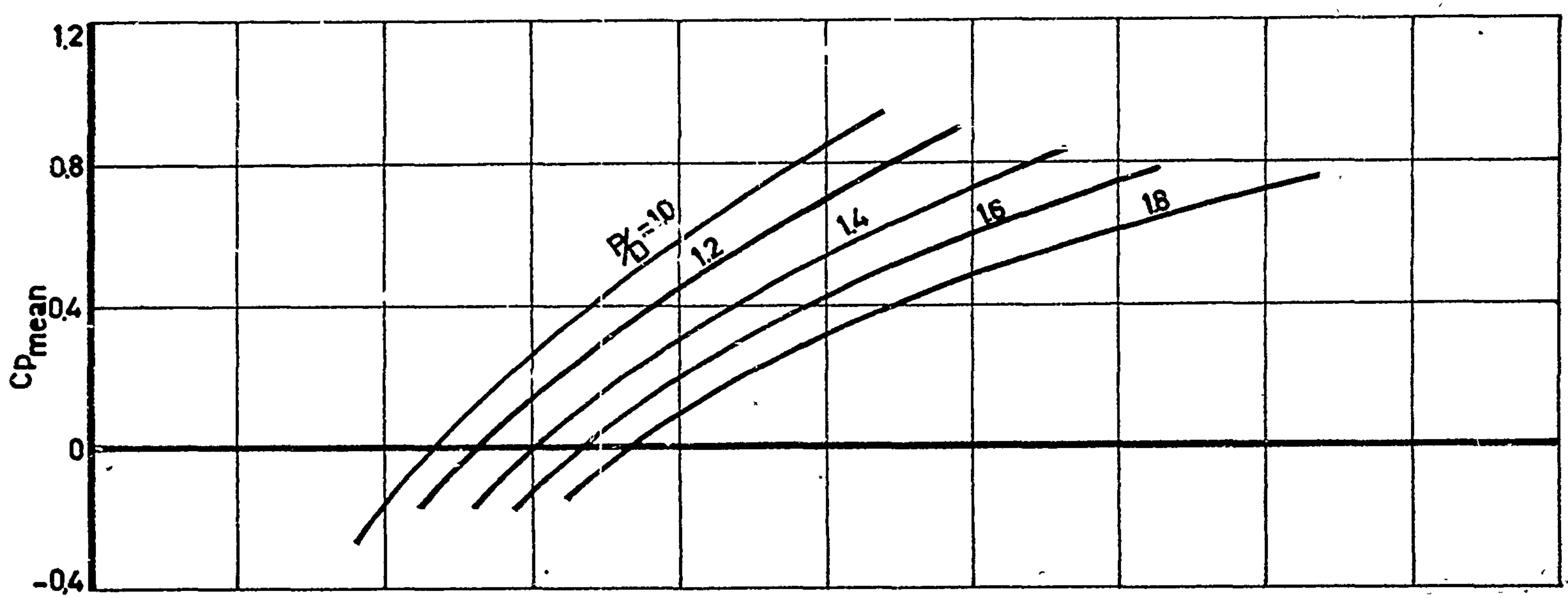
1.2
0.8
0.4
0
-0.4
$C_{P_{mean}}$
P/D=1.0
1.2
1.4
1.6
1.8

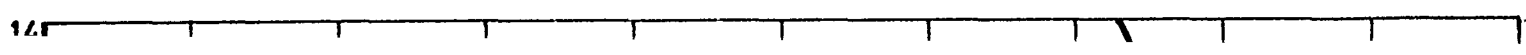

NEDERLANDS
PROEFSTATIO

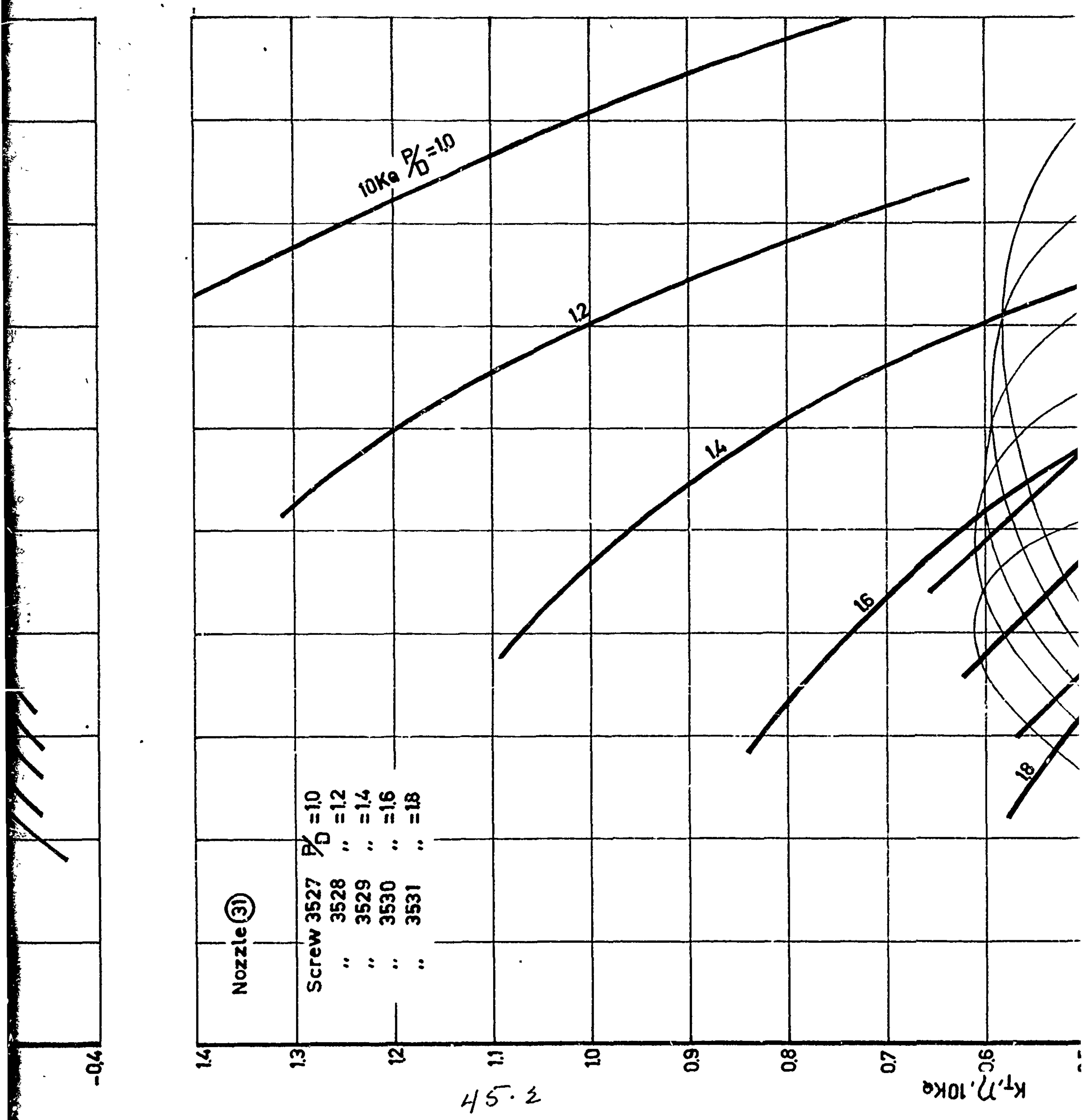

NEDERLANDSCH SCHEEPSBOUWKUNDIG PROEFSTATION WAGENINGEN	NO.	BLZ.

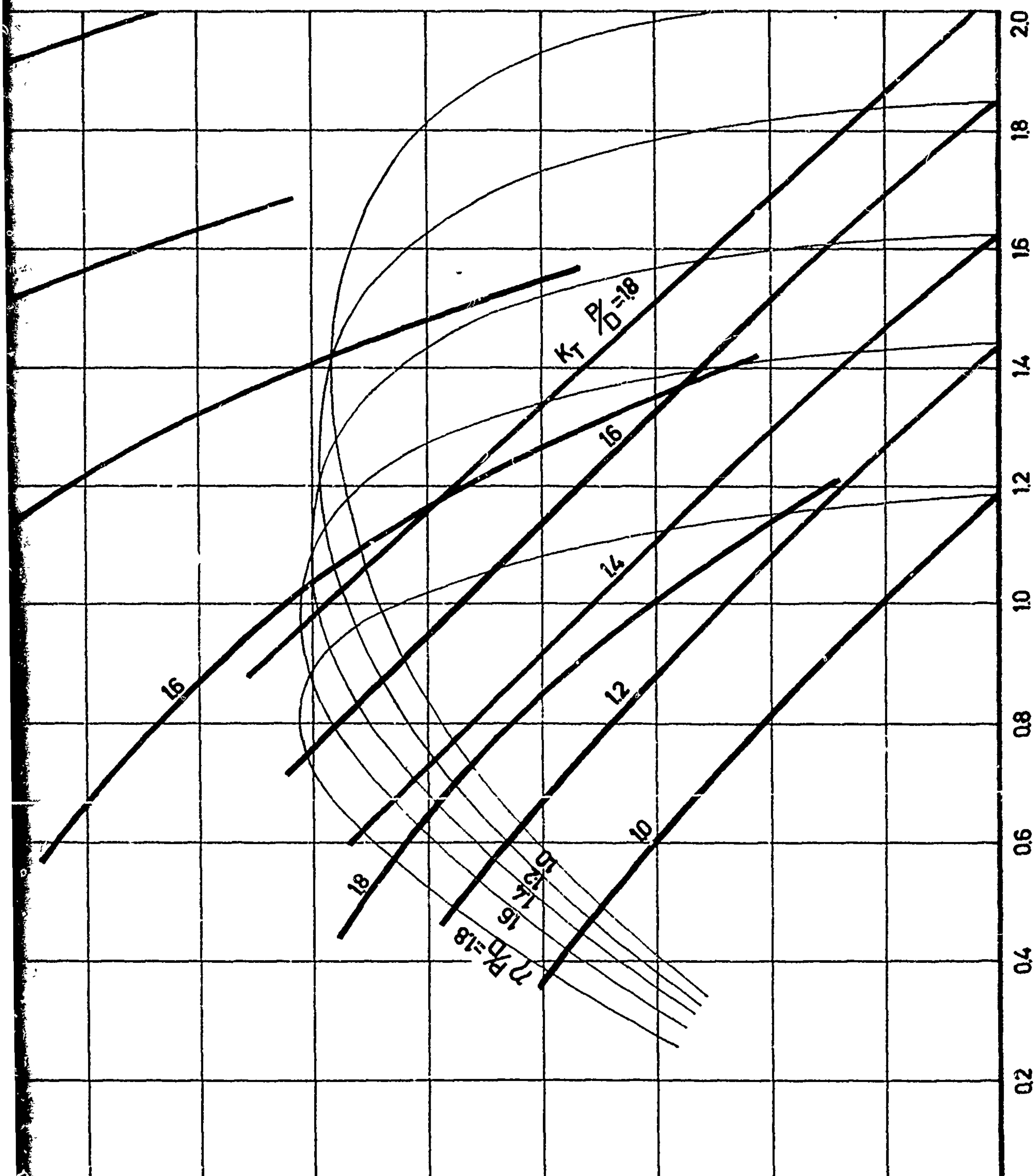

Figure 23. Experimentally obtained characteristics of nozzle No. 31

45.3

46.1

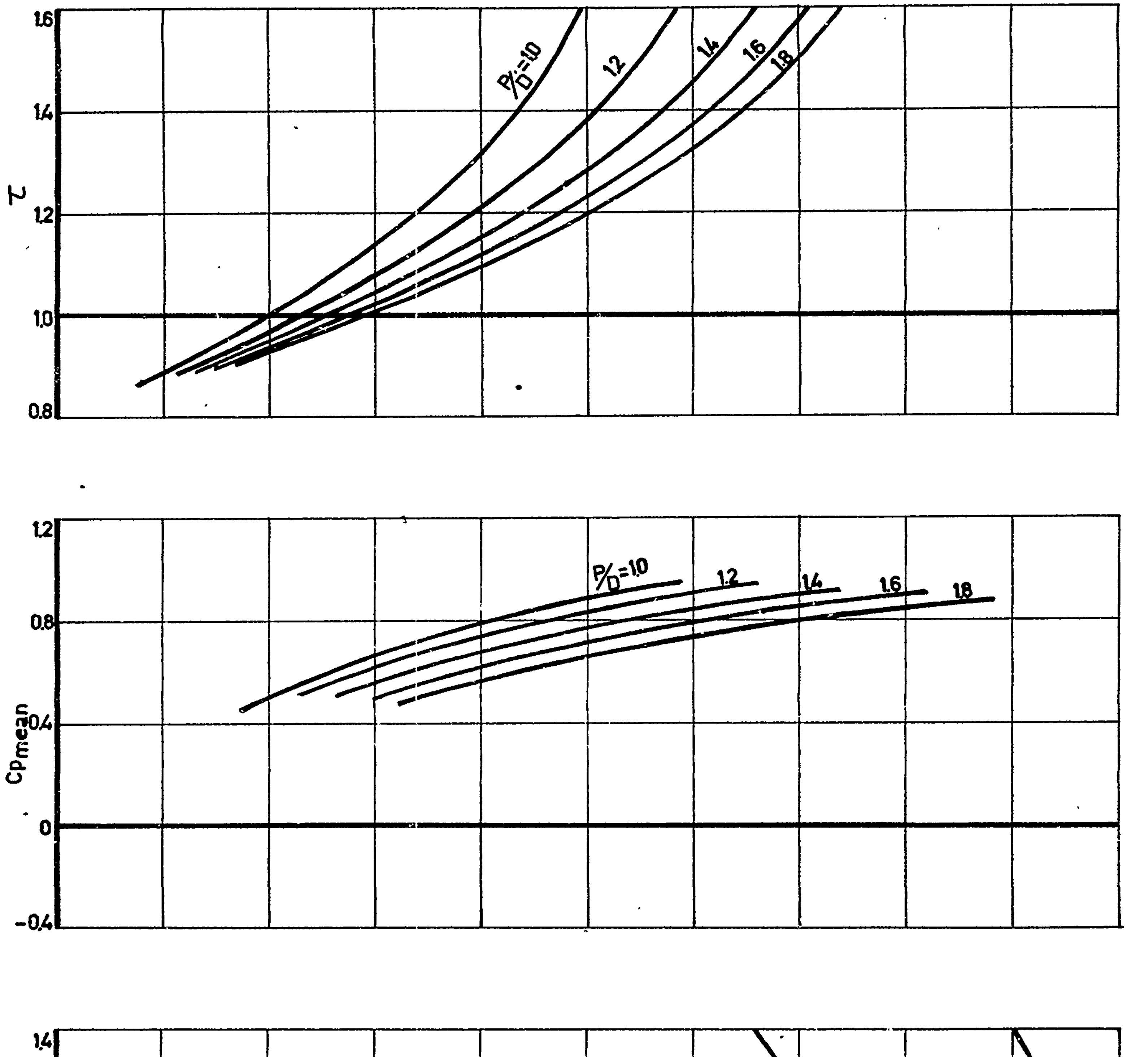
τ
1.6
1.4
1.2
1.0
0.8
P/D=1.0
1.2
1.4
1.6
1.8
Cpmean
1.2
0.8
0.4
0
-0.4
P/D=1.0
1.2
1.4
1.6
1.8
1.4

NEDERLANDS
PROEFSTATI

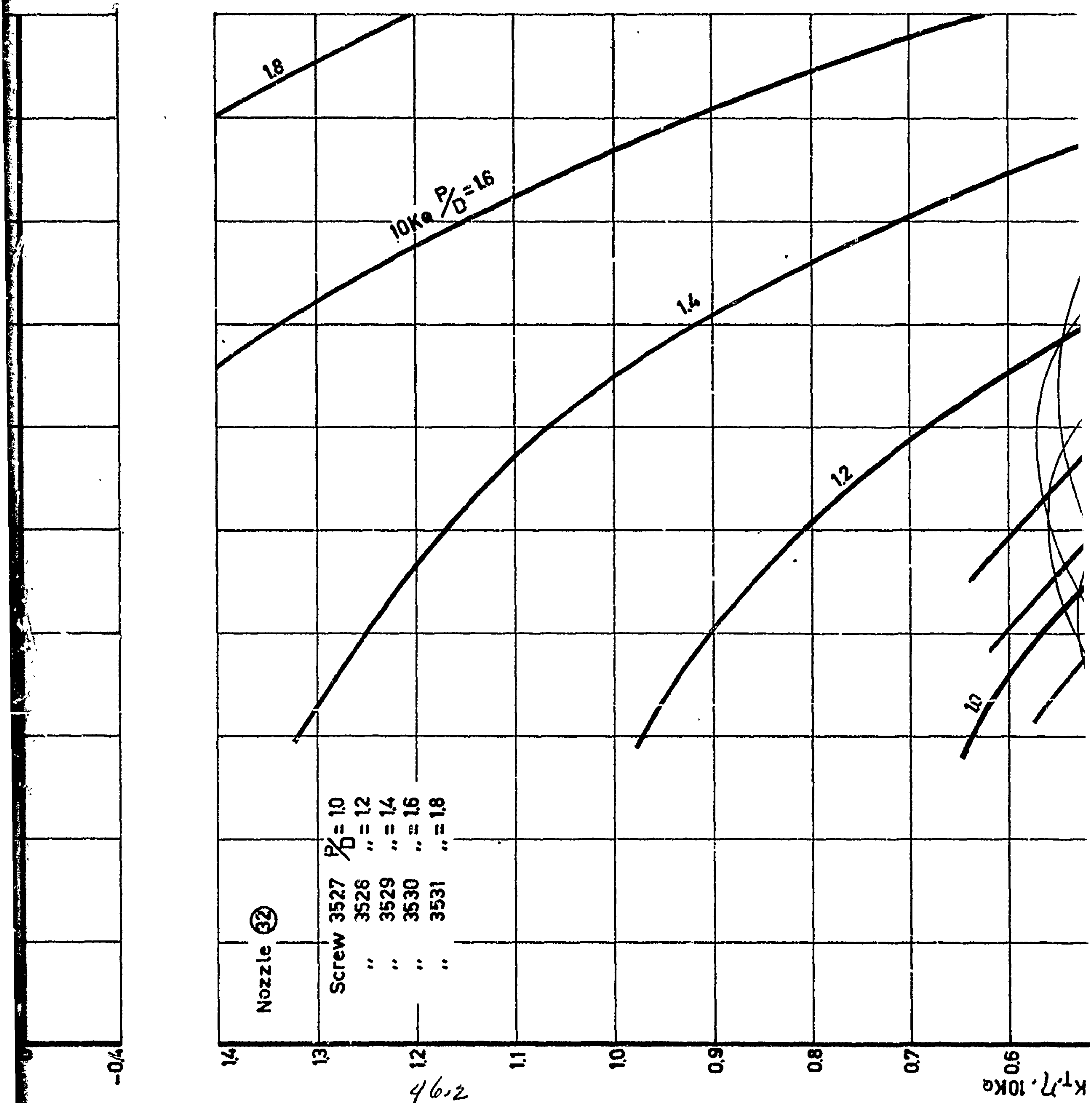

46.2

NEDERLANDSCH SCHEEPSBOUWKUNDIG PROEFSTATION WAGENINGEN	NO.	BLZ.

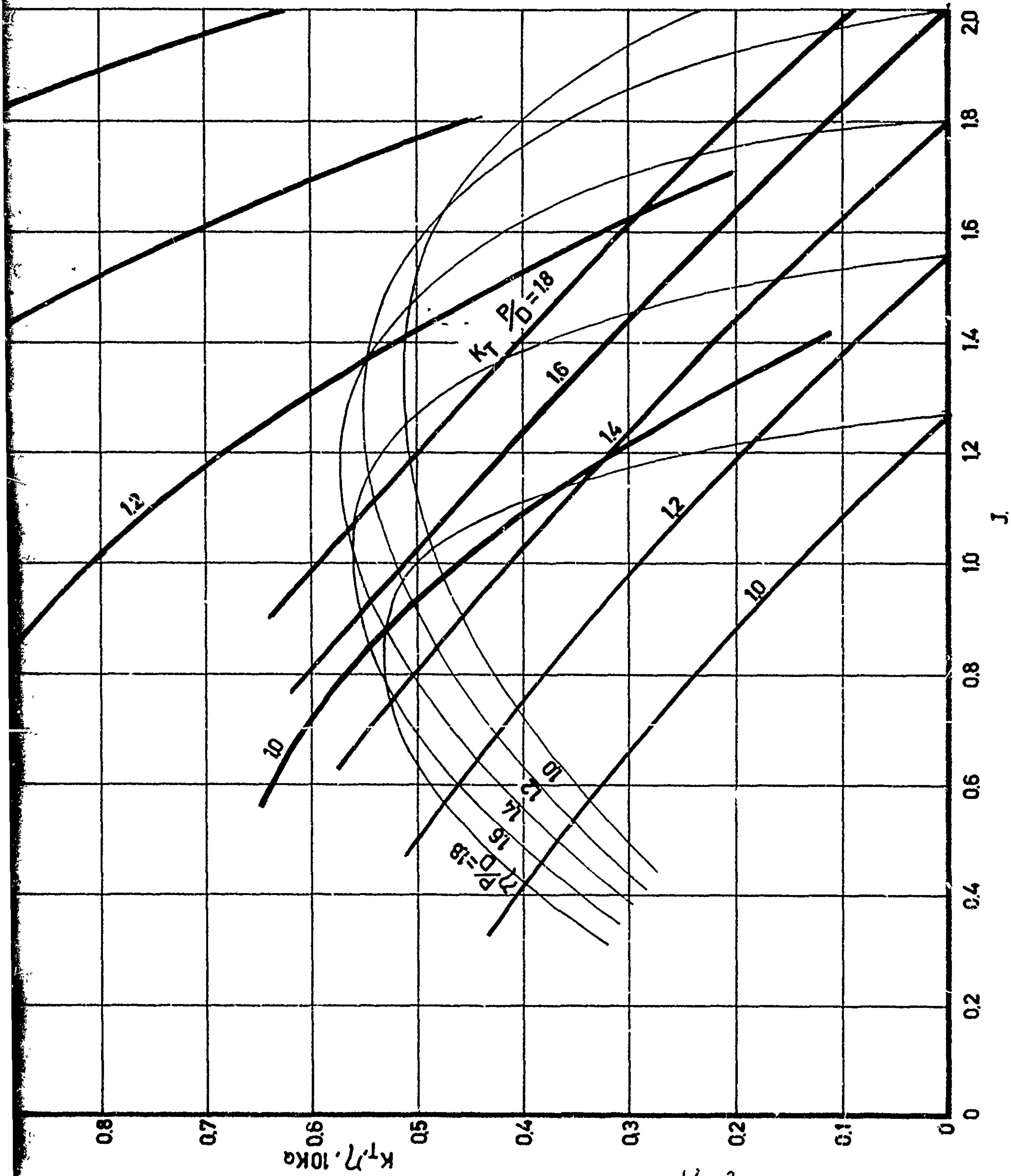

Figure 24. Experimentally obtained characteristics of nozzle No 32

46.3

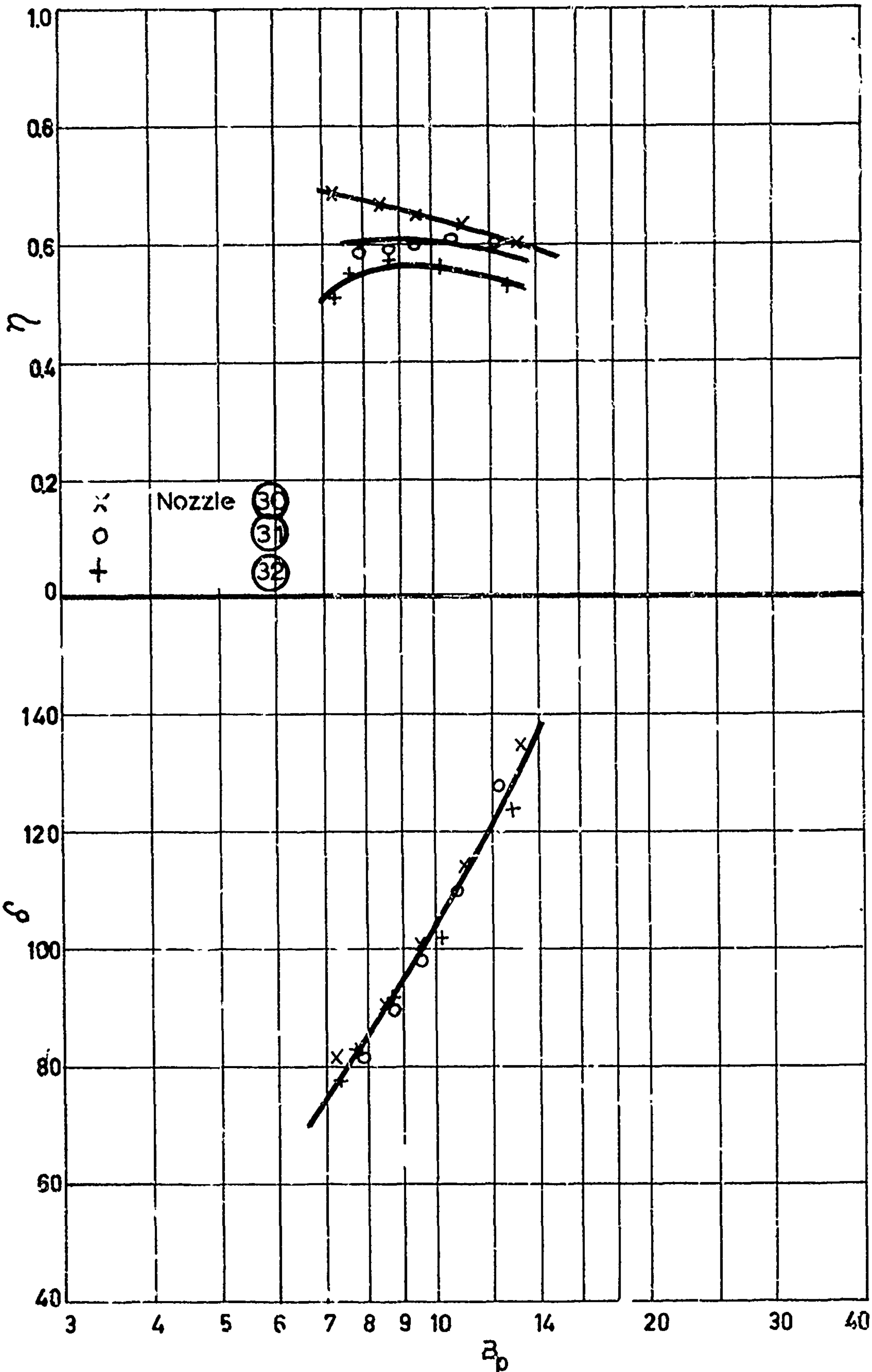

Figure 25. Optimum efficencies as a function of Bp for the various nozzles.

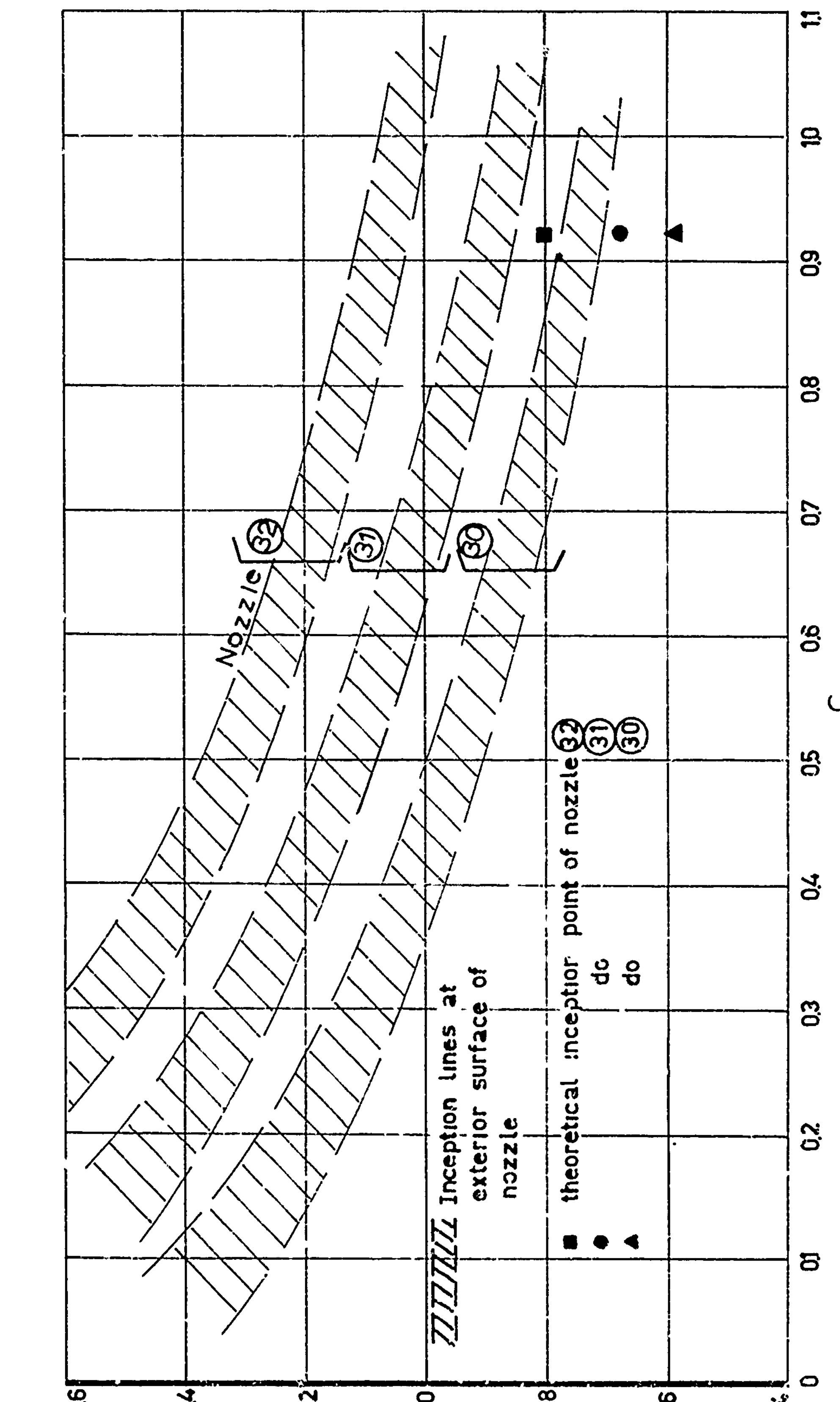

Figure 26. Inception lines for bubble cavitation at the exterior surface of the nozzles